SOLID-STATE NANOCRYSTALLINE GAS SENSOR ARRAY DEMONSTRATION

by

Nathaniel Palenaka Ambler
Bachelor of Science, University of Florida, 2006

A Thesis

Submitted to the Graduate Faculty

of the

University of North Dakota

in partial fulfillment of the requirements

for the degree of

Master of Science

Grand Forks, North Dakota
December
2008

This thesis, submitted by Nathaniel Palenaka Ambler in partial fulfillment of the requirements for the Degree of Master of Science from the University of North Dakota, has been read by the Faculty Advisory Committee under whom the work has been done and is hereby approved.

_____

Chairperson

_____

_____

_____

This thesis meets the standards for appearance, conforms to the style and format requirements of the Graduate School of the University of North Dakota, and is hereby approved.

_____

Dean of the Graduate School

_____

Date

PERMISSION

Title   Solid-State Nanocrystalline Gas Sensor Array Demonstration

Department   Space Studies

Degree   Master of Science

In presenting this thesis in partial fulfillment of the requirements for a graduate degree from the University of North Dakota, I agree that the library of this University shall make it freely available for inspection. I further agree that permission for extensive copying for scholarly purposes may be granted by the professor who supervised my thesis work or, in his absence, by the chairperson of the department or the dean of the Graduate School. It is understood that any copying or publication or other use of this thesis or part thereof for financial gain shall not be allowed without my written permission. It is also understood that due recognition shall be given to me and to the University of North Dakota in any scholarly use which may be made of any material in my thesis.

Signature _____

Date _____

TABLE OF CONTENTS

vi

LIST OF FIGURES

LIST OF TABLES

ACKNOWLEDGMENTS

ABSTRACT

Sensors in reduced pressure environments exhibit largely uncharacterized behaviors. These environments include future extra-terrestrial habitation and greenhouse environments necessary for the fulfillment of the mandated Vision for Space Exploration (VSE) laid out by President George W. Bush on January 14, 2001. Several solid-state sensors, such as the complementary metal oxide semiconductor (CMOS) indium tin oxide (In_2O_3:SnO_2) sensor, demonstrate key benefits in response rates and sensitivity when compared to highly temperature and pressure dependent sensor technologies. Suitability testing of these sensor archetypes involved developing circuitry and testing at the University of North Dakota (UND), heritage data from testing at the Kennedy Space Center and other NASA facilities, and a flight aboard the National Aeronautics and Space Administration's (NASA) High Altitude Student Platform (HASP). The project represented a large science-technology-engineering-mathematics (STEM) promotion effort in postsecondary education, and its execution served as a large inter-disciplinary and multi-institutional challenge from a management prospective. Testing utilized the indium tin oxide (ITO) thin film sensors for the measurement of ozone, developed by the University of North Florida (UNF). These sensors represent a unique, easily produced in mass, and newly designed solid-state nanocrystalline gas sensor array (patent pending). During testing, these sensors demonstrated detection to the parts per billion by volume (ppbv) level. Testing for ozone quantitatively agreed with calibration to within 15%. Flight data

acquired aboard HASP produced a highly accurate ozone profile over the flight. In all, this research addresses many serious unmet needs for miniature sensors capable of in-situ and real-time detection of gasses, such as carbon monoxide (CO), volatile organic compounds (VOCs), or carbon dioxide (CO_2), in reduced pressure and low temperature environments. Because these ITO sensors do not require the high operating temperatures of previous sensors and because these sensors maintain good stability under harsh atmospheric conditions, gas sensors of this type seem good candidates for use in extraterrestrial applications, and in space flight instrumentation. These sensor archetypes help satisfy the rigorous demands of space flight technologies and the future demands of human exploration while improving the detail of the picture and perception of home planet Earth.

CHAPTER 1

INTRODUCTION

1.1 Statement of Problem

Perception of the environment and surrounding world remains highly rooted in evolutionary predispositions and scientific inquiry; often the tools and sensors developed consistently undergo revision in order to paint the tapestry of perception closer to that of reality, increasing situational awareness and understanding. In complex engineering systems, especially in space, the need for accurate and precise data remains a top priority for safe and efficient operations and controls. These systems in space face additional and crippling complexities due to microgravity, increased radiation, and vacuum conditions. Extra-terrestrial planets' unique dynamics also make Earth based sensors potentially unreliable for direct utilization. NASA and other space agencies currently suffer from unmet needs for miniature and micro-miniature sensors, with limited power demands, capable of in situ and real-time analysis of environmental data. Current sensor technologies suffer poor selectivity, poor baseline recovery, irreversibility, long-term degradation, output signal limitations, and often-poor response times.

Operational requirements outlined in NASA's Exploration Systems Architecture Study (ESAS), in response to the VSE, include improving the human-machine symbiosis, and overall sensor technology; the complexity of the mission tasks, required by the VSE, demands the introduction of new technologies in and for hardware to achieve these vast

tasks (Krishen 2008). Specifically of interest in these demands is the ability to detect effectively very low concentrations of gasses in reduced pressure environments such as those proposed for greenhouses on the Moon and Mars. Currently, metal oxide thin films remains one of the most effective methods used for optimization of solid-state gas sensors towards these goals; these solid-state sensor designs offer considerable improvements in signal, selectivity, stability, and response rate (Korotcenkov 2007). Such improvements, address many of the critical needs of sensor technology.

One such solid-state sensor involves the application of indium tin oxide (In_2O_3:SnO_2) whose unique chemical properties contain the required structure, and bulk and surface properties to test for ozone. The behavior of these indium tin oxide (ITO) sensors in reduced pressure environments in both the lab and near vacuum conditions of a long duration and high altitude balloon flight helps to establish some conclusions into the viability of these sensors for space applications. Further, this work helps lay fundamental groundwork in the optimization of sensor parameters for optimal functioning. In addition, to their viability for space applications these sensors have high potential applicability in a wide range of environmental, chemical, refining, control, manufacturing, and industrial processes.

1.1.2 ITO O$_3$ Gas Sensor Background

Since the early 1960s, gas-sensitive resistors have existed commercially with a demonstrated capability to detect combustible gases at the ppmv level. However, recent thin film gas sensors demonstrate great promise at reliably detecting concentrations at the ppbv level (Hansford *et al.* 2004). Specifically, the use of ITO follows as the most recent solid-state gas sensor development (Patel *et al.* 2003, 2005-7).

2

Current conventional ozone sensors, such as the electrochemical concentration cell (ECC) ozonesonde, suffer from pressure sensitivities, great expense, and difficulty in their deployment. The use of ITO sensors demonstrates a great improvement over prior gas sensors, such as early models that used tungsten tin oxide, in sensor response and sensitivity. The ability to detect such low levels of concentration is critical in both ozone atmospheric sampling and in the measurement of ground level pollution, which varies on the ppbv level (Ambler and Patel 2008). In fact, such pollution has steadily increased 5 times its level at mid-latitudes from the start of the century (~10 ppbv to over ~50 ppbv) (Marenco et $al.$ 1992).

The implementation of ITO ozone sensors, such as those developed at UNF, at high-altitudes could play a key role in better understanding the current ozone situation. The structure of the ozone loss in near-space and space over time also helps to test and confirm scientific understanding about the future state of the ozone. Such understandings help also to resolve questions regarding how gas phase and heterogeneous modulation of chlorine monoxide and inorganic chlorine (ClO/Cly) partitioning affects ozone depletion. In fact, stratospheric ozone depletion depends largely on the partitioning processes that arise from the release of halogen atoms. These chemical processes in the stratospheric ozone layer help further clarify legislative effectiveness of mandated changes enacted in the twentieth century, and the potential need for further corrective actions (Solomon 1999).

1.2 Problem Background and History Prior to UND

Research into the applicability of ITO sensors for space applications began in the summer of 2007 at NASA's Space Life Sciences Laboratory (SLSL) at the Kennedy Space Center (KSC). Initial research sought to investigate and begin satisfying the robust and

rugged sensor demands required in the establishment of a Martian greenhouse. Under the direction of Dr. Phillip Fowler, Dynamac, and Dr. Vadim Rygalov, UND, among others, research on how effectively to monitor greenhouses in reduced pressures and potentially hostile environments highlighted many current sensor shortcomings. During a controlled experiment, a lettuce greenhouse maintained an internal pressure of approximately 25 kPa or ~1/4 atmospheric pressure and the resulting growth rates not only maintained normal production rates but also increased up to ~50% as compared to their control. Figure 1 depicts the setup and conditions of the laboratory.
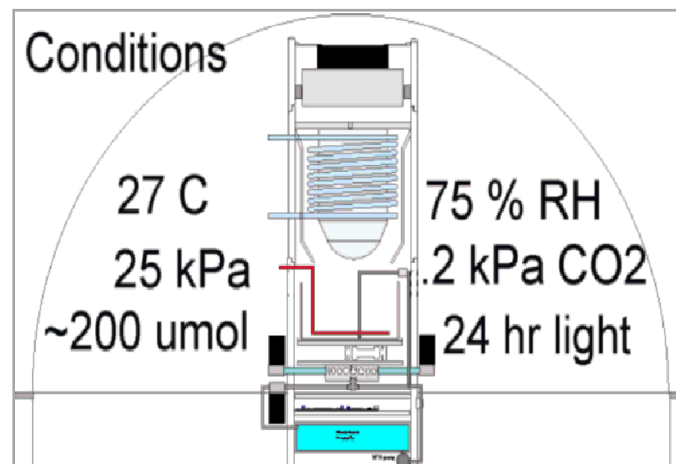
Figure 1. Reduced Pressure Martian Greenhouse Diagram (courtesy Fowler and NASA)

This resulting research is also more widely applicable as NASA realizes that reduced pressure environments extend beyond just planetary greenhouses and into every aspect of spacecraft and structural design. Decreases in internal pressure requirements reduce structural requirements, and, therefore, costs. In fact, according to the ESAS, the newly proposed Crew Exploration Vehicle (CEV), ORION, operates at a reduced pressure of 65 kPa. One consequence of such designs is the necessity to increase oxygen content

above 21% to accommodate these conditions, and hence to monitor carefully the resulting potential increased fire risk. Research suggests the use of an internal pressure below 20 kPa can eliminate risk of fire by upsetting the thermal diffusivity dynamics. The use of an evacuation treatment below this limit could mitigate fire damage in the event of an ignition event (Nakamura and Aoki 2008). Figure 2 highlights the points of ignition in regards to the ambient and partial pressures of oxygen.
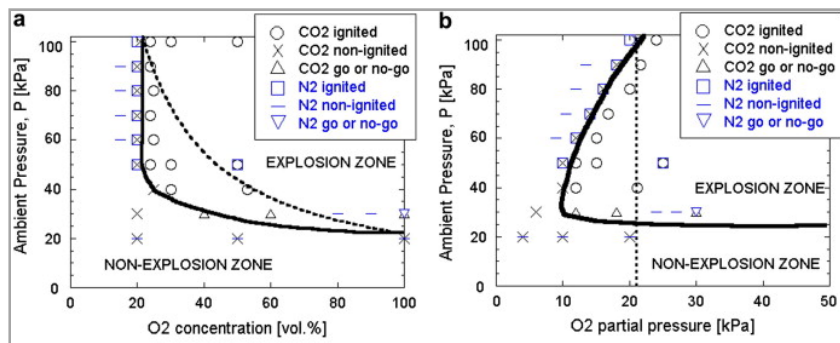
Figure 2. Fire Risks (Nakamura and Aoki 2008)

One drawback in such reactive systems is many current sensors that could help detect atmospheric parameters, such as oxygen, suffer from bulky systems with high power requirements, and suffer from large uncharacterized proportionalities to ambient pressure and temperature. For example, conventional oxygen sensors utilize large electrochemical cells, such as those with Zirconia (ZrO_2), that require high temperatures, and exhibit high power consumption. An investigation of improved sensor designs led to the selection of a novel ozone detector utilizing ITO that minimized many of these negative characterizations, and followed as an improvement over the earlier tungsten tin oxide design (Hansford *et al.* 2004). With the support of Space Florida and its students, NASA various facilities and staff, Dynamac scientists, the University of Central Florida (UCF)

research facilities, UCF faculty member Dr. Chew, UND faculty member Dr. Vadim Rygalov, and UNF partner Dr. Nirmalkumar Patel an initial attempt at sensor calibration and a balloon launch were attempted. Calibration at the SLSL occurred with the Low Pressure Test Bed Facility (LPTBF) with the help of Dr. Phillip Fowler, and Joe Benjamin, Dynamac, shown in Figure 3. After this successful calibration and positive chamber-flight results from the LPTBF, a launch aboard a high altitude-sounding balloon occurred from Kelly Park with the support of Space Florida shown in Figure 4.
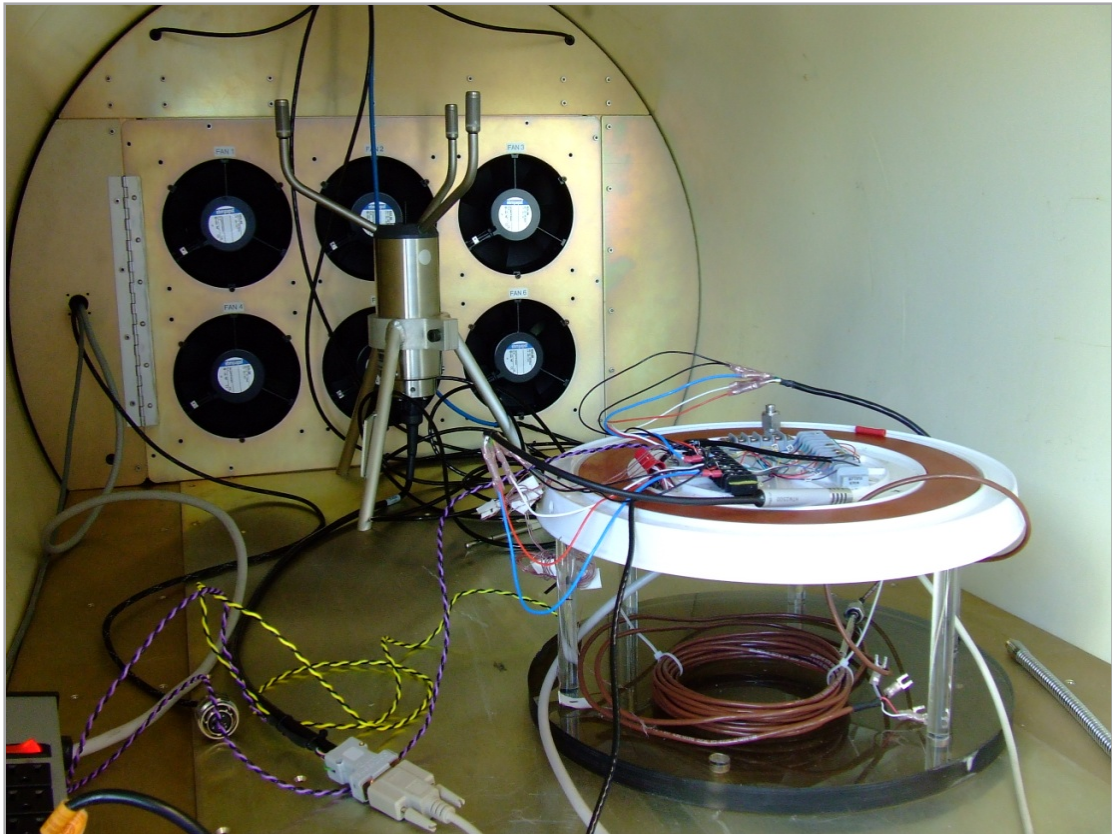
Figure 3. Low Pressure Test Bed Facility at the SLSL

Figure 4. Original Kelly Park Launch Attempt for Ozone Sounding

In the end, the payload suffered from a loss of telemetry, and as a result, the flight never produced any data and its location remains unknown. However, many positive lessons were learned through the process at KSC, including calibration techniques and technical engineering procedures. These lessons would play out during another NASA opportunity, HASP, which laid the foundations for successful data acquisition (DAQ) from a flight and sensor technology validation. This next stage in the collaborative work depended mainly on the NASA, the UNF College of Chemistry and Physics, the UND College of Engineering, and the UND Space Studies Department.

CHAPTER 2

PROJECT OVERVIEW

2.1 Roadmap and Methodology

The next evolution of the project required testing these ITO architectures in the field aboard a high altitude balloon as part of the fulfillment of the technology demonstration objectives. Through the NASA High Altitude Student Platform (HASP), this possibility arose. Participation required successfully responding to a call-for-proposal (CFP) from the host organization Louisiana Space Grant and Louisiana State University. The response to the CFP is included in appendix A with additional HASP documentation and details. This effort encompassed many aspects ranging from effective project management to technical engineering in payload development. This effort required a concerted effort from the primary investigator to wear many hats, including project manager, for the coordination of the required engineering effort, for the calibration work, and for the scientific work, including data reduction.

The overall methodology of the study involved successful DAQ through a flash memory on-board data backup and a real-time data downlink during the HASP flight from the uniquely designed UND sensor interface and supplied payload supports. Additionally, the science benefit relied on post-flight data analysis based on calibration data, flight data, and lab results. Baseline data from calibration when compared to flight data, and adjusted for pressure and temperature sensitivities, as measured by an on board test resistor,

established the desired relationship between the data received and a physical interpretation of ozone concentration. This interpretation allowed the creation of a complete ozone profile from the flight. This work represents a necessary technology demonstration for these relatively inexpensive, highly sensitive, and reliable solid-state nanocrystalline ITO gas sensors. Such solid-state gas sensors, with widespread utility, could greatly increase the understanding of Earth and its changing environment. Further, this proof of concept helps to address questions regarding the viability of these sensors in near-space applications, and potentially in fulfilling critical needs in the spaceflight hardware and architecture of both today and tomorrow.

2.2 HASP Summary

The NASA Balloon Program Office and the Louisiana Space Consortium at the Louisiana State University support the overall High Altitude Student Platform (HASP) program. The HASP enables student built payloads to fly aboard a long duration high altitude helium balloon. This platform uses a zero pressure, thin-layer polyethylene (~0.8 mil), light balloon. This helium-filled balloon spans 400 feet in diameter and expands to 11,000,000 SCF. The targeted flight duration lasts approximately 23 hours and achieves a targeted altitude of at least 36 km (~120,000 ft). This primarily student led effort provides an ideal cost-effective near space environment, offers students experience in designing and creating scientific payloads for space environments, and remains an excellent Science-Technology-Engineering-Mathematics (STEM) development resource.

The HASP includes a standard mechanical, power and communication interface for student payloads to help prevent complexity during the integration process, ensuring

student success. Further, this system provides some flexibility to the mission requirements and launch schedules, which in turn further aids the success of the student payloads.

This program fosters excitement in aerospace related careers by providing a minimal expense "space test platform" available to twelve student groups selected from respondents to the CFP from across the United States. Due to the ease of integration and minimal associated costs, this platform provided the ideal setting for the testing of the UND and UNF sensor payload.

2.2.1   Typical Flight Overview

The HASP ascends at approximately 1000 feet per minute into the stratosphere. The stratosphere rests above the Earth's troposphere, generally considered to span, at the poles, from the tropopause at ~8 km to the stratopause at ~50 km above the surface. This region includes a temperature inversion region, which helps to partially trap trace gases such as ozone, among others (*e.g.* NO_2, BrO, OClO), and small particles for long periods, often for several years, making it an exceptionally interesting zone of study. Figure 5 provides the nominal flight profile from the 2006 flight of HASP (Guzik *et al.* 2006).
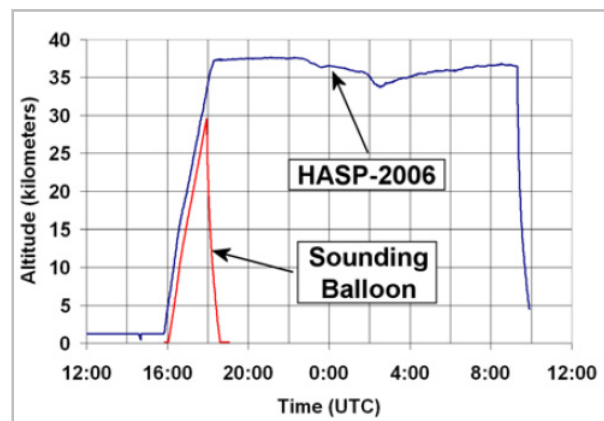
Figure 5. Altitude vs. Time for the Nominal 2006 HASP Flight Compared to Traditional Sounding Balloons (Guzik *et al.* 2006)

Additional concerns during this flight center on the platform's huge thermal variations of cooling and warming between +40°C and -80°C as shown in Figure 6. These thermal issues create hardware and avionics design challenges for consideration.
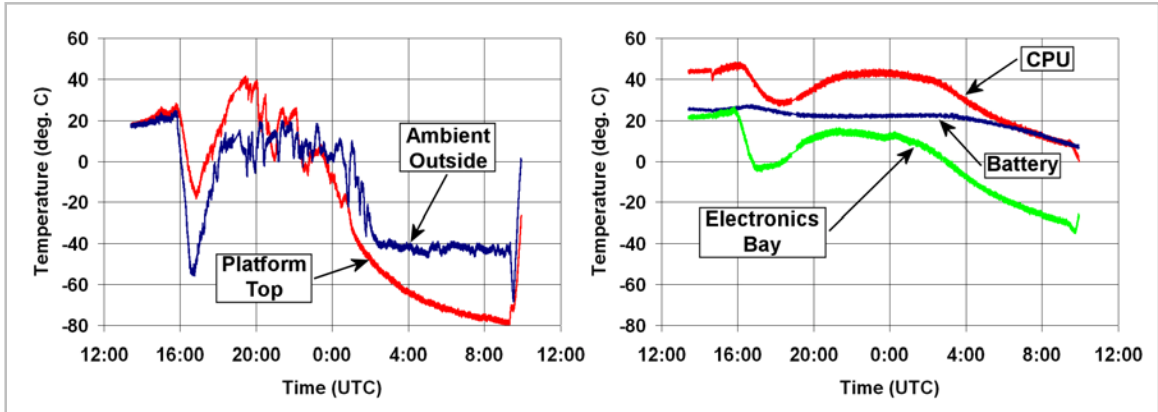
Figure 6. Typical Temperature Flight Profile (Guzik *et al.* 2006)

In addition, to this temperature profile the payload also deals with a rapidly diminishing pressure that approaches a vacuum as seen in Figure 7a. This roughly estimated relationship between altitude and pressure follows as (Jacobson 2005),

$$P = P_o \cdot e^{\frac{-M \cdot g \cdot alt}{R \cdot Ts}}$$

where

	P	pressure at given altitude, Pa
	P_o	pressure at sea level [101,325 Pa]
	M	average molecular mass of atmosphere [$0.02897 \frac{kg}{mole}$]
	g	local gravity, m/s^2
	alt	altitude of interest, m
	R	gas law constant [$8.314510 \frac{joule}{K \cdot mole}$]
	T_s	temperature at sea level [288°K]

11
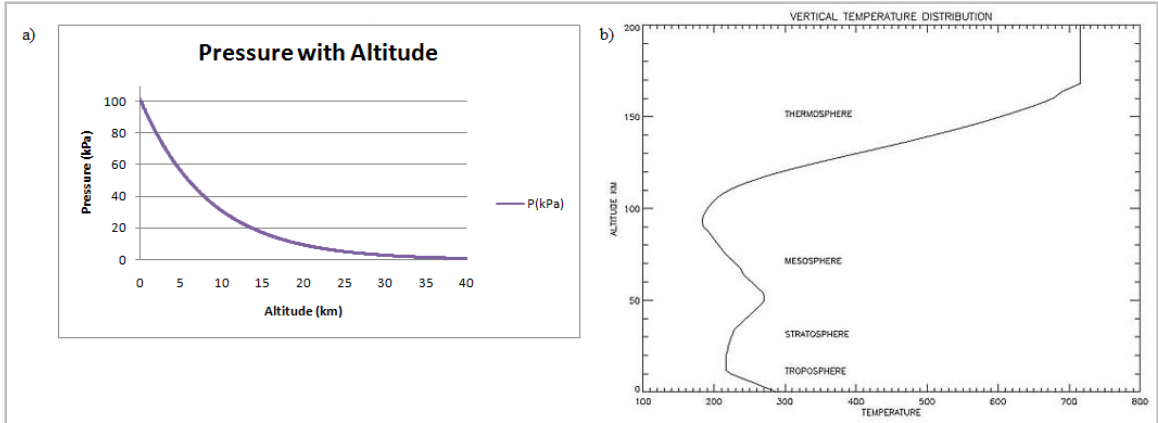
Figure 7. a) Pressure with Altitude for Dry Air, and b) Temperature with Altitude (courtesy of NASA GSFC Atmospheric Chemistry and Dynamics Branch)

These pressure issues, near-vacuum conditions, and unique thermal issues create unique engineering obstacles very similar to those found in a space environment and common in spacecraft design. At such low pressures, the molecular separation distance greatly increases and the importance of increased sensitivity of the sensor is crucial. Further, heat transfer can no longer occur through convective means. These challenges and many more underwent thorough consideration during the engineering design process.

Geographically, the HASP flight originates from Ft. Sumner, New Mexico between 05:00 and 10:00 depending on weather and ground conditions. The Columbia Scientific Balloon Facility (CSBF), NASA, oversees the flight to ensure flight termination occurs over a safe location within the United States. This geographic latitude roughly approximates to 93% of the expected equatorial ozone concentration. Due to the nature of a long duration flight, the range of uncertainty for the balloon spans several hundred miles. However, the slower nature of upper stratospheric winds at float compared, to the much quicker surface and low level winds, allows the careful monitoring and tracking of the

flight path. During the flight, NASA places a chaser aircraft on standby for purposes of recovery and tracking.

2.2.1.1 Flight Ozone Range

The maximum ozone concentration peaks and occurs in the stratosphere between 20 km and 27 km, well within the predicted flight profile for both HASP and earlier KSC efforts, as seen in ozone climatology and trend data shown in Figure 8 (Randel *et al.*1999). This consideration largely went into the decision behind the characteristic testing of ozone, a novel, yet practical selection given the flight characteristics. Aside from altitude, concentration largely depends on the latitude of interest, alluded to earlier, when moving away from the equator formation rates decrease with the cosine of the latitude. Further, temporal, and seasonal effects play an equally large role.
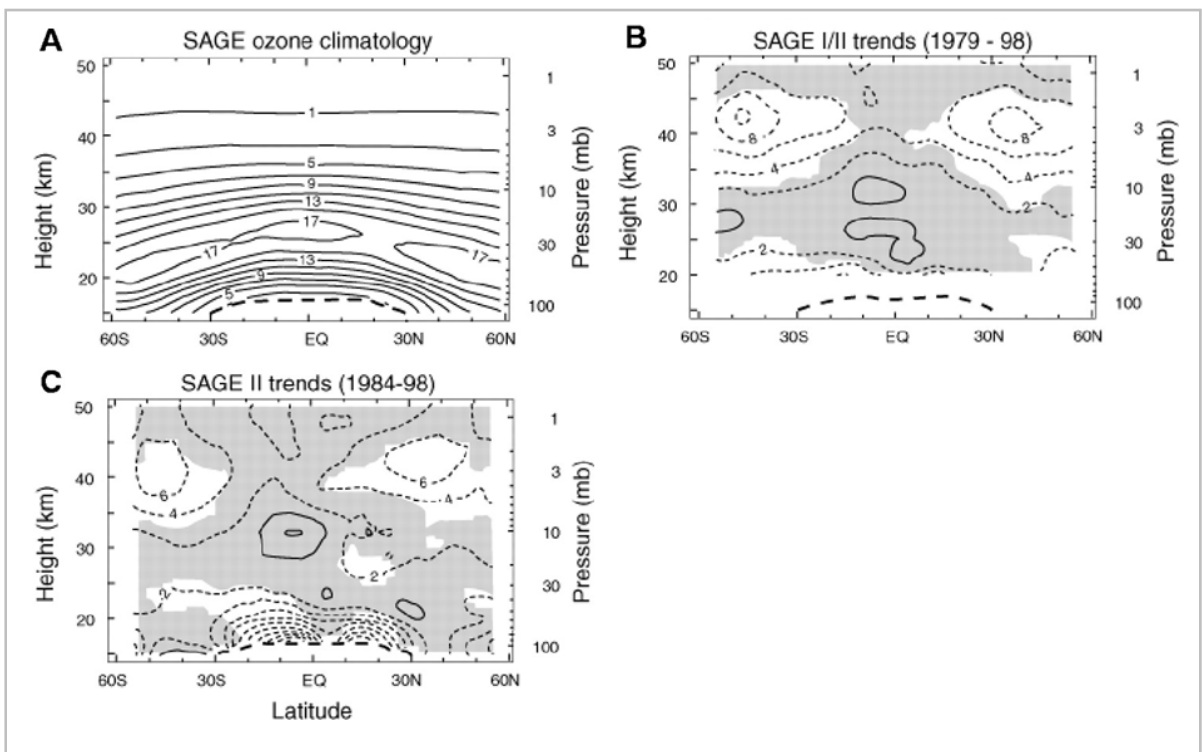
Figure 8. Ozone Concentration and Trends with Height and Latitude (Randel *et al.* 1999)

Once at the target altitude, the expected ozone concentration corresponds to between approximately 8 and 12 ppm at local noon during float at ~25 km as derived from Figure 9, primarily driven from adapted Chapman mechanism predictions.   This dimensionless correspondence from Figure 9 derives from estimating the following relationship as follows,

$$C^* = \frac{\rho \text{ (ozone)}}{\rho \text{ (total)}} \cdot \text{cosine } (\text{lat}_{\text{data}}{}^{\text{o}})^{-1} \cdot \text{cosine } (\text{lat}_{\text{int}}{}^{\text{o}}) \cdot \text{p'} \cdot \text{t'}$$

where

ρ_{ozone} density of ozone (molecules $\cdot$ cm^{-3}) $\approx$ 1 to 2 x 10^{12} molecules$\cdot$cm^{-3}

ρ_{total} density of atmosphere (molecules $\cdot$ cm^{-3}) $\approx$ 3 x 10^{17} molecules$\cdot$cm^{-3}

p'   seasonal variation factor $\approx$ 1.4

t'   local temporal variation factor

$\text{lat}_{\text{data}}{}^{\text{o}}$ latitude of data from the graph, degree(s)

$\text{lat}_{\text{int}}{}^{\text{o}}$ latitude of interest for concentration estimation, degree(s)
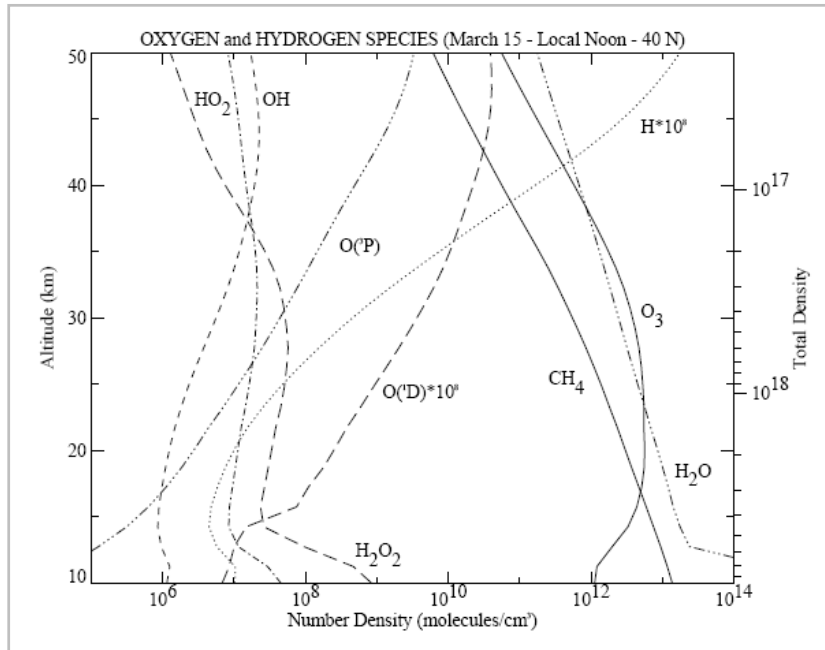
Figure 9. Oxygen and Hydrogen Species Concentrations (Demore *et al.* 1997)

The dominant adapted Chapman mechanism greatly explains the expected flight ozone profile and the presence of ozone in the stratosphere through a series of dynamic reactions between ozone's creation and destruction. In short, the mechanism stems from the necessity for very energetic UV radiation to (λ < 183 nm) to breakdown oxygen molecules, and the capability for any short wave radiation up to near IR (λ < 1180 nm) to break down the ozone molecule. In the troposphere, this process plays a passive role due to photolysis where radiation reacts with ozone and releases heat and oxygen faster than ozone creation. However, this mechanism can greatly underestimate various photolytic effects and overestimate predicted ozone. Chapman explained this general reaction sequence and fundamental phenomena as follows (Chapman 1930),

$$\text{i)} \quad O_2 + hv \rightarrow O + O$$

$$\text{ii)} \quad O + O_2 + M \rightarrow O_3 + M$$

$$\text{iii)} \quad O_3 + hv \rightarrow O + O_2$$

$$\text{iv)} \quad O + O_3 \rightarrow O_2 + O_2$$

$$\text{v)} \quad O + O + M \rightarrow O_2 + M$$
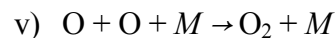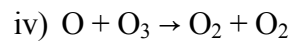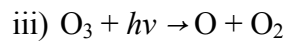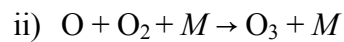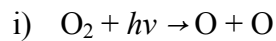
where hv represents photonic energy, electromagnetic radiation

M represents any molecule involved in the termolecular reaction

2.2.2 Technical Overview

The HASP platform provides the BUS support for up to 12 payloads through a gondola that provides a mechanical, electrical, power, and data support structure. Each payload keys to a specific payload ID number, payload ID 7 in the instance of UND. In

addition to the technical specifications and interface documentation in reference to HASP, each individual payload has to withstand vertical shocks ($\pm G_z$) of 10 g, and horizontal shocks ($\pm G_x$) of 5 g for flight certification. The mass budgeting excluded the mass of the payload mountings plates; however, the mass budget constrains all other mounting hardware (*e.g.* screws, and bolts). All payloads undergo testing for conformity prior to integration. These payloads vary in two classes in regards to size and respective support as outlined in Table 1.

Table 1. HASP Technical Interface Summary and Requirements

	Small Student Payloads:	Large Student Payloads:
Available Slots:	8	4
Maximum Weight:	3 kg (6.6 lbs)	20 kg (44 lbs)
Maximum Footprint:	15 cm x 15 cm (~6"x6")	38 cm x 30 cm (~15"x12")
Maximum Height :	30 cm (~12")	30 cm (~12")
Supplied Voltage:	29-33 VDC	29-33 VDC
Available Current:	0.5 Amps @ 30 VDC	2.5 Amps @ 30 VDC
Maximum Serial Downlink (bitstream):	1200 bps 2 bytes per command	4800 bps 2 bytes per command
Serial Interface:	1200 baud, RS232 protocol, DB9 connector	4800 baud, RS232 protocol, DB9 connector
Analog Downlink:	2 channels 0 to 5 VDC	2 channels 0 to 5 VDC
Discrete Commands:	Power On, Power Off	Power On, Power Off
Analog & Discrete Interface:	EDAC 516-020	EDAC 516-020

Figure 10 illustrates the gondola support structure of HASP, where at each outward and inner corner rest the student payloads. Each payload interacts with the HASP through its electronics and the Science Stack and the Serial Commanding Unit (SCU) as shown in the schematic of Figure 11.
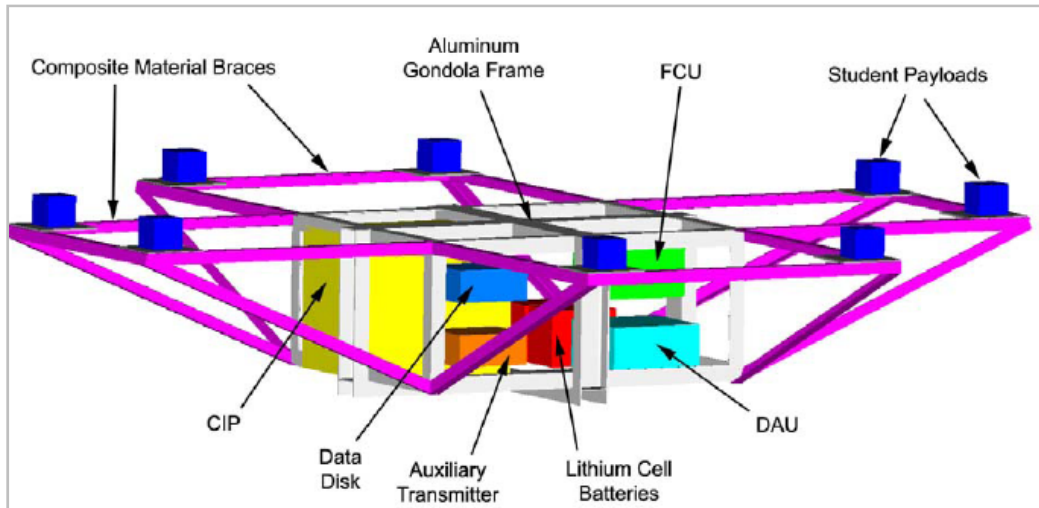
Figure 10. HASP Gondola and Configuration (Guzik and Wefel 2004)
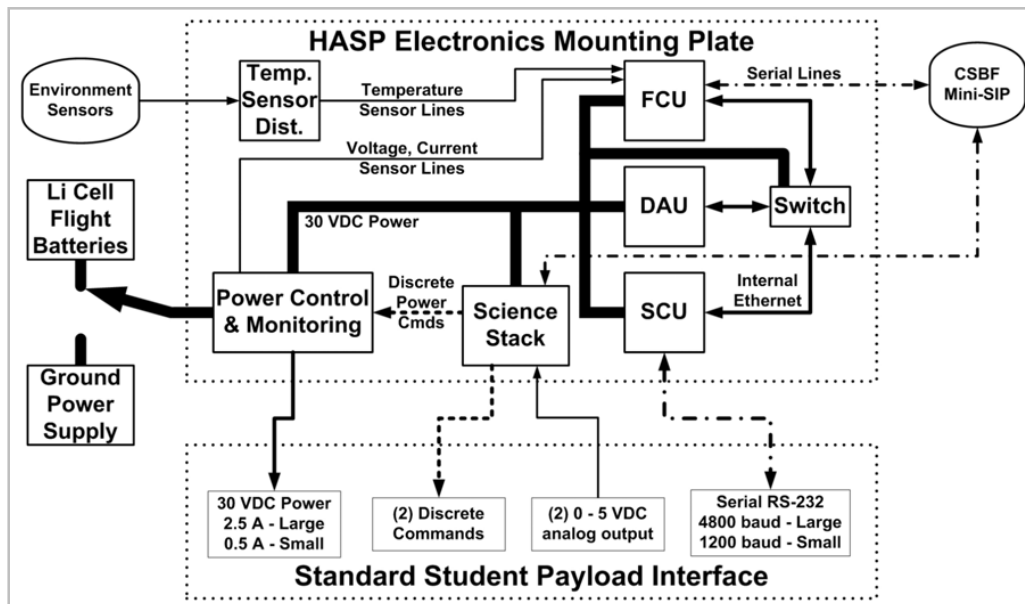
Figure 11. Student Payload Interface to the HASP Flight Electronics (Guzik *et al.* 2006)

Each class of payload receives their respective ¼" thick PVC mounting plate as shown in Figure 12 and Figure 13 (Guzik *et al.* 2006). The UND payload required only the smaller payload demonstrated in Figure 13a, and illustrated on the left of Figure 12.
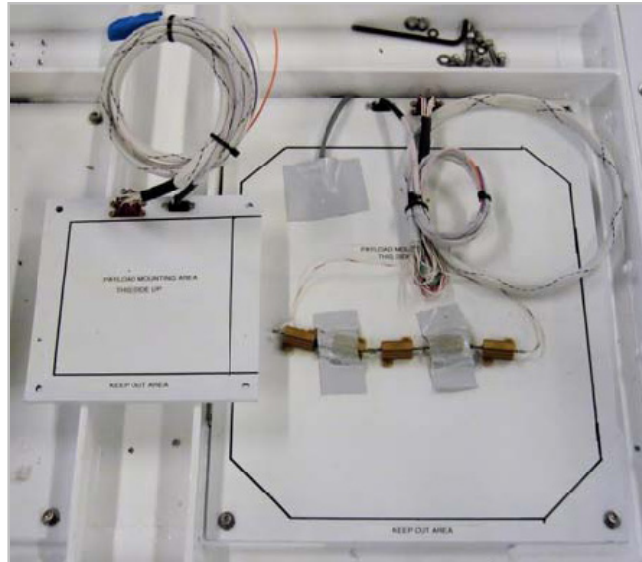
Figure 12. Mounting Plates Photograph (Guzik *et al.* 2006)
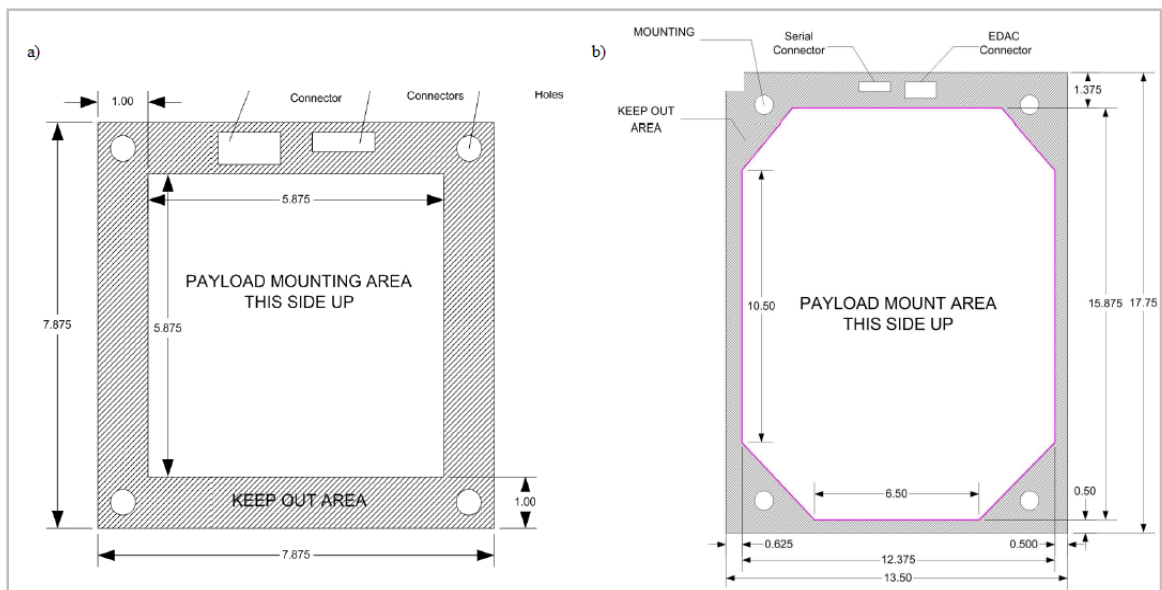
Figure 13. a) Small Payload Mounting Plate, dimensioned in inches, that UND utilized, and b) Large Payload Mounting Plate, dimensioned in inches (Guzik *et al.* 2006)

As outlined in the technical and interface specifications, these payload-mounting plates include a DB9 data terminal equipment (DTE) connector for serial uplink and downlink and an EDAC 516-020 for power, discrete commands, and analog outputs. Payloads each receive commands and send data to the HASP flight system through a single RS-232 connection using 8 data bits, no parity, 1 stop bit and no flow control at 1200 baud for the UND and UNF payload and other smaller payloads, and 4800 baud for larger payloads. On the connector, only the signal ground pin, received data pin, and transmitted data pin operate. According to specifications, student payloads must wire the DB9 pigtail as a NULL modem where pin 3 receives, and pin 2 sends. Figure 14a, adopted from the HASP technical specifications, shows the configuration for the DB9 pins. The connector EDAC 516-020 used to interface to power, analog downlink channels, and discrete commands requires pins L and R for signal return for both analog and discrete channels. Figure 14b, adopted from the HASP technical specifications, displays the EDAC 516-020 pin layout. Table 2 specifies the pin layout of the EDAC 516-020.
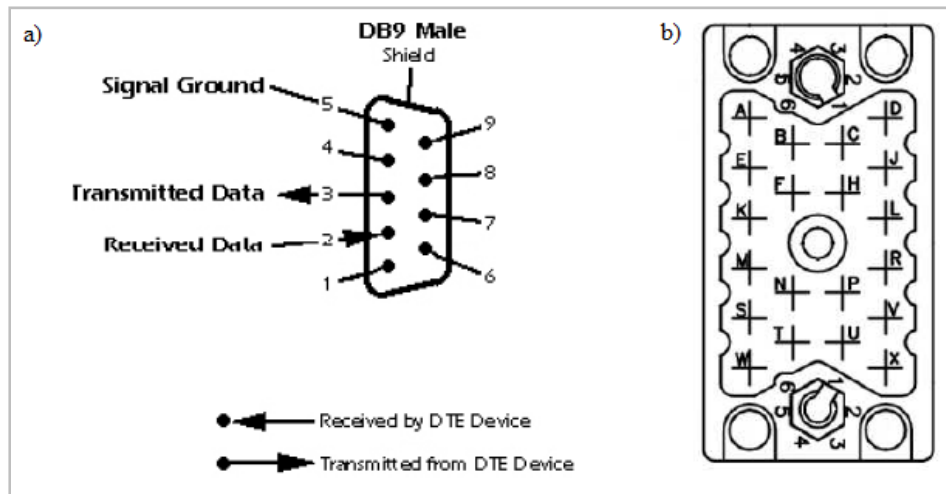
Figure 14. a) DB9 Receptacle Pin Layout, b) EDAC 516-020 Receptacle Pin Layout (adopted from the HASP specifications document)

Table 2. EDAC 516-020 Pin Layout

Pin	Wire Color	Function
A, B, C, D	White with red stripe	+30 VDC
W, T, U, X	White with black stripe	Power Ground
K	Blue	Analog 1
M	Red	Analog 2
L, R	Black	Signal Return
F	Brown	Discrete 1
N	Green	Discrete 2
H	Large Payloads (unwired)	Discrete 3
P	Large Payloads (unwired)	Discrete 4

The A, B, C, and D pin on the EDAC 516-020 connector supplies the ~+30 VDC in parallel from the HASP system; however, the batteries may initially provide up to 33 V and diminish down 29 VDC during the course of flight. The correct pin configuration is crucial in preventing a blown circuit on HASP or non-functionality of payloads. Also through the EDAC connector, two 0 to +5 VDC analog channels sample once a minute, digitize, and downlink real-time data of two parameters. Pins K & L represent channel one, and pins M & R represent channel two. The fused power supply limits current draw to 0.5 amps for the smaller payloads and 2.5 amps for the larger power supply.

Once a serial command is transmitted and onboard, HASP formats and routes serial command strings to the payload over the serial link. Each command string includes 7 bytes and Table 3 shows the format for HASP command strings from the interface manual.

Table 3. HASP Command String Format Sent to Student Payloads (adopted from the HASP Interface Manual).

Hex Value	Byte	Description
1	1	Start of Heading
2	2	Start of Text
command byte 1	3	First byte of command from ground
command byte 2	4	Second byte of command from ground
3	5	End of Text
D	6	Carriage Return
A	7	Line Feed

The HASP operator transmits commands at limited times each hour. Each command takes 1 minute to execute and confirm. The payload design highlights the adapted UND and UNF payload command format.

2.3 Project Management

The measure of success of any project depends on an appropriate management stance, a careful balance of project needs, resources, and intangible human interactions. The dynamics of managing complex medium sized student directed groups in engineering projects, such as HASP, remains an underexplored area of human-interaction research; study of these interesting dynamics also benefits the understanding of project management, especially for general medium sized unstable dynamic projects. In this process, the UND and UNF HASP student group maneuvered through the project phase with contemporary project engineering techniques that minimized the risks to successful project management resolution, such styles included the use of extreme project management (XPM) or agile project management, and contingent systems based thinking. Although the process largely evolved to suit the needs, this project serves to help better document an underdeveloped area of management research. Documentation and quantification for such extreme project

management cases remains an active area of research and requires inclusion of traditional project management techniques. This agile management technique, in the more fluid XPM environment, supplemented itself with traditional project management tools such as the work breakdown schedule (WBS), the program evaluation and review technique (PERT) critical path method (CPM), and the use of Gantt charts. In this specific case many of these tools were only implemented midstream; however, ideally, future projects would spend considerable planning efforts in creating these at the outset of a project.

The utilization of an extremely agile model, a contingent based perspective, foresight of participant's schedules as a function of semester progression, encouragement of strong student commitment with financial and experiential incentives, virtual engineering groups through Adobe® Breeze conferencing software, and a strong continual reliance on faculty advocates and faculty functional managers all played fundamental roles in the project's successful completion. These roles propelled and maintained forward momentum for the project. A highly adaptive, highly agile, highly innovative, and highly creative management style, originally used in software engineering, effectively navigated the student led research group through rapidly changing revisions of hardware, software, and mechanical qualifications as the project largely centered on ongoing research with uncertain and changing requirements.

Although the successful completion of the project relied on no one tangible aspect, it is clear that this student led research project lent itself to a dynamic interacting complex project requiring constant monitoring and a willingness for flexibility within the limits of the project's temporal limitations. The unique and busy nature of student participants required much flexibility; however, in this project the need for flexibility also had to reflect

the more rigid requirements of the NASA HASP guidelines, and external agents. Ultimately, the research project demonstrated the fundamentals of project management. It suggested that the successful balance between the need for agility and the rigidity of project requirement is the function of a project manager. The implications of these fundamentals in the selection of an appropriate project manager implied the necessity for a manager that had both the technical expertise and leadership experience to balance project requirements, maintain channels of effective communication, demonstrate strong commitment through intimate involvement, establish well-defined goals, and create an effective monitoring and control system. All of these demands in the fashion of a team and learning environment.

The classification and use of XPM largely symbolized and resulted from an attempt at hitting a moving target, and remains inherently difficult to quantify. However, the success of XPM in regards to HASP manifests through the effective management of the following categories: scope, schedule, resources and costs, risk, quality, collaboration, performance and motivation, and learning.

2.3.1 Project Structure

The control of many of the characteristics of effectiveness depended on a clear understanding of the project type and appropriate structure. The project followed a near projectized organizational structure due to the intrinsic nature of a research project with new technology. In addition, due to its academic STEM value, it largely aimed to promote what Senge refers to as a learning organization. Although projectized on the surface to allow mobility between aspects of the project, the structural organization remained largely fluid and organic to empower teams and growth. The team composition consisted of 6 primary undergraduate engineering students at UND, 2 undergraduate students at UNF,

multiple graduate students from Space Studies at the organizational level, and central faculty members at UND to help handle many of the transactional managerial responsibilities for the technical UND group.

As mentioned, the learning component stood as an essential consideration in both promoting individual learning, and improving the process and quality of the project. Although the organizational goal remained to support a broad mixture of hard systems thinking with holistic considerations, the decision to classify the organization structure as projectized is due to the appropriateness of such a structure in dealing with uncertain, technologically new, complex, time-critical, and important projects. Robert Youker outlined these characteristics for organizational decision making as seen in Table 4.

Table 4. Criteria for Organization Design Decisions (Youker 1997)

	Favors Functional	**Favors Matrix**	**Favors Project**
Uncertainty	Low	High	High
Technology	Standard	Complex	New
Complexity	Low	Medium	High
Duration	Short	Medium	Long
Size	Small	Medium	Large
Importance	Low	Medium	High
Customer	Diverse	Medium	One
Interdependency (within)	Low	Medium	High
Interdependency (between)	High	Medium	Low
Time Criticality	Low	Medium	High
Resource Criticality	Depends	Depends	Depends
Differentiation	Low	High	Medium

The HASP Project, with its unique considerations, deviated qualitatively the least from this projectized style. As seen in Figure 15, from this conclusion the organizational

continuum implied the majority of the organization directly related to the project (Youker 1997). The project experience validates this logical conclusion of direct organizational contact to the project.
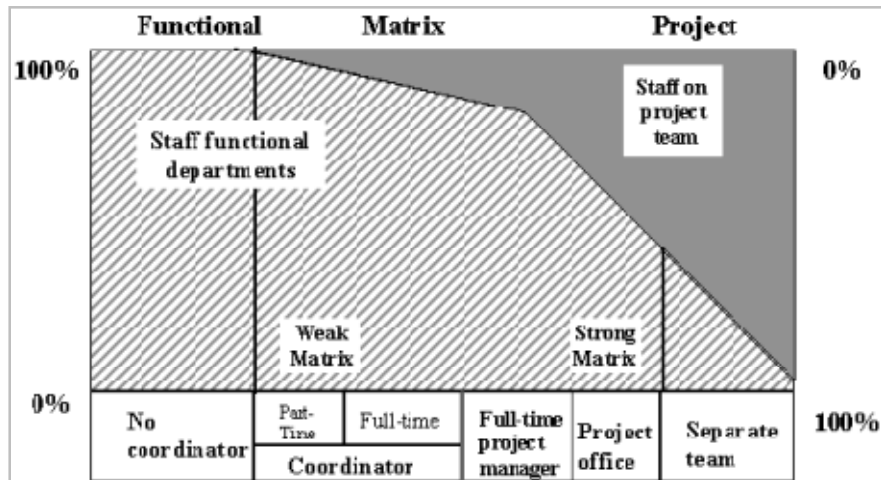
Figure 15. Organizational Continuum (Youker 1997)

The projectized structure also carefully considered systems engineering (SE) aspects, especially in light of the fact that according to INCOSE Systems Engineering Center of Excellence 15 to 20% of the total project should optimally involve SE efforts (Honour 2004). According to similar studies, most projects typically fail to reach their maximum potential because of low investitures (*i.e.* 3 to 8%) on SE activities (Kludze and NASA 2004). The application of the SE process proved highly compatible with XPM management techniques in that the project had continual feedback and methods to incorporate and integrate changes back into the system. The projectized structure most closely matched the objective to stimulate learning, successfully fly the HASP payload, and generate the necessary scientific and engineering gains. In this project, the main technical scope of concern remained limited to the engineering, and scientific aspects of the project.

Figure 16 shows the larger organizational structure supporting the project in the ideal. It is important to note that the Dakota Space Society remained intimately involved because the organization's main purpose at the time centered on conducting student related research, with the HASP effort the only current and active project.
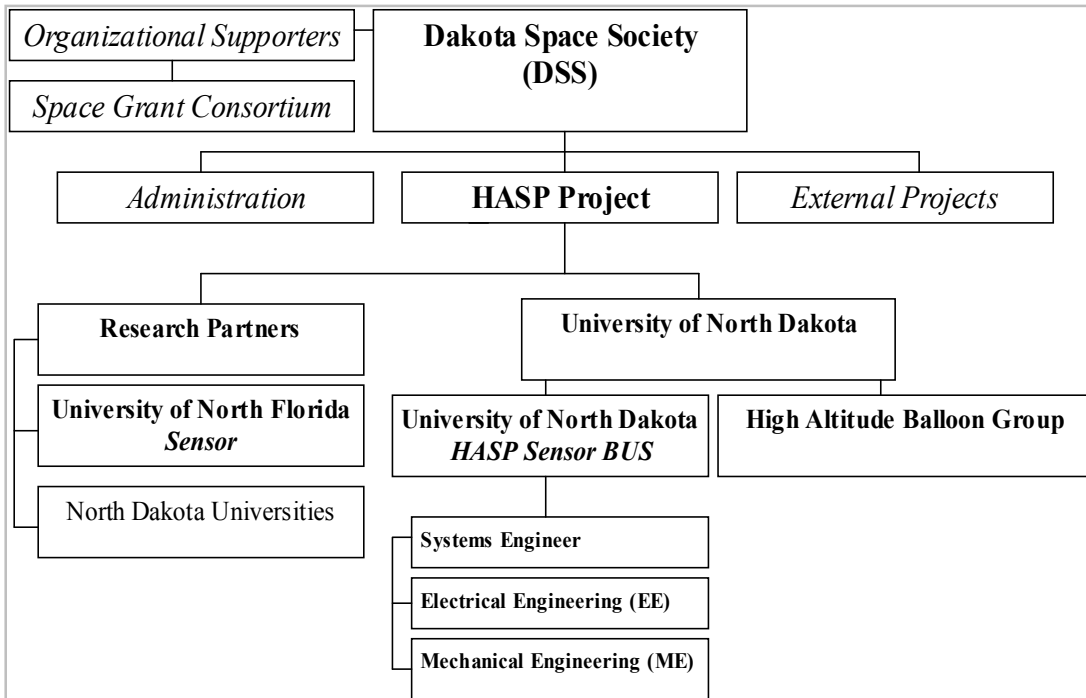
Figure 16. HASP Organizational Structure

In this organizational structure DSS is a student organization at the University of North Dakota acting as the overall umbrella organization for the project; the DSS internal structure has several offices with varying administrative duties. In this case, the presiding officer of DSS acted as the PM and remained largely responsible for the project, including helping to direct functional managers, direct technical leads, and coordinate research partners. This organizational structure helped to increase feedback, and demonstrated a

high degree of commitment from the organization to the project, further supporting the projectized nature of the HASP research effort.

The measurement of success for any organizational structure, including HASP, largely stems from a matter of perception, cost adherence, and schedule success (Might and Fischer 1985). The HASP project remained largely on target, ultimately proved successful in promoting STEM, gained valid scientific data from flight, and served as a technology demonstration for both the DoD and NASA.

2.3.2 Management and Systems Methodology

Part of managing such a dynamic and uncertain project inevitably simplifies to managing chaos. A large part of the chaos in HASP grew from inherent instability in working with a new technology and grew from the use of many student researchers with varying responsibilities and external pressures. Of relevance to note, some of the students received stipends; however, the primary motivation remained the experience and the personal learning experience of the project. As both objectives of the participants and the project included continual learning and development, the fostering of the learning organization remained extremely pertinent to the success of HASP. The learning environment promoted the gradual evolution of the project's organization and processes to adapt to its needs, much as an organic system. These project characteristics match the systems thinking perspective, a projectized structure, and an XPM style, partially concluded *ex post-facto*.

The HASP project demonstrated that many of these elements naturally fit together and share many of the same greater underlying principles, particularly valuable conclusions to similar sized and characterized future projects. Although XPM remains a relatively new

practice for many PMs, XPM actually bases itself on a revolution from sound fundamentals, not a departure. The relationship between these structures, designs, outlooks, and styles seem naturally congruent and appear a logical fit to the purposes of the HASP effort and student projects.

In regards to the operations of the project, the project held standard weekly meetings to assess progress and to monitor and control the project. During these weekly meetings, each paired-team discussed their progress, needs, or setbacks. These meetings ultimately demonstrated a necessary component to assessing the progress of the group. These meetings eventually turned into design meetings between fewer key contacts in the summer. This decrease largely developed from the fact that many student researchers could only participate through the conceptual and early design phase as the summer carried other obligations for many of the students. The PM consistently monitored the project while balancing minimal interference and direct involvement in the project, including directly participating in the engineering process. This careful balance offered the most realistic feedback to the project, and the most accurate assessment of the project's overall status. Further, milestones or in software engineering terms, "versions" of the project underwent inspection during milestones (*e.g.* the critical design review). Student teams typically worked continuously in an integrative fashion to limit interruptions to the progress and to enable accurate tracking of the holistic system.

Due to its uncertainty, complexity, and nature, the HASP project type most resembles a systems project. Figure 17 demonstrates the classification régime for projects.
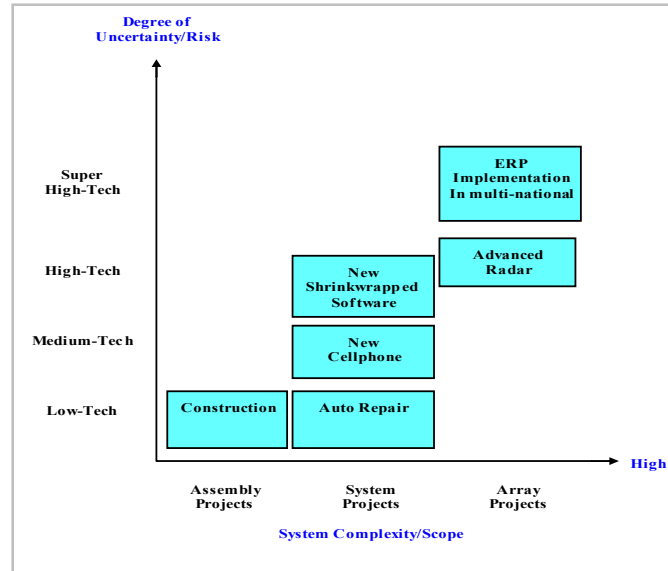
Figure 17. Shenhar's Taxonomy of Project Types (adapted from Shenhar 2001)

This systems approach aligns well with the previous discussion of the engineering systems process, the learning organization goal, the organizational structure, and the utilized XPM style. System thinking stresses the importance of viewing the final product as a dynamic and complex whole that remains independent of individual components of the design (*i.e.* the whole does not equal the sum of its parts; the whole can synergistically equal more or the whole can degrade to equal less). When combined with systems theory, the systems engineering process clearly benefited. HASP demonstrated that as engineers worked in pairs and rotated to other aspects of the project they naturally viewed the project as a whole system, allowing an integral system to continue as a thematic concern to the process. In fact, the SE importance to the goals of the project expended approximately roughly 20% of the project's human resource, fulfilling the 15-20% optimization requirement for SE efforts according to INCOSE Systems Engineering Center of Excellence (Honour 2004).

Similarly, the decision to apply an agile model of management seemed an obvious necessity in the HASP project due to its dynamic, interactive, and complex nature. Definition of the HASP organization as dynamic, as in the prior characterizations, remained largely qualitative. This HASP configuration most logically fit the interacting and dynamic environment in the structural dynamic interaction matrix from the Maylor & Vidgen's model (2006) in Figure 18.

	Independent	Interacting
Structural	1. Independent structural complexity	2. Interacting structural complexity
Dynamic	3. Independent dynamic complexity	4. Interacting dynamic complexity

Figure 18. Structural Dynamic Interaction (SDI) Matrix (Maylor and Vidgen 2006)

Such dynamic and interacting characteristics make XPM an ideally suited management style suited with an elastic approach that handles rapid changes within such a complex project. Further, such a style allowed for frequent revisions to the project without costly transactional changes. It allowed the project to make these revisions and to test these changes continually in concentric loops of planning and feedback; this cycle limited any delays to items on the critical path and avoided delays in the life cycle of the project. Moreover, this feedback process became an almost unnoticeable and unconscious behavior. As stated, the XPM approach originally stemmed from methods involving managing software projects; however, its applicability extends beyond just computer programming,

and its utility benefits any complex or uncertain task, as seen in this project. Don Wells (2003) points out that XPM is a series of not just new rules, or some forgotten ones, it concerns human values and teamwork, and much more. When considering XPM it is also important to make note that it requires a high intensity of communication and interaction; therefore, research suggests it should limit itself to small or medium groups, such as HASP, with 12 or less, although this does not preclude an underdeveloped distributive XPM approach for larger groups (Kalstorin 2004).

Certain criticisms of the XPM style stems from the misperception that XPM is an attempt to justify a lack of planning; however, planning is actually more important in XPM than any other management style (Wells 2003). XPM in no way detracts from the 6P, Prior Planning Precludes Poor Project Performance, rule of management. In fact, XPM enhances the 6P rule by planning a capacity for flexibility to deal with unforeseen, yet minimized as much as possible, turbulence or risks, in an open, organic, and undeterministic approach (Klastorin 2004). One of the concerns for many projects with XPM is that the non-technical participants and the technical participants must remain intimately involved with each other, and understand each other, in the process. This requires a high commitment from all levels of the organization and management, and technical understanding from the leadership. However, such requirements also benefit the fidelity of feedback from this high level of interaction. Concerning stimulating a learning organization, XPM stands out as it relies on a team approach and collective mind to drive the process, continually evolving and organic. However, this is difficult to plan as much of these anecdotes are ideal insights and methodologies stemming from the hindsight of a final evolved version of the project's

characteristics, where each project has varying circumstances and defining characteristics important to the management decision process.

These reported methodologies may seem to buck the traditional PM concepts and stereotypes that focus strictly on meeting times, budgets, and project requirements, the pinnacles of the project management triangle. However, these traditional concepts, when taken alone, suffer from an operational mindset that does not recognize the uniqueness and intricacies of projects, especially highly complex and uncertain projects. The traditional operation PM concept must evolve to incorporate aspects of transformational leadership as well, especially in highly dynamic projects, made easier with XPM. The effective project management design of the future stands to evolve the project management triangle to Shenhar's new strategic project leadership (SPL) star shown in Figure 19. These aspects of tools, spirit, organization, strategy, and process all align to the systems outlook and learning organization approach necessary in the intrinsic HASP project characteristics of study.

Figure 19. Strategic Project Leadership Star (Shenhar 2007)

2.3.3 Systems Engineering and Project Tools

According to the Project Management Institute (2000), a project is a "temporary endeavor undertaken to create a unique product or service," with a well-defined life span. HASP adheres to these requirements as it has a specific start date, and end date. These date definitions arise from the flight requirements, and grow out of the requirements selected by

the NASA and the HASP program managers. However, monitoring these dates and the project as a whole requires not only effective management philosophy but also effective tools. Each major event, or progress, includes dependencies on prior events and activities, such as the submission of a payload integration plan. The project time line with assigned dependencies, shown in Figure 20, plays a large role in the creation of the critical path.

Task	Duration	Earliest Start	Latest Finish	Dependencies
HASP Proposal	17 days	11/15/2007 8:00	12/7/2007 17:00	
HASP Review and Selection Process	28 days?	12/10/2007 8:00	1/16/2008 17:00	1
Preliminary Design Phase	24 days?	1/17/2008 8:00	2/19/2008 17:00	2
PDR	1 day?	2/20/2008 8:00	2/20/2008 17:00	3
Critical Design Phase	34 days?	2/21/2008 8:00	4/8/2008 17:00	4
CDR	1 day?	4/9/2008 8:00	4/9/2008 17:00	5
Final Design Phase	19 days?	4/10/2008 8:00	5/6/2008 17:00	5
FDR	1 day?	5/7/2008 8:00	5/7/2008 17:00	7
Local Flight Preparations	10 days?	5/8/2008 8:00	5/21/2008 17:00	7
FAA Review and Design Integeration	118 days?	1/17/2008 8:00	6/30/2008 17:00	2
Local Flight	1 day?	5/22/2008 8:00	5/22/2008 17:00	8,10,9
Scientific Testing and Calibraiton	1 day?	5/23/2008 8:00	5/23/2008 17:00	8,11,1
HASP Paylod Specification and Integration Plan	62 days?	5/8/2008 8:00	8/1/2008 17:00	7
HASP Specification Submission	1 day?	8/4/2008 8:00	8/4/2008 17:00	13
HASP Integration	2 days?	8/5/2008 8:00	8/6/2008 17:00	12,14
BEMCO Thermal / Vacuum Test	1 day?	8/7/2008 8:00	8/7/2008 17:00	15
Correct for Deviation	1 day?	8/8/2008 8:00	8/8/2008 17:00	16
BEMCO 2nd Test	1 day?	8/9/2008 8:00	8/9/2008 17:00	17
HASP Payload Integration Certification	1 day?	8/10/2008 8:00	8/10/2008 17:00	18
Pack and Ship to Ft. Sumner	1 day	8/11/2008 8:00	8/11/2008 17:00	17,19
HASP Flight Operation Plan	63 days?	5/23/2008 8:00	8/15/2008 17:00	11
HASP Ops Plan Submission	1 day?	8/18/2008 8:00	8/18/2008 17:00	21
Flight Operations and Payload Oversight	11 days?	8/19/2008 8:00	9/1/2008 17:00	22
Launch	1 day?	9/1/2008 8:00	9/1/2008 17:00	1,14,15,19,22
Flight/Science Information Keeping	193 days?	12/11/2007 8:00	9/1/2008 17:00	1
Flight/Science Conclusions for Report	87 days?	9/2/2008 8:00	12/31/2008 17:00	25,24
Final Report Submittal	1 day?	1/1/2009 8:00	1/1/2009 17:00	24

Figure 20. HASP's Project Timeline and Dependencies from Microsoft Project

Microsoft Project 2.0 generates the network analysis and critical path method (CPM) from the WBS, the project plan found with additional project details in appendix B, and the individual task slack characteristics. The project management tools associated with maintaining these organizational goals, and demands vary in necessity and complexity. One of the benefits of XPM is the avoidance of rigid schedules and traditional tools. However, traditional program management tools supplement the XPM approach with HASP but do not focus on unnecessary heavy formalism. These traditional approaches,

tools, and software, such as Microsoft Project Professional 2.0 and Palisade @Risk 4.0 for

Project, generate the basic schedule, WBS, CPM, and risk analysis discussed.

2.3.3.1 WBS, Schedule, & Gantt

The WBS in HASP remained an extremely important reference, and the most

important part of the planning phase for the project, it served as the bill of material

equivalent for objectives and the timeline. The timeline for the project included the

expected task duration and potential variance calculated from the WBS as shown below

(Klastorin 2004):

$$\mu = \frac{t^0 + t^p + 4t^m}{6}$$

$$\sigma^2 = \frac{(t^p - t^o)^2}{36}$$

where $\quad$ t^o $\quad$ optimistic time estimate

$\quad$ t^p $\quad$ pessimistic time estimate

$\quad$ t^m $\quad$ most likely time estimate

After calculating expected task durations, establishing precedence relationships,

and constraining the start and finishing times of the tasks from the WBS, the Gantt chart

schedule emerges as shown for illustrative purposes in Figure 17, project schedule.
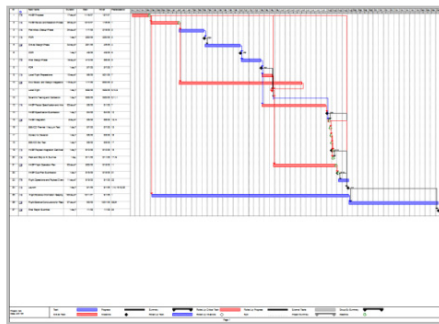
Figure 21. Project Schedule

2.3.3.2 CPM and Risks to Schedule

The highlighted path in the schedule represents the critical path to the project. These highlighted tasks in HAPS required completion on time for the project to avoid costly project crashing. Figure 22 shows the larger project critical path, taken from the schedule, for illustrative purposes.
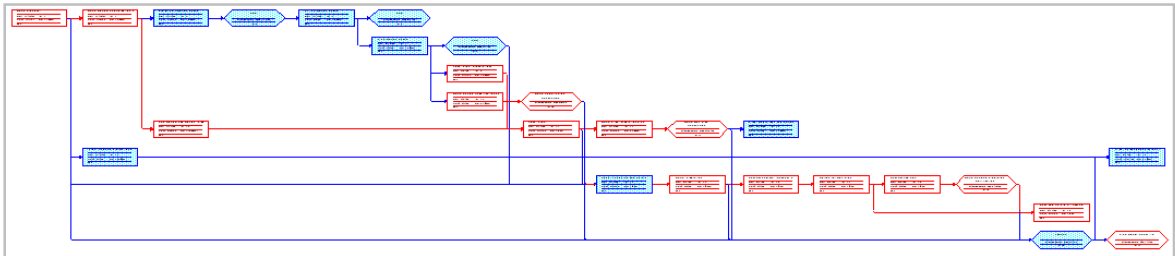
Figure 22. Overall Critical Path from HASP

From this CPM, a Monte-Carlo simulation with @Risk 4.0 and the Project file highlighted potential deviations to the schedule. Figure 23, shows the Rayleigh fit from the resulting risk assessment to the schedule.
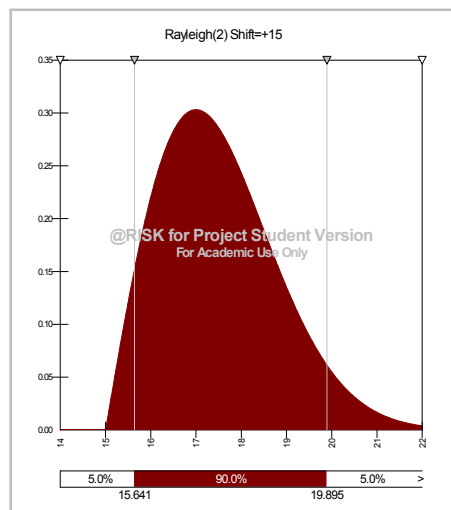
Figure 23. HASP Schedule Risk Example

The result of these risk simulations depends on the amount of dependent channels, duration of preceding tasks, and slack in tasks. The risk simulation for this example schedule from HASP showed that at task number 17 there existed a 30% chance that the schedule would experience a delay to the schedule. Such simulations would have allowed the possibility for corrective measures to be performed early, such as increased monitoring, to ensure the on time delivery of task 17, the critical design review (CDR). Simulations help prepare for the event of encountering instability, such as bringing in additional resources early instead of addressing a crisis with a crash to the project schedule. However, the benefit of XPM is the increased flexibility to schedule, at a cost.

2.3.3.3 Virtual Teams and Communications

Another interesting aspect of the HASP project revolved around utilizing virtual engineering teams and fluent effective channels of communication. Virtual teams eased the tasks of managing a cross-geographic research effort. An illustrative screenshot from the conferencing software Breeze during the CDR, seen in Figure 24, demonstrates Dr. Patel at the UNF and other remote participants dynamically interacting with the UND engineering team. The UND Engineering student appears in the upper left of the screen, and the thermal circuit diagram of discussion appears in the main window for remote participants.
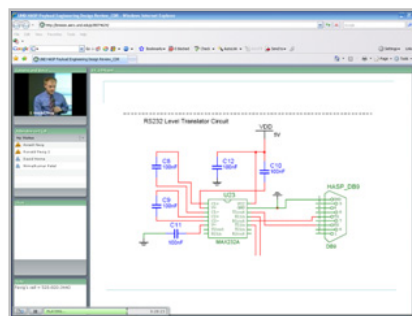
Figure 24. HASP Virtual Teams

To obtain the required open channels of communications, the UND team primarily used lateral and informal forms of communication; however, an administrative officer from the organizational level greatly helped to maintain communications. Maintaining communication also enveloped the main role of the PM. Of all the activities communication related or dependent activities represented nearly 80% of the PM's time. However, open lines of communication represent the lifeblood of an XPM project. The PM monitored these lines for feedback to help prevent turbulence. This meant monitoring the channels of communication, where the number of channels in a process includes:

$$m = \frac{n(n-1)}{2}$$

where   m   channels

               n   number of participants

In HASP, the number of lines varied depending on the phase; however, there were at a minimum 105 communication channels to monitor for the PM. This remained a top priority, as communication in any style of management is one of the top four elements to a project (Klastorin 2004). As Brooks (1995) notes, the importance of communication transcends modernity and cites that the construction of the Tower of Babel where construction immediately stopped as soon as different languages were introduced (Klastorin 2004). Having everyone on the same page proved essential and required a high degree of effective communication from and to the PM and functional mangers.

In addition, communication was especially important in student group. As with any student group, the exigency of external pressures (*e.g.* class) and the pressures from the project at times seemed overwhelming for some of the participants. To avoid escalation of

too much pressure, open communication about schedule stresses and concerns continually fed into the process to adapt and balance with the students' outside obligations. Communication was also important to the motivation of the students, especially that they knew that considerations for academic obligations remained a priority to the process.

Finally, communications also fulfilled one of the foundations to organizational learning (Senge 1990). As mentioned, the HASP project maintained a system through regular meetings where communication remained as opened as possible; meetings included active inquiry and feedback, clear mutual respect and support as described by Senge (1990). Given the foundations of the project, including the organizational structure, organizational plan, and schedule, it fell primarily to the PM, and faculty advisor, to manage successfully the project to completion and termination.

2.3.4 Management Conclusions and Insights

Through careful consideration of the current literature, the HASP project benefited from a sound organizational foundation and structure as the project developed. Although much of the project remained a learning process, it is clear that the project's conscious and unconscious use of XPM still required some of the basics of PM, while avoiding the fixation on these tools. The tools of the PM played important roles in helping maintain a complex project on a moving target; the agility of an XPM approach helped quickly maneuver the project to adapt and hit that target through a systems level approach. Further, the research and management process suggested that the "learning organization" is naturally congruent with the aspects of the XPM style, systems engineering, and the projectized structure.

The active engagement of the PM in the process helped to demonstrate a strong degree of commitment to the project. The use of communication technologies, such as Breeze remote conferencing software, PM tools, and engineering management efforts helped to increase effective communication. These tools helped to effectively monitor and regulate the HASP project. Ultimately, hindsight from the project's conclusion suggests a successful project manager (PM), in this type of student research effort, possesses both the technical expertise and leadership experience to balance needs and to step in when necessary. This ultimate leadership style manifested itself as effective communication. Effective communication of the changing needs and parameters of the project helped to define the goals and objectives of HASP, and helped to monitor the system while promoting and taking continual feedback to the process. The success of these efforts mainly involved promoting and maintaining learning, promoting STEM, and gathering science, all of which this HASP project managed to accomplish.

CHAPTER 3

PAYLOAD AND SENSOR DESIGN

3.1 Payload Design

The payload design process is a rigorous process where all payload developers from

had to meet the specifications laid out in the HASP technical summaries; further, each

payload had their own requirements defining their successful operation. For the UND and

UNF payload, examples of these requirements included successfully integrating with

HASP, taking real-time data samples from the ITO sensor and transmitting these data to the

ground, storing all data on board, and maintaining a sensor temperature of $24^{o}C \pm 15^{o}C$ at

any time during the flight profile. Largely the payload development constraints fell into

two categories: mechanical design, and electrical design.

3.1.1 Mechanical Design

The UND and UNF payload, with a mass of less than 2 kg (~4 lbs), only required

the smaller class of payload. This classification of payload also limited the design to

certain dimensions as well, which included 15 cm x 15 cm for the base and 30 cm for the

height. After taking into account the thickness of the chosen insulation, these dimensioning

requirements only left an inner volume of approximately 0.0055 m^3.

The designed support structure utilized an aerospace grade aluminum (*i.e.* Al 6061-

T6) alloy. The support structure included three center holes and a corner hole to attach the

mounting plate to via carriage screws with locknuts. Similarly, in the case of the corner

hole, a threaded rod ran the length of the payload and attached at the top lid via a locknut to ensure the lid maintained a snug fit. In addition, prior to flight, Kapton tape ensured a secure attachment to the lid. Inside the supports rested a 1" R12 polyurethane rectangular housing, reducing the expected heat transfer at extremes to -1.64 W. Figure 25 illustrates the primary structure in meters.
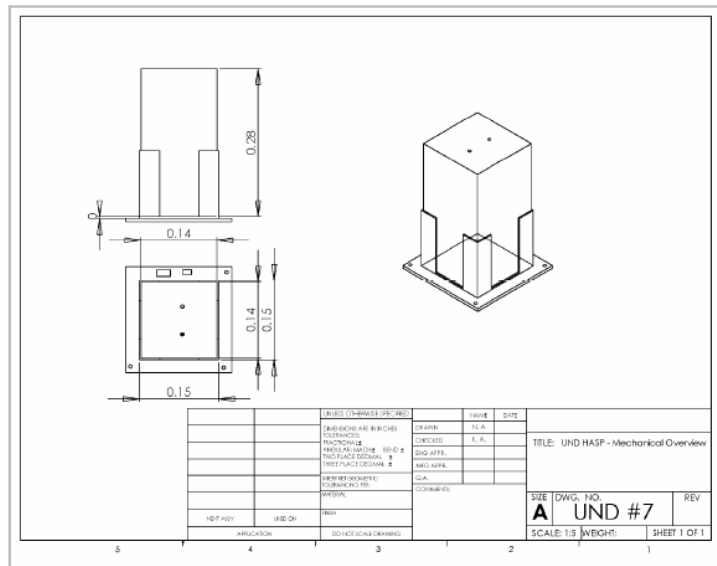
Figure 25. Primary Structure (m)

The design accounted for thermal considerations to ensure that the payload remained within ideal operating conditions under a near zero convection state. Under these conditions, thermal insulation and heat dissipation arises as a serious consideration. Metalized plastic sheets (MPS), space blankets, when layered over the R12 insulation helped to retain and reflect back up to 95% of the heat. The final payload structure includes Kapton (polyimide) thermally conductive tape to further support the top and side structure. Figure 26 shows the SolidWorks model of the integrated payload.
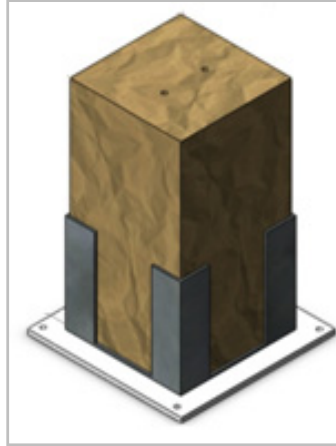
Figure 26. Payload Solid Model

The structure housed the sensor, shown on top, and the accompanying electronics, shown on bottom, via mounting screws, as in Figure 27. Additionally, Figure 28 shows the final integrated UND and UNF payload on the HASP gondola.
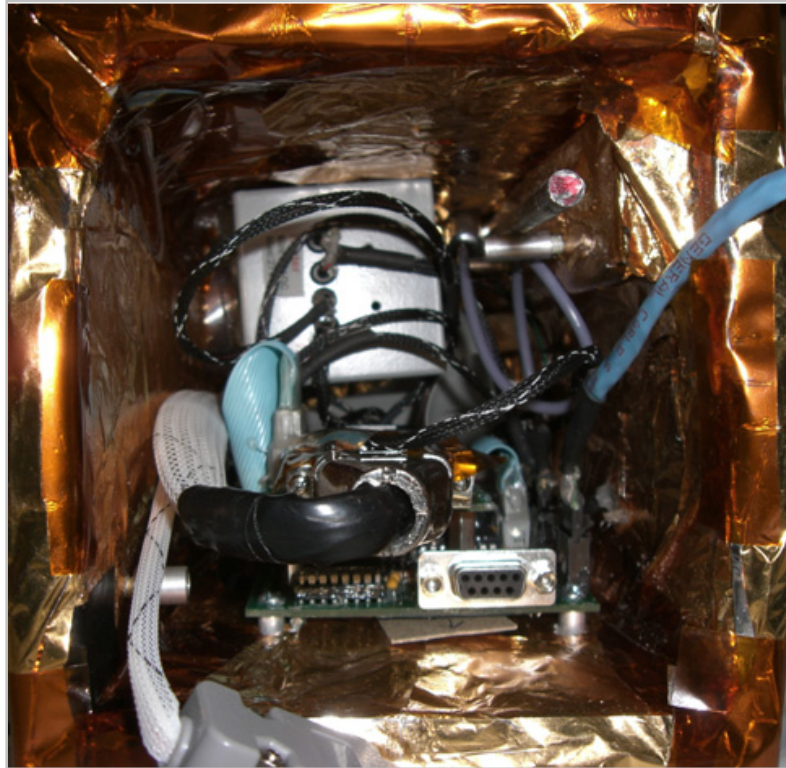
Figure 27. HASP Internals

Figure 28. Payload Integrated on HASP Gondola

The integrated payload structure had to support the completed sensor and electronics system while ensuring the mass budget remained within the requirements for integration and flight. Overall, the payload, including all subsystems, had a total mass of 1.79 kg during integration, only 40 g more than the estimated mass cited in the HASP proposal, and comprised several components as listed in Table 5.

Table 5. Mass Budget for Payload

	Item	Mass (grams)	Dimension (cm)
Sensor			
	Metal Case	111.80	12.7x5.6x5.6
	Circuit board	14.50	13.0x4.2
	24 sensors slide	4.60	7.5x2.5
	6 metal clips	8.40	
	Fan with wires	12.00	
	25 pin cable	36.00	
	Omega (KHLV-0504/10) heater with wire	1.60	1.2x9
	Omega (SA1-T) thermocouple	1.90	36" coil
	2x 9V Battery for heater	96.00	
	1x9V battery for Fan	48.00	
	Screws and nuts	10.00	
Structure			15x15x30
	Power supply	~190	
	Printed circuit board and cabling	~380	
	MPS	~40	
	Fasteners and tape	~300	
	Insulation and corner supports	~532	
		Total = 1,787	

3.1.1.1 Structure

Hang and spin tests during integration, confirmed the structure's design viable to withstand the required vertical 10 g force and horizontal 5 g force, as laid out in the technical requirements for HASP payloads. Structural stress modeling, seen in Figure 29, also confirmed that the main support structure would sustain the required load factors. Tungsten inert gas (TIG) welding connected the corner bracket segments to the base connector segment of the structure. In addition, welded to the midsection of the braces included a load distributive thick wire gauge element.
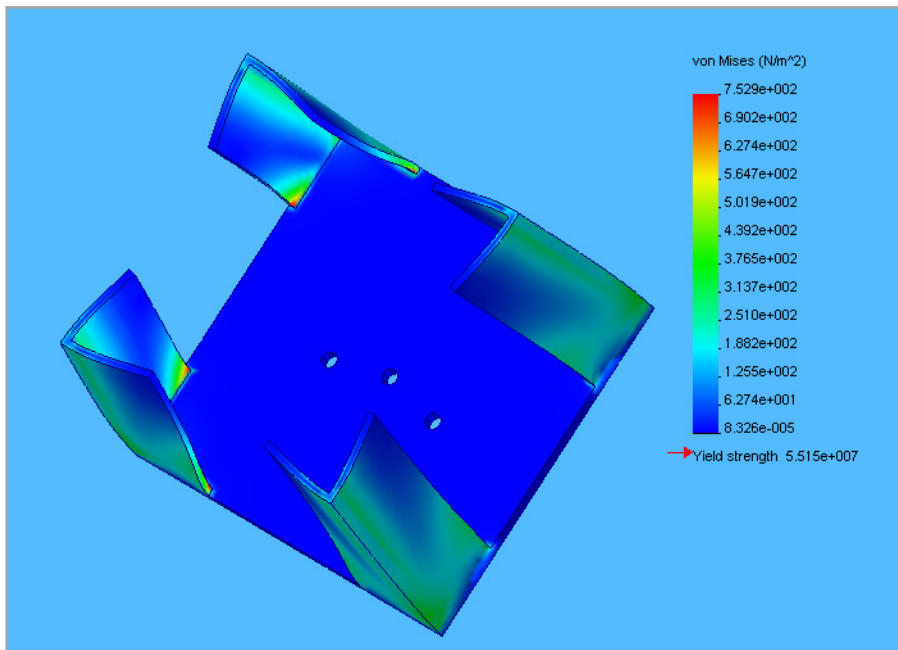
Figure 29. Structural Stress Model

3.1.1.2 Thermal

The thermal engineering goal for the payload concerned ensuring the successful operation of the onboard electronics and the successful operation of the sensor. In addition to the R12 insulation and MPS, the Omega flexible heater element (KHLV-0504/10)

mounted on the sensor helped to maintain the payload at the target temperature of ~24°C for the sensor. The thermal design underwent validation through BEMCO vacuum and thermal testing. During these thermal tests, payloads underwent thermal extremes (0°C ± 60°C) for sustained periods. The internal temperature maximum reached and maintained 58°C during this test. On the negative temperature, the internal temperature minimum reached ~11°C, whilst the heater remained turned off during this test. However, when the heater turned on the temperature quickly reached a temperature of just under 40°C when trying to maintain the targeted temperature range of 24°C to 40°C. These conditions all fell under the well-agreed standards for the sensors' optimal operation. At the coldest region, during the flight profile, the sensors' temperature profile remained within the operational range, and was consistent with thermal testing, as shown in Figure 30.
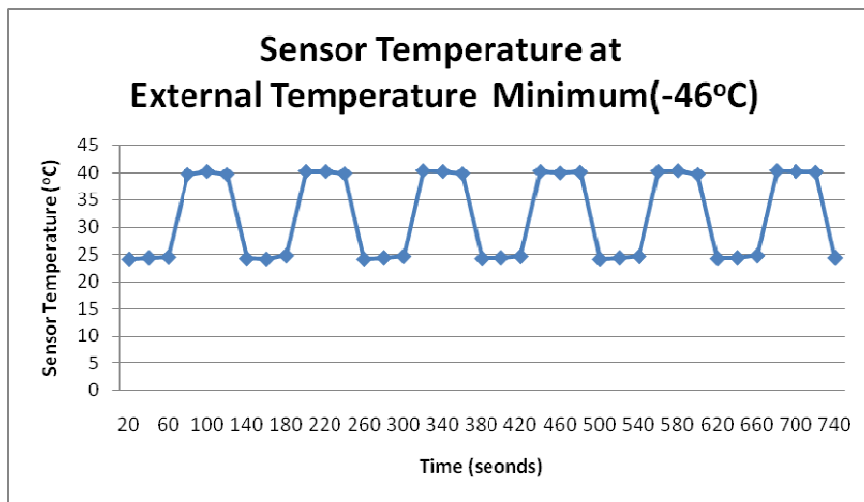
Figure 30. Sensor Temperature during Flight

The onboard heater used approximately 2.25 W of power when on. The heater element maintained the necessary temperature throughout the flight and exceeded the

theoretical minimum (1.64 W) according to a 1-D Fourier steady-state estimate from the following equation,

$$q_x = -k\,A\frac{dT}{dx}$$

where
    q_x heat transfer rate under steady-state, one-dimensional conditions

    k   thermal conductivity of wall $\approx$ 0.0046 W/m $\cdot$ ^{o}K

    A   conductive surface area $\approx$ 0.225 m^{2}

    dT   temperature differential $\approx$ 70 ^{o}K

    dx   cross sectional length $\approx$ 0.0254 m

3.1.2 Electrical Design

The UND developed electronic circuit board measured, stored, and transmitted the voltage signals from the ozone sensors as well as from the resistance temperature detectors (RTDs). A multiplexed Wheatstone bridge converted the resistances of each individual ozone sensor to voltages. Further, the circuit board controlled the heater to maintain the targeted internal temperature. A second board supplied the power for the main circuit board and contained a DC-to-DC converter with a linear regulator. The power supply took in 24-32VDC from the HASP platform and provided to the main circuit ±5VDC for the fan and +15VDC sensor heater.

3.1.2.1 Telemetry and Software

During the initial start up sequence, a solid LED indicated to the ground crew that the power was on and a blinking LED indicated that the payload was actively sampling data. A second LED faced the interior of the platform making it viewable from HASP's web camera, CosmoCam, which allowed a visual confirmation of nominal operation during

the night portion of the flight, independent of the payload's telemetry data. HASP ground controllers initialized the payload's operation through a programmed hex command (0x7878). During its normal operation, each of the 24 ozone sensors and environmental sensors sampled three times every minute. Onboard memory recorded this data and the circuit assembled the information into a data packet that transmitted the data back to the ground station. In the event of an anomaly, the payload resumed operation through a secondary hex command (0x7272) from HASP to the payload. In the case of a hard restart during the flight, the system's programming checks the onboard memory for errors and continues recording data after the last correct recorded value. Figure 31 shows an overview of these required software routines.

Figure 31. Payload Software Routines

The 256-byte packet construction sent every one minute adhered to the recommended construction of HASP as shown in Table 6.

Table 6. Payload Packet Format

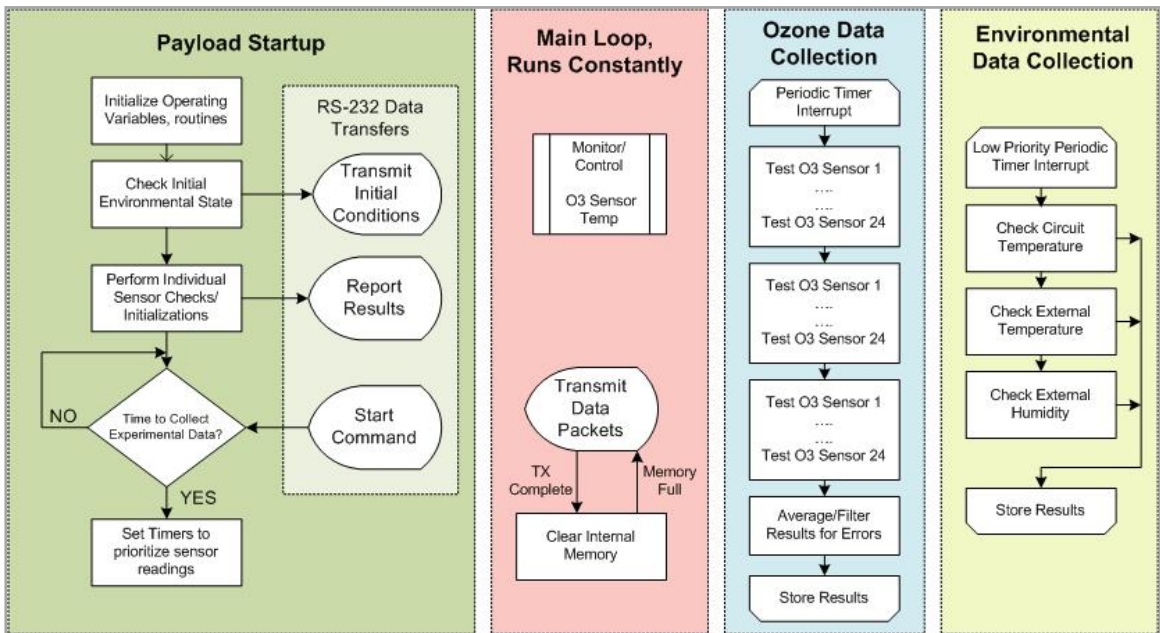| Packet Part	15	14	13	12	11	10	9	8	7	6	5	4	3	2	1	0
			Upper Byte								Lower Byte					
Start Bytes	1	1	1	1	1	1	1	1	0	0	0	0	0	0	0	0
Packet Number	PN15	PN14	PN13	PN12	PN11	PN10	PN9	PN8	PN7	PN6	PN5	PN4	PN3	PN2	PN1	PN0
Data CRC8/16																
Ozone 1 SN 1	SN5	SN4	SN3	SN2	SN1	SN0	V9_1	V8_1	V7_1	V6_1	V5_1	V4_1	V3_1	V2_1	V1_1	V0_1
	SN5	SN4	SN3	SN2	SN1	SN0	V9_2	V8_2	V7_2	V6_2	V5_2	V4_2	V3_2	V2_2	V1_2	V0_2
	SN5	SN4	SN3	SN2	SN1	SN0	V9_3	V8_3	V7_3	V6_3	V5_3	V4_3	V3_3	V2_3	V1_3	V0_3
Ozone 2 SN 2	SN5	SN4	SN3	SN2	SN1	SN0	V9_1	V8_1	V7_1	V6_1	V5_1	V4_1	V3_1	V2_1	V1_1	V0_1
	SN5	SN4	SN3	SN2	SN1	SN0	V9_2	V8_2	V7_2	V6_2	V5_2	V4_2	V3_2	V2_2	V1_2	V0_2
	SN5	SN4	SN3	SN2	SN1	SN0	V9_3	V8_3	V7_3	V6_3	V5_3	V4_3	V3_3	V2_3	V2_3	V0_3
Ozone 3 SN 3	SN5	SN4	SN3	SN2	SN1	SN0	V9_1	V8_1	V7_1	V6_1	V5_1	V4_1	V3_1	V2_1	V1_1	V0_1
	SN5	SN4	SN3	SN2	SN1	SN0	V9_2	V8_2	V7_2	V6_2	V5_2	V4_2	V3_2	V2_2	V1_2	V0_2
	SN5	SN4	SN3	SN2	SN1	SN0	V9_3	V8_3	V7_3	V6_3	V5_3	V4_3	V3_3	V2_3	V2_3	V0_3
Ozone 4 SN 4	SN5	SN4	SN3	SN2	SN1	SN0	V9_1	V8_1	V7_1	V6_1	V5_1	V4_1	V3_1	V2_1	V1_1	V0_1
	SN5	SN4	SN3	SN2	SN1	SN0	V9_2	V8_2	V7_2	V6_2	V5_2	V4_2	V3_2	V2_2	V1_2	V0_2
	SN5	SN4	SN3	SN2	SN1	SN0	V9_3	V8_3	V7_3	V6_3	V5_3	V4_3	V3_3	V2_3	V2_3	V0_3
….	SN5	SN4	SN3	SN2	SN1	SN0	V9_1	V8_1	V7_1	V6_1	V5_1	V4_1	V3_1	V2_1	V1_1	V0_1
	SN5	SN4	SN3	SN2	SN1	SN0	V9_2	V8_2	V7_2	V6_2	V5_2	V4_2	V3_2	V2_2	V1_2	V0_2
	SN5	SN4	SN3	SN2	SN1	SN0	V9_3	V8_3	V7_3	V6_3	V5_3	V4_3	V3_3	V2_3	V2_3	V0_3
Ozone 24 SN 24	SN5	SN4	SN3	SN2	SN1	SN0	V9_1	V8_1	V7_1	V6_1	V5_1	V4_1	V3_1	V2_1	V1_1	V0_1
	SN5	SN4	SN3	SN2	SN1	SN0	V9_2	V8_2	V7_2	V6_2	V5_2	V4_2	V3_2	V2_2	V1_2	V0_2
	SN5	SN4	SN3	SN2	SN1	SN0	V9_3	V8_3	V7_3	V6_3	V5_3	V4_3	V3_3	V2_3	V2_3	V0_3
R Test 1 SN 25	SN5	SN4	SN3	SN2	SN1	SN0	V9_1	V8_1	V7_1	V6_1	V5_1	V4_1	V3_1	V2_1	V1_1	V0_1
	SN5	SN4	SN3	SN2	SN1	SN0	V9_2	V8_2	V7_2	V6_2	V5_2	V4_2	V3_2	V2_2	V1_2	V0_2
	SN5	SN4	SN3	SN2	SN1	SN0	V9_3	V8_3	V7_3	V6_3	V5_3	V4_3	V3_3	V2_3	V2_3	V0_3
R Test 2 SN 26	SN5	SN4	SN3	SN2	SN1	SN0	V9_1	V8_1	V7_1	V6_1	V5_1	V4_1	V3_1	V2_1	V1_1	V0_1
	SN5	SN4	SN3	SN2	SN1	SN0	V9_2	V8_2	V7_2	V6_2	V5_2	V4_2	V3_2	V2_2	V1_2	V0_2
	SN5	SN4	SN3	SN2	SN1	SN0	V9_3	V8_3	V7_3	V6_3	V5_3	V4_3	V3_3	V2_3	V2_3	V0_3
External Temp SN 27	SN5	SN4	SN3	SN2	SN1	SN0	V9_1	V8_1	V7_1	V6_1	V5_1	V4_1	V3_1	V2_1	V1_1	V0_1
	SN5	SN4	SN3	SN2	SN1	SN0	V9_2	V8_2	V7_2	V6_2	V5_2	V4_2	V3_2	V2_2	V1_2	V0_2
	SN5	SN4	SN3	SN2	SN1	SN0	V9_3	V8_3	V7_3	V6_3	V5_3	V4_3	V3_3	V2_3	V2_3	V0_3
Internal Temp SN 28	SN15	SN4	SN3	SN2	SN1	SN0	V9_1	V8_1	V7_1	V6_1	V5_1	V4_1	V3_1	V2_1	V1_1	V0_1
	SN5	SN4	SN3	SN2	SN1	SN0	V9_2	V8_2	V7_2	V6_2	V5_2	V4_2	V3_2	V2_2	V1_2	V0_2
	SN5	SN4	SN3	SN2	SN1	SN0	V9_3	V8_3	V7_3	V6_3	V5_3	V4_3	V3_3	V2_3	V2_3	V0_3
Humidity SN 29	SN5	SN4	SN3	SN2	SN1	SN0	V9_1	V8_1	V7_1	V6_1	V5_1	V4_1	V3_1	V2_1	V1_1	V0_1
	SN5	SN4	SN3	SN2	SN1	SN0	V9_2	V8_2	V7_2	V6_2	V5_2	V4_2	V3_2	V2_2	V1_2	V0_2
	SN5	SN4	SN3	SN2	SN1	SN0	V9_3	V8_3	V7_3	V6_3	V5_3	V4_3	V3_3	V2_3	V2_3	V0_3
Buffer for Extra Data if needed, fan speed, heater condition … etc. (74 bytes total initialized to 0's)																
End Bytes	0	0	0	0	0	0	0	0	1	1	1	1	1	1	1	1

Color Key:

SNx	Sensor x Number Bit
Vx_1:	Sensor x Voltage Bit (1st Measurement)
Vx_2:	Sensor x Voltage Bit (2nd Measurement)
Vx_3:	Sensor x Voltage Bit (3rd Measurement)

Total Packet Length:
256 Bytes (Exact) without RS232 Start/Stop bits

Transmission Interval:
Roughly Every Minute

3.1.2.2 Circuit and Electronics Design

The overall electronics design for the payload followed a general systems flow diagram depicted in Figure 32. Figure 33, illustrates the overall UND designed circuit diagram, including the C programmable PIC18F4520 setup. Appendix C includes additional relevant engineering information (*e.g.* Wheatstone bridge theory for circuit).
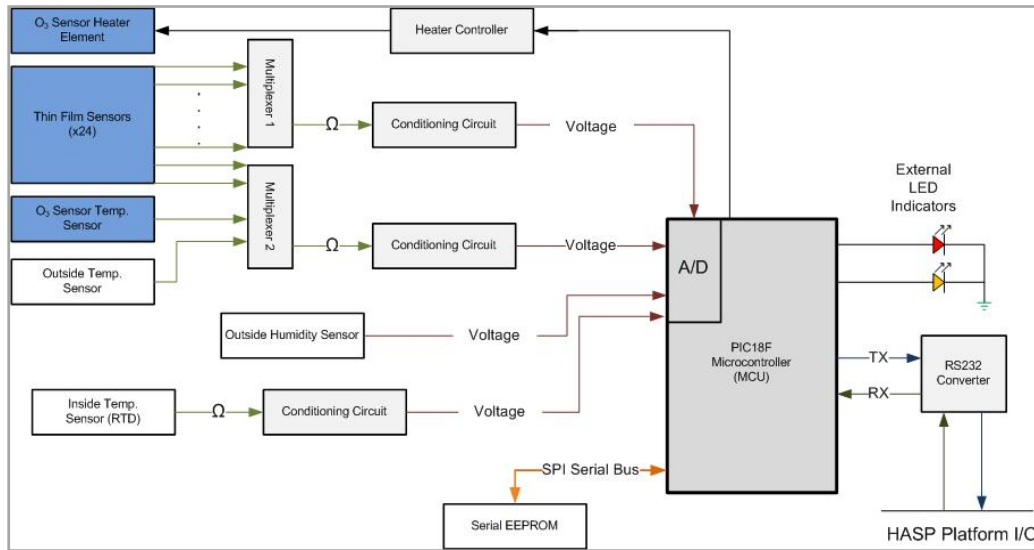
Figure 32. Payload Systems Diagram
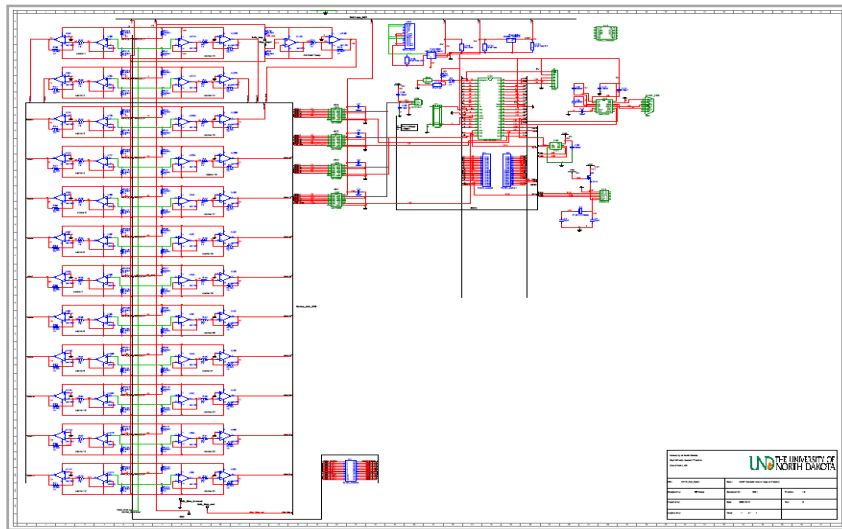
Figure 33. Overall Circuit Diagram

Similarly, Figure 34 shows the diagram for the power supply. Figure 35 highlights the solid models for these electrical designs prior to fabrication. After assembly of the circuit board and power supply unit, an application of conformal coating helped to protect the circuit board against moisture and extreme temperatures. Figure 36 shows the finished product of the power supply mounted on top of the main printed circuit board, with the conformal coating, that flew aboard HASP. All of these components supported the collection of the necessary data from the sensors, supported communication with HASP, and supported sending the correct telemetry to the ground.
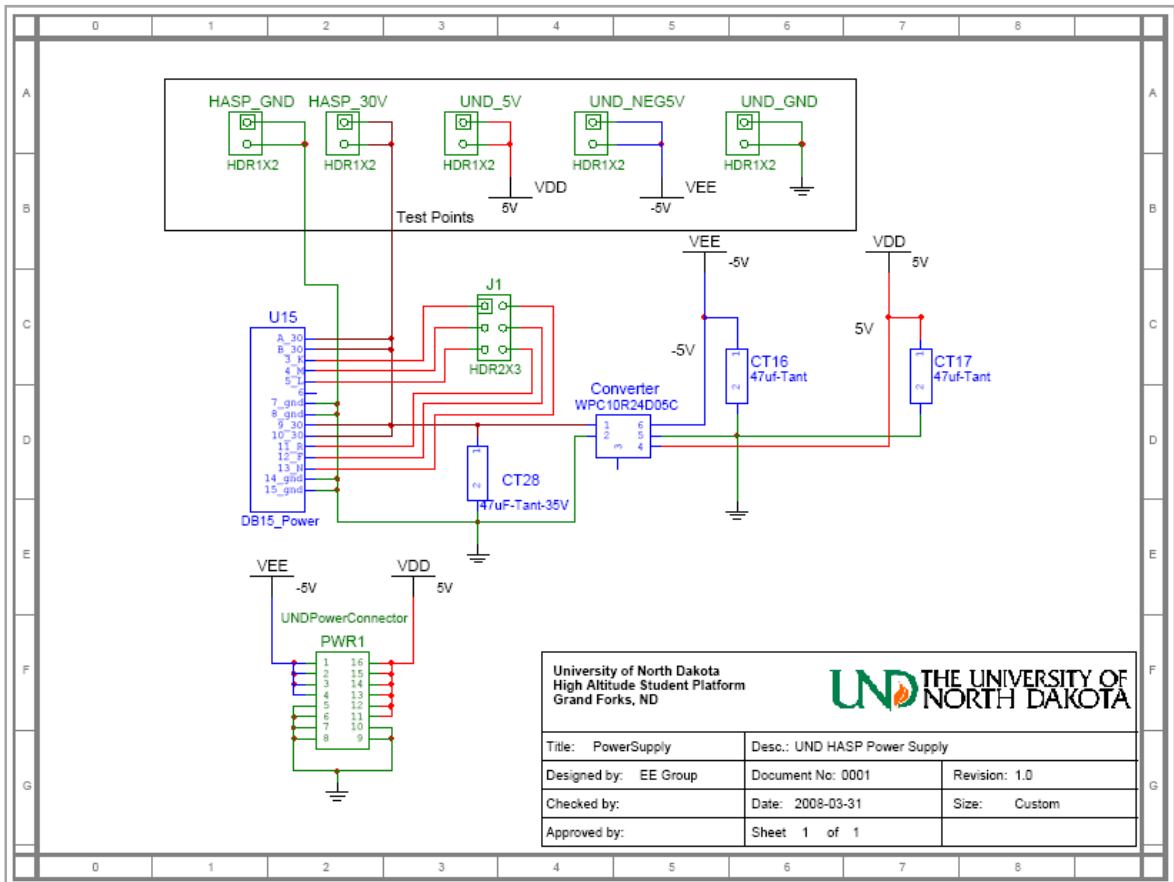
Figure 34. Overall Power Supply Diagram
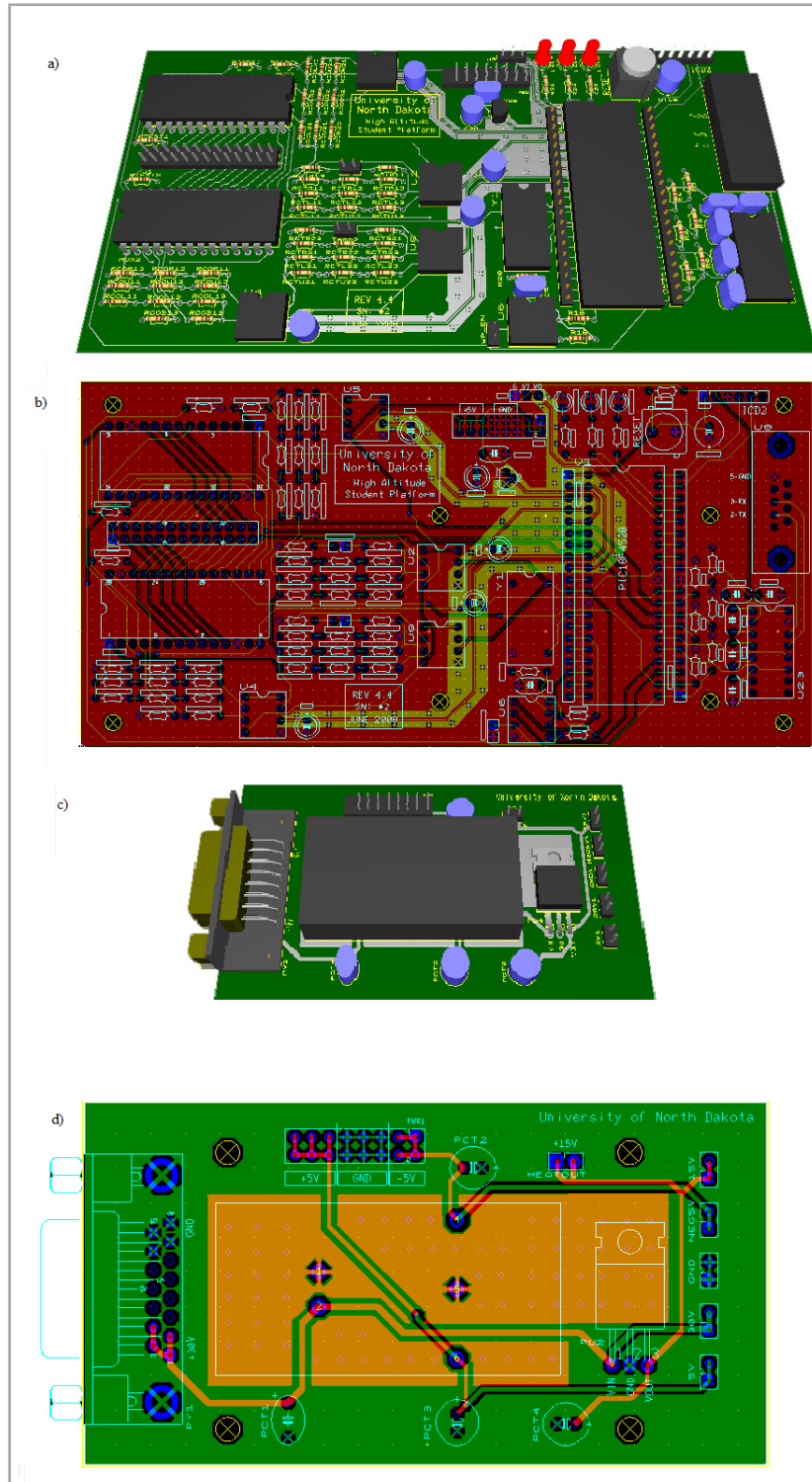
Figure 35. Solid Models of a) Main Circuit Board, b) Top of Main Circuit Board, c) Power Supply, d) Top of Power Supply

Figure 36. Conformal-Coated Circuit Board and Power Supply for Flight

3.2 Sensor Operating Principle

The detection of bio-spherical ozone and other gasses remains extremely important due to their physiological relevance (Ambler and Patel 2008). Because typical concentrations of ozone remain very low, gas sensors need high sensitivity together with good selectivity in order to avoid any cross interference with other gases. Gas sensors in the form of thin films appear more promising over the pellet form or thick film form because they are low in cost and rugged. Gas sensors using oxide semiconductors remain the subject of extensive investigation after more than four decades; primarily the focus rests on tin oxide semiconductors for the HASP technology demonstration. Indium tin oxide (ITO) thin film currently in widespread use serves as a transparent conductive electrode for

several optoelectronic devices and for less studied gas sensing applications. Thin film ITO gas sensors underwent development at UNF as reported earlier (Patel et al. 2003, 2005-7).

Gas sensors based on ITO utilize selective chemical sensitivities of their surface to different adsorbed gases. This causes changes to the electrical resistance of the sensor. Appropriate doping in ITO provides electronic defects that increase the influence of oxygen partial pressure on electrical conductivity. Because oxygen vacancies on metal-oxide surfaces exist as electrically and chemically active, these vacancies function largely as n-type donors decreasing the electrical resistivity of the ITO element. Reducing gases such as CO, H_2, and alcohol vapors result in detectable decreases in the electrical resistance of n-type ITO semiconductors by way of producing oxygen vacancies and conduction of electrons at higher temperatures. At high temperatures, vacancies in the oxide lattice at the gas-sensor interface occur when thermal pressure ejects the oxygen atoms from the lattice. Similarly, upon adsorption of charge accepting molecules at the vacancy sites, namely from oxidizing gases such as ozone (O_3) and NO_2, these electrons effectively deplete themselves from the conduction band of the semiconductor. This leads to an increase in the electrical resistance of n-type ITO.

3.2.1 Sensor Fabrication

Fabrication of gas sensors and sensors arrays utilized thermal evaporation methods. The thermal evaporation method employed a high vacuum system consisting of a metal box chamber. Cleaned glass microscope slides and alumina served as the substrates for deposition by the different ITO thin film sensors. Indium tin oxide (ITO) bulk powder from Alfa Aesar acted as the source material. The thicknesses of the films varied from approximately 800 to 3000 Å, while the substrate temperature varied from 200 to 300°C.

54

Further, gold thin film, deposited on both sides of the ITO thin film, established the necessary ohmic electrical contacts.

Each array consisted of 24 sensors fabricated on one glass slide. In one processing of the deposition, 96 sensors on four glass slides simultaneously underwent fabrication under the same general fabrication conditions. Each sensor on the array has an active surface area of about 25mm x 25mm. During operation, each sensor can work individually or as part of an array, and all 24 sensors generate electrical signals simultaneously which then depended on the developed UND electrical circuitry and HASP support.

Of the arrays, a chosen glass slide substrate interfaced with a specially designed printed circuit board. This array mounted inside a small metal box with a small fan on one side in order to blow uniformly the air molecules over all 24 sensors during operation. The mounted sensor included a flexible Kapton heater (Omega) and RTD on the backside of the glass slide in order to maintain a constant temperature across the array at approximately $24^{o}C$ during flight. It is important to note that the power consumption of the element remained minimal, as these sensors do not require the high operating temperature, such as the $530^{o}C$ reported with the tungsten oxide sensors (Hansford et al. 2004).

3.2.2 Sensor Properties

Examination of the surface morphology of the ITO thin film used a FEI Quanta 200 Environmental Scanning Electron Microscope (ESEM) at the University of North Florida under Dr. Nirmalkumar Patel from the Department of Chemistry and Physics. Confirmation of the chemical composition used an Energy Dispersive Analysis of X-rays (EDAX) at the same aforementioned workstation.

Electron micrographs demonstrated these reported morphologies and layups. Figure 37 displays the gold electrodes that make ohmic contacts for the ITO thin film sensors. This electron micrograph represents a typical ITO thin film sensor with gold electrodes. The next micrograph in Figure 38 shows the scanning electron micrograph surface of the ITO thin film. This micrograph revealed and confirmed that the ITO thin film contains nanocrystalline grain sizes, with an average ITO grain size of 45 ± 12 nm. Figure 39 further supports this grain size finding as it confirms this nanocrystalline structure in a 500 nm resolution image and depicts the nanotubules of the ITO sensor. This crystalline structure is crucial to the sensor's selectivity as decreased grain size directly relates to an increased surface area.
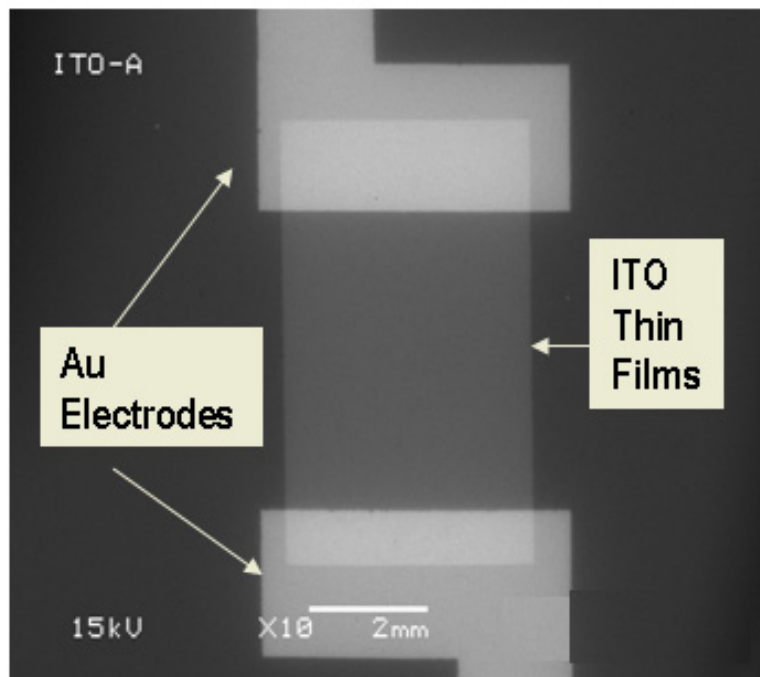
Figure 37. Typical ITO Sensor with Gold Electrodes
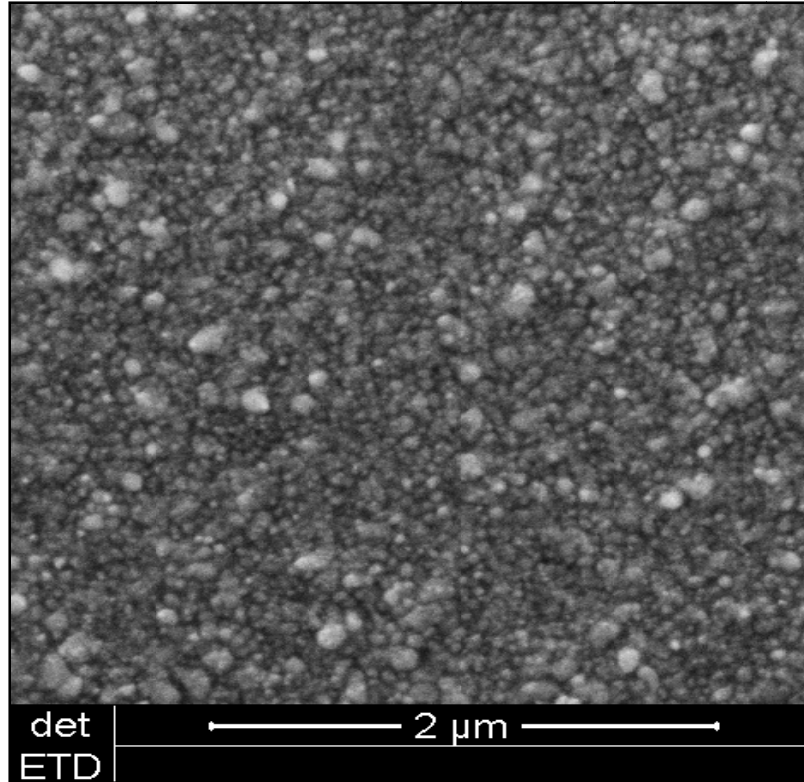
Figure 38. ITO Surface Nanocrystalline Morphology
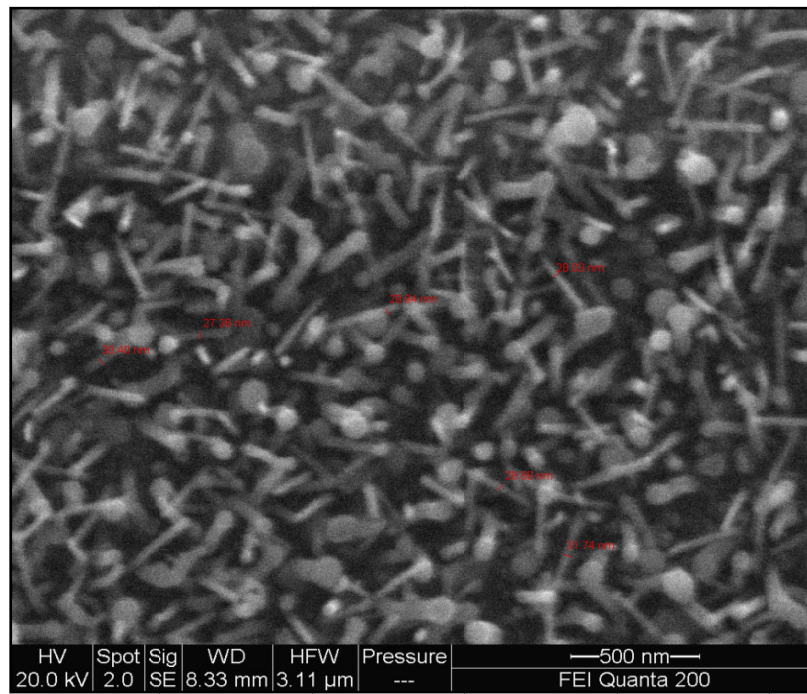
Figure 39. ITO Nanotubules

The characteristic reason for nanocrystalline ITO thin film sensors sensitivity to oxidizing ozone gas is due to this large surface area to volume ratio and the large number of unsatisfied bonds in the nanocrystals this represents. The bixbyite-type cubic lattice structure of indium oxide governs its atomic behavior which is noted with additional sensor details and operating principles in appendix D. Adsorption of the electron acceptor gaseous species leads to band bending and formation of a surface depletion layer due to the capture of the free charge carrier at the surface. All available conduction electrons remain trapped in the surface states of nanocrystalline ITO, which enhances the sensor response. The overall mathematical representation of this is adapted from Hansford *et al.* (2005),

$$O_o \rightarrow V + \tfrac{1}{2}\,O_2$$

$$V + O_2 \rightarrow O_o + \tfrac{1}{2}\,O_2$$

$$O_o \rightarrow V + \tfrac{1}{2}\,O_2$$
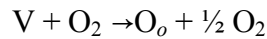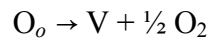
where $\quad O_o \quad$ represents the a lattice oxygen site

$\qquad\quad V \quad$ represents an oxygen vacancy

This mathematical representation represents the physical phenomenon stemming from thermal pressure that ejects oxygen atoms discussed in the sensor operating principle introduction. This thermal pressure creates vacancies, which appear in the oxide lattice. These vacancies require oxygen or ozone to fill; however, ozone reacts at a much faster rate and, as a result, allows ozone a minimum detectability level of part-per-billion volume (Hansford *et al.* 2005).

The overall research supports the conclusion that the gas sensing effect in metal oxides is complex and depends on an intricate relationship between the various metal oxide parameters such as grain size, porosity, agglomeration, bulk conductivity, surface stoichiometry, catalytic reactivity, band gap, electronic band structure, and many more. The sensor behavior also clearly depended on several sensor parameters stemming from its deposition process and treatments (Korotcenkov 2008). Research from Korotcenkov (2008) suggests that the addition of one-dimensional metal oxides improves thermal stability, and the use of transition metals modifies the catalytic reactivity and surface morphologies of the thin film. The conditions of the ITO metal oxide thin film for the sensing of ozone took all of these considerations into account to create the necessary properties. The final deposition resulted in 24 ITO sensors arrays overlaying a unique printed circuit board that allows the measurement of the resistance from the gold leads as seen in Figure 40.
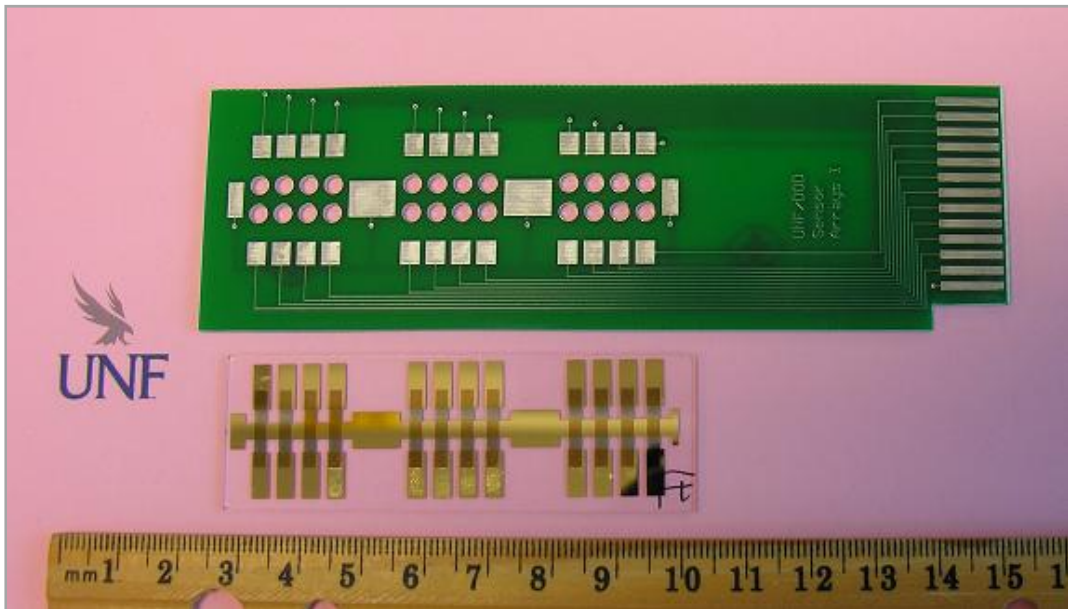
Figure 40. Solid-State ITO Gas Sensor Array (courtesy of Patel 2008)

CHAPTER 4

DISCUSSION AND RESULTS

4.1 Calibration and Lab Data

The first step in supplementing and even replacing current ozone sensor techniques requires accurate calibration and testing of new designs. Calibration of the UNF ITO gas sensors occurred under different concentrations of ozone (0 ppm to 14 ppm) and under different total pressures. Testing of the solid-state ITO sensors required a reduced pressure and temperature setting to mimic a near space environment. Testing occurred at the Low Pressure Test Bed at NASA's Kennedy Space Center (KSC) Space Life Science Laboratory facility, the University of North Dakota (UND), NASA's Columbia Scientific Balloon Facility (CSBF), and in the upper atmosphere aboard NASA's High Altitude Student Platform during flight. All calibration and in flight conditions remained thermally regulated to maintain the sensor at roughly 24°C.

4.1.1 Calibration Methods and Setup

As noted, the calibration of these sensors occurred under varying ozone concentration, pressures, and ambient temperatures at several facilities. Each calibration method, setup, and procedure slightly varied depending on the facility. In general, these procedures involved taking a known production rate of ozone, known flow rates, comparison to a calibrated sensor, and known volumes to interpolate and verify the partial pressure of ozone. These partial pressures then underwent comparison to the resistance

measurements from the sensors. Each setup also involved testing for pressure and thermal effects.

4.1.1.1 KSC Calibration

This procedure required the use of the Low Pressure Test Bed Facility (LPTBF) at the Space Life Sciences Laboratory (SLSL), KSC. Figure 41 shows the LPTBF at the SLSL. This operation required the support of Raymond Wheeler, NASA Biological Science Office, additional NASA personal, and the consultation of Dr. Phillip Fowler and Joe Benjamin who oversaw the calibration setup, procedures, and operations in coordination with the Space Florida research team. In this setup, a PRO 3,400 V5 ozone generator, using pure oxygen, produced ozone at known percentage and flow rate out of the generator (3.6 g/hr). After leaving the generator, the flow then mixed with an inerting gas, Nitrogen, at a known flow rate to prevent fire risks. These combined flows then fed into a bell jar with a known volume within the LPTBF.

Figure 41. LPTBF at KSC for Calibration

In brief, the setup and theory can be represented by the developed equations and is summarized as follows,

$$C^* = \frac{Q_{O2}\rho_{O3}\alpha}{Q_{O2}\rho_{O2} + Q_{N2}\rho_{N2}} + \delta_\gamma$$

$$\frac{P_1 V_1}{T_1} = \frac{P_2 V_2}{T_2}$$

$$\frac{P_1 Q_1}{T_1} t = \frac{P_2 Q_2}{T_2} t \qquad \therefore \frac{P_1 Q_1}{T_1} = \frac{P_2 Q_2}{T_2}$$

where C^* is the relative concentration in the bell jar and is unitless

Q volumetric flow rate, $\frac{m^3}{s}$

ρ density (*e.g.* $\rho_{o3} = 2.14$ kg/m³, $\rho_{o2} = 1.43$ kg/m³, $\rho_{N2} = 1.25$ kg/m³)

α efficiency of ozone generation (part of O_3 per O_2) ≈ 0.00833

δ_γ reaction differential of ozone with inerting gas ≈ 15 ppbv

P pressure, kPa

V volume, m³

T temperature, $^\circ$K

t time, s

These overall relationships allowed for calculation of the concentration, C^*, inside the bell jar within the LPTBF, when multiplied by a million gives ppm. In this setup, the mass of the ozone was dependent on the amount of oxygen passing through the ozone generator, where approximately 0.83%, according to manufacturer's specifications, of the oxygen disassociated into ozone. This mixture required the addition of an inerting gas, N_2, to prevent a safety hazard. In addition, the ideal gas law derivation helped to estimate

effects to concentration from reduced pressures. Additional theoretical characteristic signal response equations for the sensor used in calibration is included in appendix C.

4.1.1.2 UND Calibration

The procedure at UND involved using two calibrated sources: an OMC-1108 ozone sensor, from Ozone Solutions, and the OMZ-3400 ozone generator, from Ozone Solutions, with a known ozone output of 3.4 g/hr from air at atmospheric pressure. The OMC-1108 was calibrated with an Advanced Pollution Instruments 401X O_3 Photometric Calibrator – serial number 331. The analyzer remains actively certified under NIST standards and is actively calibrated according to API specifications. The certificate of calibration is included with additional technical and engineering details in appendix C.

Initial testing utilized the calibrated OMC-1108 to give real time readings of internal ozone partial pressure in parts per million (ppm) generated with the ozone generator, OMZ-3400. The OMZ-3400 sat internally in the 0.1058 m^3 chamber, generating a known amount of ozone from the chamber air, and the calibrated OMC-1108 sensor further validated theoretical outputs. Some differences between the theoretical and the OMC-1108 ozone meter resulted from the high reactivity and small size of ozone, making it hard to contain fully within the chamber or maintain steady-state operations.

The chamber, shown in Figure 42, used a vacuum pump to reduce the pressure of the chamber. A Baratron pressure manometer read pressures from within the chamber. Electrical power and cable connectors were also supplied and sealed in the chamber from the outside. On the outside of the chamber, several Flutes measured the resistances of the individual sensors. Hand measurements and a data logger, using the UND designed circuit, recorded resistance measurements.

After completing these basic measurements, the chamber setup changed to allow it to empty into a smaller airtight container with a pressure gauge. This allowed, with the ideal gas law, allowed for the calculation of concentration of ozone in the secondary container, verified with the OMC-1108. This chamber, shown in Figure 43, acted as a quick injection system to allow for the measurement of response rates. The secondary chamber was allowed to empty to various concentrations to record the negative response of the sensor as well.
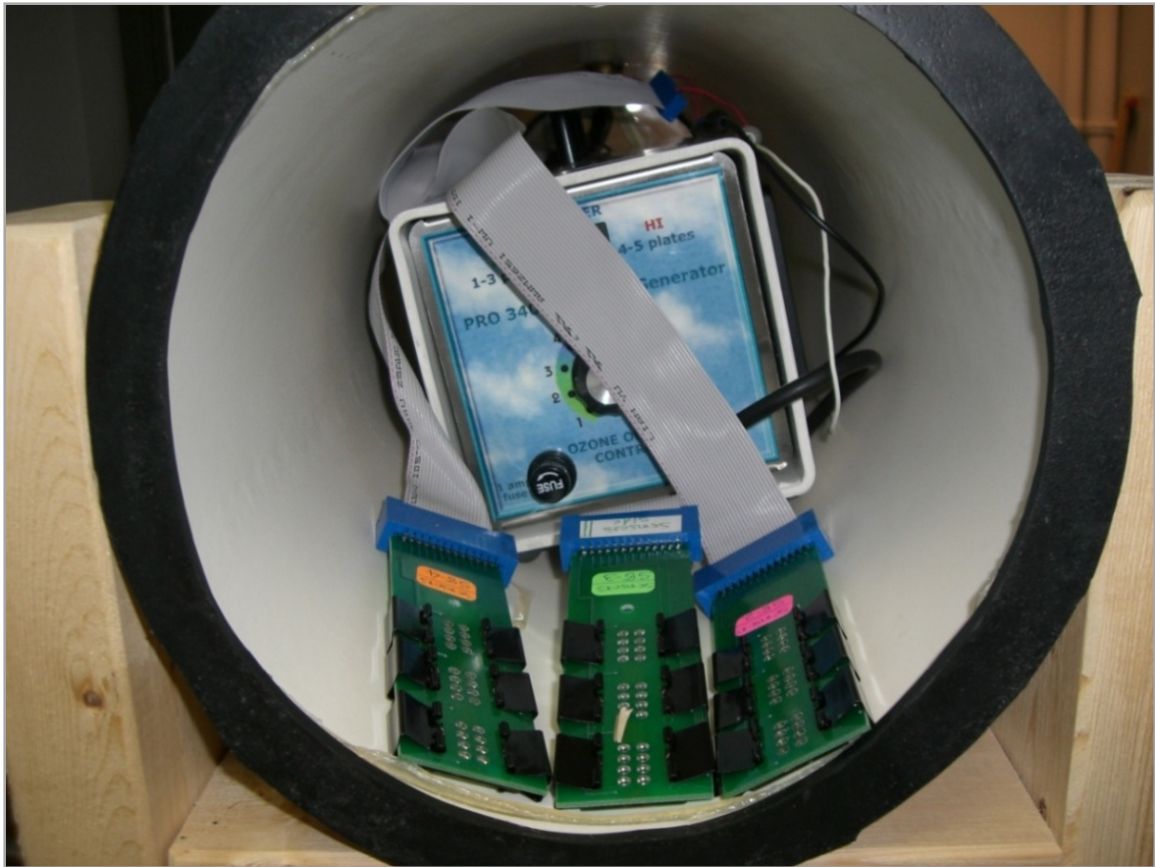
Figure 42. UND Calibration
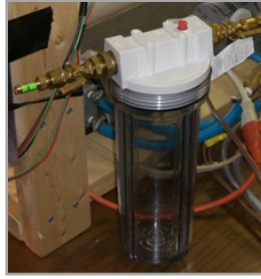
Figure 43. UND Injection System

4.1.1.3 CSBF Calibration

After these calibrations, the integrated payload withstood a series of tests at the
NASA-CSBF, Palestine, TX facility. Testing included a BEMCO thermal and vacuum
space simulation test shown in Figure 44. During this test, the payload experienced
recorded temperatures ranging from $56^{o}C$ to $-45^{o}C$ and pressures from atmospheric
pressure down to 1mBar of pressure. These variations allowed for the quantification of
pressure and temperature effects on the sensor necessary to perform data corrections and
data reduction later. There was a clear indication of changes in voltage readings with the
changes detected in pressure and temperature. These tests fulfilled the requirements
necessary for the certification of flight readiness that is included appendix A.
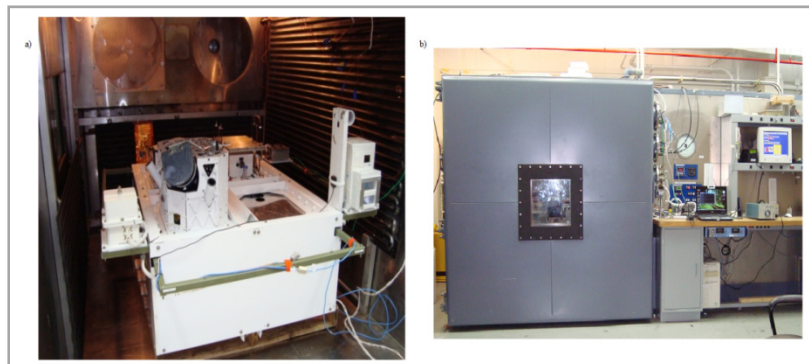
Figure 44. BEMCO Environmental Thermal/Pressure Chambers and Space Simulations
Systems a) inside with HASP Gondola and Payloads, b) outside of BEMCO when
Operating

4.1.2 Calibration and Lab Results

Of the multiple sensor types tested, each underwent testing at pressures near standard pressure, partial vacuum, and near vacuum. These calibrations helped in the selection of the best-suited sensor for this application. At both KSC and UND there was a clear linear relationship at low concentration among all of the sensors; however, this linear relationship changes characteristic slopes at certain mid-concentrations. Figure 45 shows the clear linear relationship for low concentrations of ozone from the KSC ITO sensors. These relationships established from the KSC stem from the averaged data seen in Table 7.

Table 7. KSC Calibration of ITO Gas Sensors on Glass Slide and on Ceramic a) for Pressure at 3 kPa, b) for Pressure at 10 kPa

a)	Ozone Gas ppm	Sensor's Resistance Glass Ohms	Sensor's Resistance Ceramic KOhms	Pressure KPa	b)	Ozone Gas ppm	Sensor's Resistance Glass Ohms	Sensor's Resistance Ceramic KOhms	Pressure KPa
	12.457	234	2.3098	3		1.548	231.1	2.33	10
	9.365	232.62	2.278	3		2.517	232.09	2.34558	10
	7.297	231.6	2.269	3		3.995	233.039	2.358	10
	3.995	230.09	2.263	3		7.297	234.023	2.37	10
	2.5169	229.7	2.251	3		9.365	234.5	2.377	10
	1.548	228.9	2.24	3					

The overall relationship in much of the calibration at normal pressure remained clearly linear only in three different and distinct regions of concentrations low, medium, and high. KSC first demonstrated this and UND testing confirmed this as shown in Figure 46 and in the data table established in Table 8.
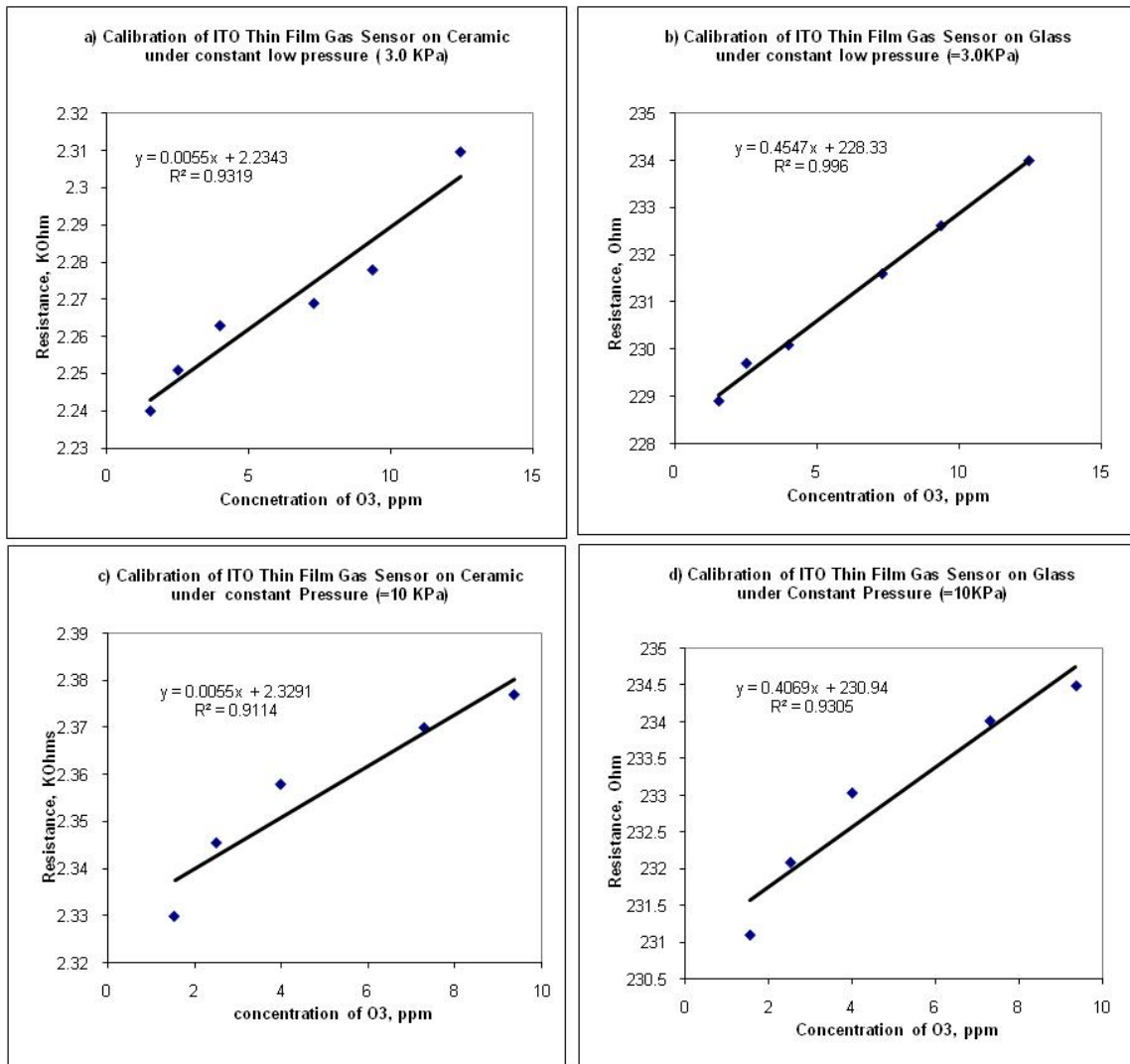
Figure 45. KSC Calibration of ITO Thin Film Gas Sensors a) on Ceramic at 3 KPa, b) on Glass at 3 KPa, c) on Ceramic at 10 KPa, d) on Glass at 10 KPa

These tests helped also gain some insight into the type of sensor that best suited HASP. The glass slide demonstrated the better overall relationship and power requirement after the course of several tests. Although, the deposition parameters slightly varied from KSC, the ceramic deposition sensor developed into the S8-2 sensor tested at UND, and the glass deposition sensor developed into the S8-3 and S8-4 type tested at UND.

67

Table 8. Summary of UND Calibration of ITO Gas Sensors under Various Pressures

Test#	Concentration	Pressure	Sensor Type	Equation	R^2
1	0 to ~4 ppm	1 atm	S8-2A	y = 3.3449x + 5.9673 * kOhm	$R^2 = 0.9798$
2	0 to ~4 ppm	1 atm	S8-3B	y = 27.084x + 260.17	$R^2 = 0.9203$
3	0 to ~4 ppm	1 atm	S8-4A	y = 70.131x + 547.07	$R^2 = 0.8571$
4	0 to ~4 ppm	0.5 atm	S8-2A	y = 849.7x - 477.83 *kOhms	$R^2 = 0.7638$
5	0 to ~4 ppm	0.5 atm	S8-3B	y = 76.796x + 201.41	$R^2 = 0.9936$
6	0 to ~4 ppm	0.5 atm	S8-4A	y = 109.55x + 490.08	$R^2 = 0.9424$
7	**0 to ~10 ppm**	**1 atm**	**S8-2A**	**y = 44584x - 121645**	**$R^2 = 0.7777$**
7b	*0 to ~4 ppm*	*1 atm*	*S8-2A*	*y = 2202.3x + 1203.1*	*$R^2 = 0.5065$*
7c	*~4 ppm to ~10 ppm*	*1 atm*	*S8-2A*	*y = 96686x - 467536*	*$R^2 = 0.8745$*
8	**0 to ~ 10 ppm**	**1 atm**	**S8-3B**	**y = 872.96x - 2069.8**	**$R^2 = 0.947$**
8b	*0 to ~4ppm*	*1 atm*	*S8-3B*	*y = 32.732x + 266.64*	*$R^2 = 0.9703$*
8c	*~4ppm to ~10ppm*	*1 atm*	*S8-3B*	*y = 1031.8x - 3267.7*	*$R^2 = 0.9815$*
9	**0 to ~10ppm**	**1 atm**	**S8-4**	**y = 12891x - 31335**	**$R^2 = 0.9277$**
9a	*0 to ~3ppm*	*1 atm*	S8-4	y = 237.11x + 542.18	$R^2 = 0.9808$
9b	*~3ppm to ~10ppm*	*1 atm*	S8-4	y = 14170x - 40931	$R^2 = 0.9382$
10	0 to ~2 ppm	0.4 atm	S8-3C	y = 1392.4x + 1988.8	$R^2 = 0.9473$
11	0 to ~4 ppm	0.7 atm	S8-3C	y = 612.65x - 40.262	$R^2 = 0.9352$
12	0 to ~4 ppm	1 atm	S8-3C	y = 297.53x + 1706.2	$R^2 = 0.8661$

Figure 46 demonstrates sample relationships found during UND tests. These results largely follow a typical linear calibration equation of $y = \alpha \cdot x + \beta$. As denoted in Table 8 and Figure 46, and as expected, the slope, α or $(\frac{\partial R}{\partial C^*})$, of these relationships increases for reducing pressures largely as there are less reducing gasses. These calibration

equations also follow from convective dominated diffusion models (>~10 to 25 kPa) compared to the molecular diffusion models, seen in appendix C.
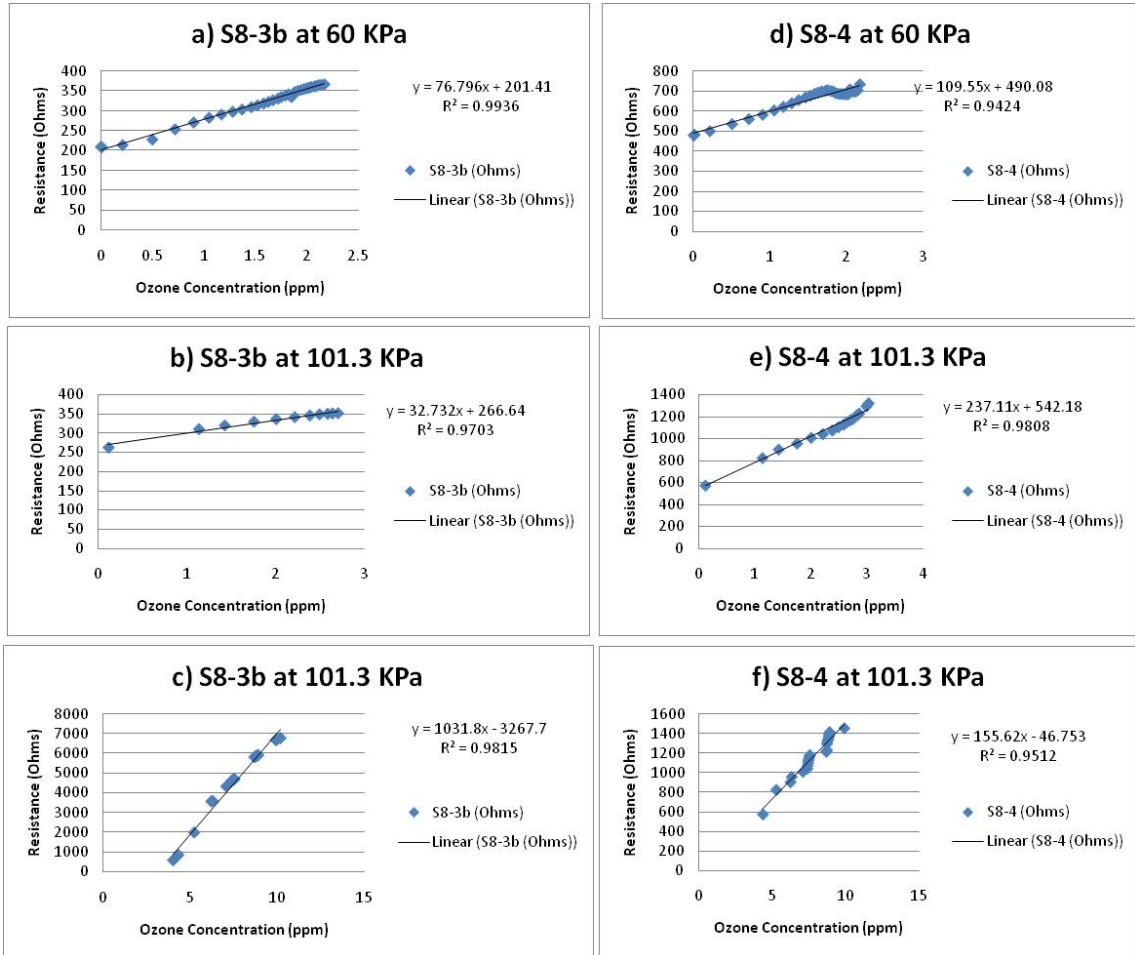
Figure 46. UND Calibration of ITO Thin Film Gas Sensors a) S8-3b under 60 KPa of Pressure with Low Ozone Concentration, b) S8-3b under 101.3 KPa of Pressure with Low Ozone Concentration, c) S8-3b under 101.3 KPa of Pressure with Intermediate Ozone Concentration, d) S8-4 under 60 KPa of Pressure with Low Ozone Concentration, e) S8-4 under 101.3 KPa of Pressure with Low Ozone Concentration, f) S8-4 under 101.3 KPa of Pressure with Intermediate Ozone Concentration

The overall calibration profile curve demonstrates the discussed typical sensor response behavior. An example from the S8-3b, the same design as the sensor flown, shows such an overall sensor profile in Figure 47.
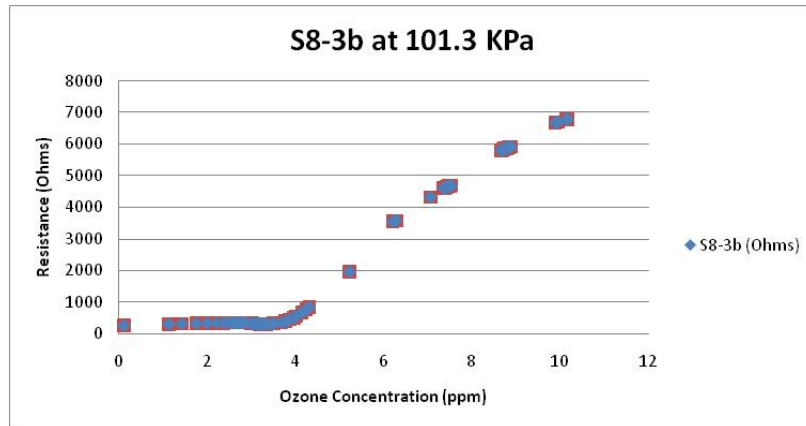
Figure 47. UND Calibration of S8-3b ITO Thin Film Gas Sensors at 101.3 KPa of Pressure

The overall sensor response rate demonstrates that the sensors respond quickly; however, the sensors took longer to disassociate. Figure 48 shows this overall response rate profile for the ITO S8-3c sensors. The various numbers on the graph, printed with each cycle, represents the concentration of ozone in ppm.
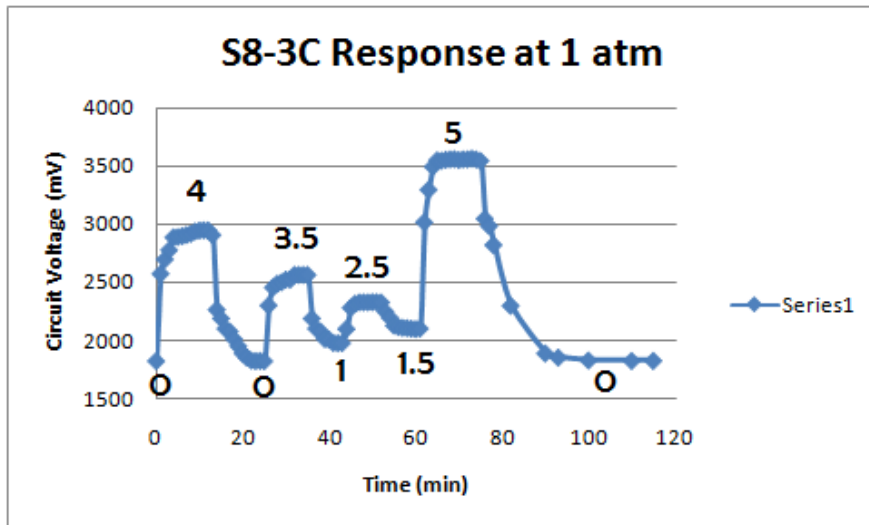
Figure 48. UND Response Rate of S8-3b ITO Thin Film Gas Sensors at 101.3 KPa of Pressure

4.2 Flight Data

The flight forecast data for the day of launch indicated surface winds of S-SE at 4-6 knots, low level winds S-SE at 11-13 knots, and high-level altitude (7 mbar to 5 mbar) winds resulting from Hurricane Ike. The resulting forecast track for the flight in Figure 49 predicted that winds would carry HASP north and then higher altitude winds would carry it west, then south, and finally east. Overall, the projected trajectory estimated an impact at 62 nm SE of Clines Corner, New Mexico.
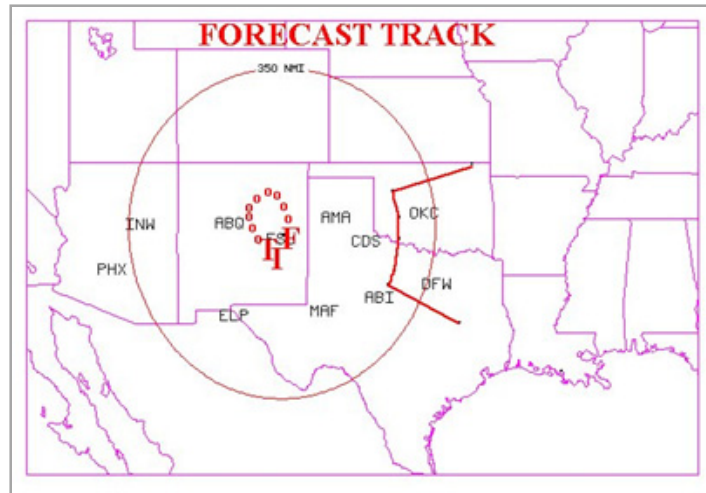
Figure 49. HASP 2008 Forecasted Flight Path from CSBF

HASP was launched on September 15, 2008 at 13:33:44 UTC from Ft. Sumner, New Mexico with operational support provided from CSBF. This flight achieved record durations for the program with 31.8 hours of flight, and approximately 30 hours of flight at float. The platform maintained an average altitude at float of 36.6 km and a peak altitude of ~38.6 km. Figure 50 summarizes the HASP 2008 flight profile. The flight path, shown in Figure 51, varied by approximately 200 miles from the forecast path due to this longer than expected flight duration and intermediate winds.
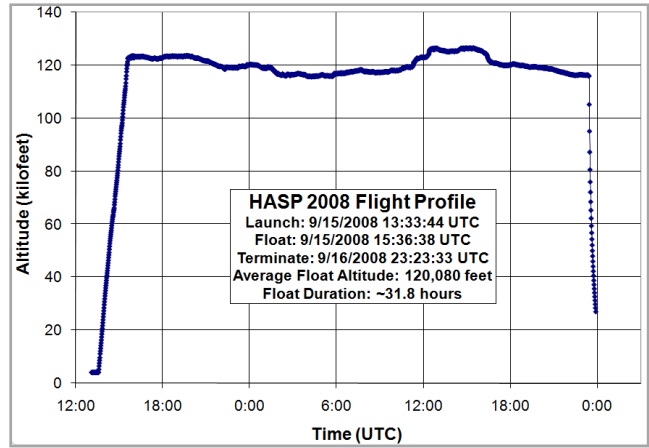
Figure 50. HASP 2008 Flight Profile
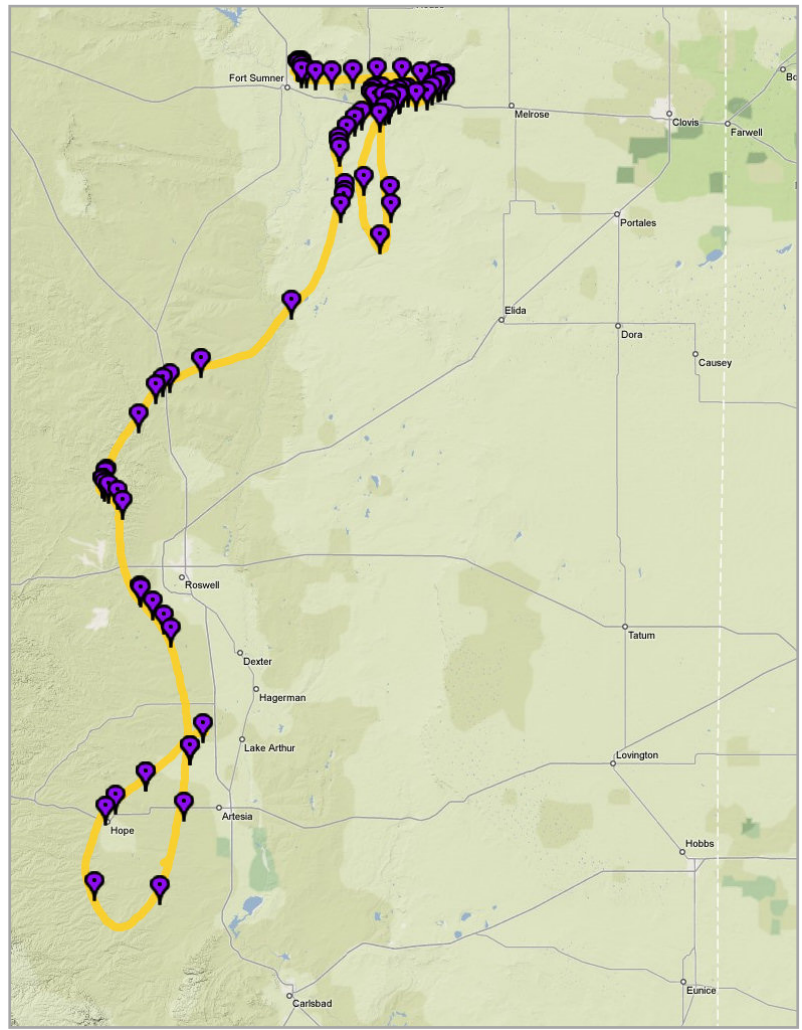
Figure 51. HASP 2008 Flight Path

4.2.1 Environmental Data

The HASP gondola underwent extreme environmental conditions. The health and status of the UND/UNF payload was carefully monitored to ensure nominal operations. During the course of the flight, the temperatures greatly varied as expected with over $50^{\circ}C$ swings shown in Figure 52. A majestic view of the payload at float, with the Earth's curvature in the foreground, is shown in Figure 53.
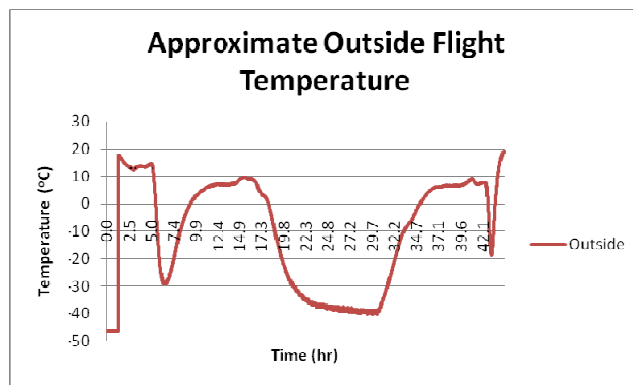
Figure 52. HASP 2008 outside Temperature Profile from Flight

Figure 53. UND/UNF Payload at Float

4.2.2 Sensor Flight Data

The UND/UNF payload performed as expected during the flight. The raw data prior to processing came in the form of counts and in time intervals of 20 seconds. Each raw count represented a 0.25 mV equivalent, which directly and linearly relates to resistance as in appendix C. Figure 54 shows this raw overall output from the RTDs, ozone sensors, pressure sensors, and humidity sensor from the flight.
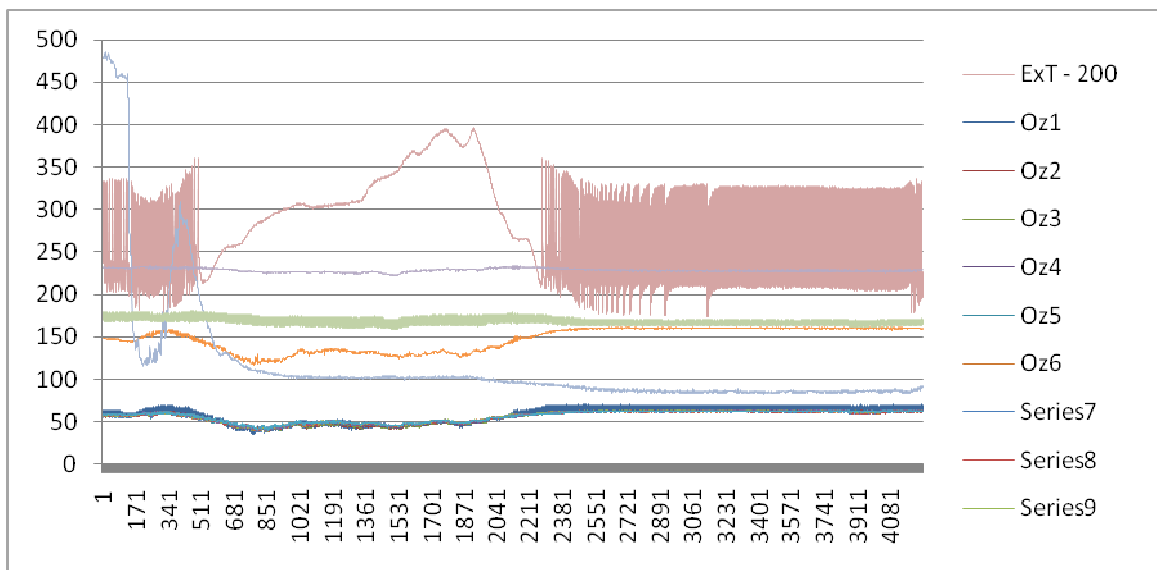
Figure 54. UND/UNF Payload Raw Output in Counts per 20 Second Time Interval

Onboard test resistors recorded variations aside from the desired signal, ozone concentration, over time (*e.g.* pressure variations, $\frac{dR}{dP}$, and temperature variations, $\frac{dR}{dT}$). Although, these test resistors had different resistance values their variations with time were nearly equal in magnitude. Further, the ozone sensors on the ground were assumed to be at similar conditions as those used in the calibration of both temperature and pressure. For instance, according to these calibrations, the ozone sensor detected 0.074 ppm (220.8 mV)

prior to launch, and its reading was consistent with theoretical values for ground level

ozone concentrations in that region. Additionally, calibration averages showed that under

inert gas the ozone sensor output is ~218 mV. However, the issue arises as to how to

isolate variations due to increases in ozone concentration from other variations (*e.g.*

psychometric and physical changes). Therefore, these considerations and discussed

relationships allowed the following ratio relationships and equalities to be made,

$$V_{test\ resistor} = k + \frac{dV}{dP} + \frac{dV}{dT}$$

$$\therefore \frac{dV}{dP} + \frac{dV}{dT} = V_{test\ resistor} - k$$

$$* \ For\ Resitor\ 2\ on\ circuit, k = 650\ mV$$

$$V_{ozone\ sensors} = \frac{dV}{dO_3} + \frac{dV}{dP} + \frac{dV}{dT}$$

$$V_{corected\ ozone\ sensors} = \frac{dV}{dO_3} - (V_{test\ resistor} - k\ )$$

$$\overline{V_{RMS\ corected\ ozone\ sensors}} = \frac{\sqrt{(V_{cs_1}{}^2 + V_{cs_2}{}^2 + V_{cs_3}{}^2 + \ ... \ V_{cs_j}{}^2)}}{n_j}$$

where V voltage, mV

      P pressure, kPa

      k voltage on circuit inherent from its resistance

   These averaged values from the ozone sensors gave an accurate picture of the

voltage across the sensor, and therefore, the resistance. This resistance value, when

accounting for daily fluctuations (temporal variation) in ozone concentration observed in

flight, in turn allowed for the calculation of the ozone concentration. As seen, this methodology involved taking the root mean square difference between the adjusted baseline, from the test resistor and the sensor. These averaged differential values were then correlated to ozone concentrations according to the earlier performed calibrations. This process enabled the creation of a profile for the ozone over Ft. Sumner, NM on September 15, 2008. This flight concluded on the "International Day for the Preservation of the Ozone Layer" the subsequent day of launch, and its resulting ozone flight profile is seen in Figure 55.
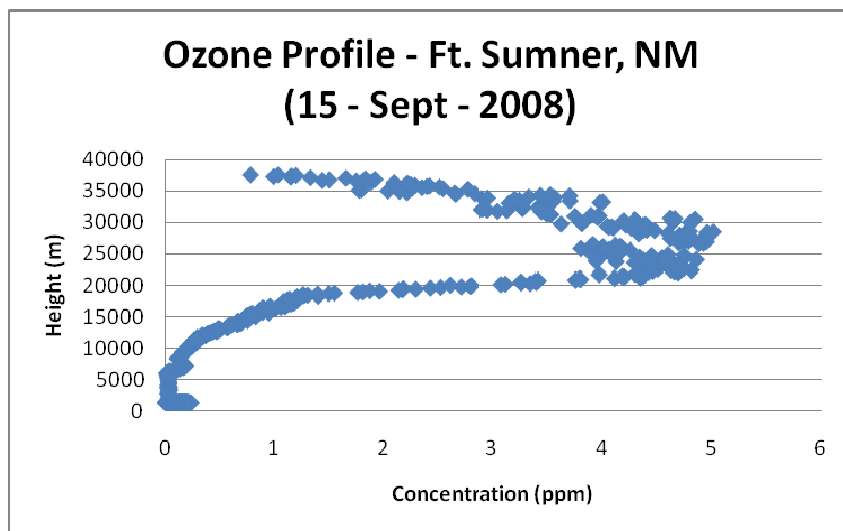
Figure 55. HASP 2008 Sensor Ozone Profile for Ft. Sumner, NM

Data supports calibration and lab findings; however, the results demonstrate a lower than expected ozone concentration. Most likely explanations include the possibility that Hurricane's Ike's circulation affected the distribution and budget of ozone and other trace gasses (Ambler and Patel 2008). This is a similar phenomenon as the one noticed over East Asia in spring 2004 (Chan *et al.* 2007). In addition, the model used to predict the expected concentration is prone to over-estimation due to its predominant dependence on the

Chapman mechanism. The Chapman prediction fails to capture sufficiently other photolytic effects, and can overestimate concentrations by as much as several orders of magnitude. The model used in the JPL NASA document typical seems to underestimate observed ozone by approximately 20%. Finally, an additional explanation could include the low-resolution bridge of the circuitry not falling within the expected values.

4.3 Conclusions

The lower expense and versatile nature of ITO sensors over conventional sensors, such as ECC sensors, make them prime candidates as gas sensors and the subject of further research. The reusability of these sensors makes it possible to increase the frequency of gathering ground truth data regarding the upper atmosphere. Such increased frequencies could lead to a better understanding of the mechanisms of ozone depletion and help to lessen some of its potentially harmful consequences. These sensors archetypes already have a demonstrated capability at detecting other GHGs as well, such as methane.

This research also helps to address many serious unmet needs for miniature sensors capable of in situ, real-time analysis of gases that can detect environmental factors such as contaminants in regenerative life support systems. Further, such solid-state sensors offer a method to study physical phenomena such as the mechanisms of water transfer and diffusion in reduced-pressure environments. Because of the stability of the response with temperature, pressure, and time, gas sensors of this type are ideal candidates for use in extraterrestrial applications and space flight instrumentation (Ambler and Patel 2008). Further, the rugged nature, small size, low mass, increased response rate, and limited power demands of these sensors begin to satisfy the rigorous demands of many space flight technologies. The characterization of these sensors' behaviors, under varying conditions,

remains crucial to the application of sensors in upper atmospheric applications, and space applications necessitated in the Vision for Space Exploration (VSE), including the creation of a prolonged human presence on the Lunar and Martian surfaces. In all, this work successfully promoted STEM, and served as a good initial technology demonstration, showing great promise for development.

4.3.1 Future Work

Future work in demonstrating ITO solid-state gas sensors requires independently verifying and establishing, through an outside agent, that the minimum concentration of the ozone analyte is detectable to the ppbv level using the American Society for Testing & Materials (ASTM) standard. This includes demonstrating the sensors' operational ability in the field. The ASTM standard requires a confidence interval of 99% that the sensor is detecting the ozone analyte above zero, near the low standard of concern. Future field tests should next occur in simultaneous operation with an electrochemical concentration cell (ECC) ozone sonde, as well as in a region with sufficient real time atmospheric satellite monitoring (*e.g.* OMPS on the NPOESS) for a secondary means of comparison. Plans, already afoot, include flying several of these sensors to detect various GHGs and atomic elements aboard a rocket to 130 km to collect an atmospheric profile.

Additionally, further work in developing theoretical modeling into calibration curves could also help increase the accuracy of these sensors. If successful, such sensors could perform the necessary calculations onboard to give real-time useful data that requires no further processing, of great interest to many potential end-users.

APPENDICES (COUNTED BUT NOT NUMBERED) - NONNUMBERED PAGE AT END GETS INSERTED HERE; SIMILIARLY THE DEDICATION PAGE GOES BEFORE THE ABSTRACT

APPENDIX A

HASP Documentation and Details

The HASP documentation provides additional information about the initial intentions of the project, and details the project process through its application and certification for flight provided in Figure 56 and 57. Further additional information in this section regards the HASP balloon and ballast, provided in Table 9.

HASP Student Payload Application for 2008

Payload Title: O_3 Sensor Technology Development and Atmospheric Experimentation

Payload Class: (circle one) Small Large	Institution: Dakota Space Society Research Consortium, University of North Dakota	Submit Date: 17-Dec-2007

Project Abstract

There are several significant and unanswered questions regarding ozone (O_3), and ozone depletion in the atmosphere. These issues demand the development of new reliable and cost effective sensors to monitor ozone over the Earth. One such unique, easily produced in mass, and newly developed (patent pending) sensor array, by the University of North Florida (UNF), is the solid-state nanocrystalline Indium Tin Oxide (ITO) thin film gas sensor. These sensors do not need to operate at very high operating temperature and follow as an improvement compared to the earlier reported tungsten oxide sensors by Hansford *et al.* (2005). In recent months, ITO gas sensors were tested and calibrated with different concentration of ozone (0.5 ppm to 14 ppm) under different pressures using the Low-pressure Test Bed at the Space Life Science Lab (SLSL), Kennedy Space Center (KSC-XA) as a student project through Space Florida with the support of NASA. Our next goal in this process is to launch the sensors with their interface circuitry into the upper atmosphere using a long duration high altitude balloon. This flight compares and validates ITO sensors with the currently used electro-chemical ozone sensors. This project continues through the Dakota Space Society student led consortium.

Team Name: Dakota Space Society	Team or Project Website: http://groups.google.com/group/UND-HASP
Student Team Leader Contact Information:	Faculty Advisor Contact Information:

Name:	Mr. Nathaniel P. Ambler	Dr. Ronald Fevig
Department:	Space Studies	Space Studies, Electrical Engineering
Mailing Address:	Department of Space Studies University of North Dakota Clifford Hall Room 512 4149 University Ave Stop 9008	Department of Space Studies University of North Dakota Clifford Hall Room 512 4149 University Ave Stop 9008
City, State, Zip code:	Grand Forks, ND 58202	Grand Forks, ND 58202
e-mail:	nambler@ufl.edu, nathaniel.ambler@und.nodak.edu	rfevig@aero.und.edu
Office telephone:	(701) 777-2480	(701) 777-2480
Cell:	(352) 284-3087	(520) 820-3440
FAX:	(701) 777-3711	(701) 777-3711

1

Figure 56. HASP 2008 Payload Application

Figure 56 cont.

O₃ Sensor Technology Development and Atmospheric Experimentation

Nathaniel P. Ambler, University of North Dakota
Dr. Ronald A. Fevig, University of North Dakota
Dr. Vadim Rygalov, University of North Dakota
Dr. Nirmal Patel, University of North Florida

Abstract & Background Information

Climate change involves complex issues pertaining to ozone, other greenhouse gases, and additional measurable parameters. There are numerous significant and unanswered questions surrounding ozone (O_3), and ozone depletion in the atmosphere, which demand the development of new reliable and more cost effective sensors. Such sensors can monitor the Earth's atmosphere and can easily undergo validation with remotely sensed data (*e.g.* satellite data). One such unique and newly developed (patent pending) sensors array by the University of North Florida (UNF), easily produced in mass, is the solid state nanocrystalline Indium Tin Oxide (ITO) thin film gas sensors. These sensors arrays follow as an improvement compared to the earlier reported tungsten oxide sensors (Hansford *et al.*, 2005). Here arrays of 24 sensors were fabricated on glass and alumina. These arrays of sensors were developed and fabricated at University of North Florida with support of the Department of Defense (DoD), Office of Naval Research and US Army, ECBC. Each sensor on the array is capable of working individually, in-concert with other sensors, or simultaneously with all sensors. During last summer, ITO gas sensor arrays fabricated over alumina and glass substrates were successfully tested and calibrated with different concentrations of ozone (0.5 ppm to 14 ppm) under varying pressures using the Low-pressure Test Bed at the Space Life Science Lab (SLSL), Kennedy Space Center (KSC-XA), as a student project through Space Florida with the support of NASA. It was found that ITO gas sensors have good sensitivity and response time with low concentrations of ozone, reasonable selectivity for ozone gas, good reversibility, and stability. This endeavor was aided by Dynamac Corporation scientists, Dr. Phillip A. Fowler and Joseph Benjamin; University of Florida and University of North Dakota research scientist, Dr. Vadim Rygalov; University of North Florida materials research scientist, Dr. Nirmal Patel; and the support of Dr. Sager and associated NASA personnel. The next step in this process is to successfully fly the sensor aboard a long duration high altitude balloon to gain atmospheric calibration data, as well as compare this data with current data (i.e., satellite data from the Total Ozone Mapping Spectrometer (TOMS).) Eventually this technique can validate current solid-state ozone sensors. This project continues through the Dakota Space Society Consortium student group with the additional support of the North Dakota Space Grant Consortium and the University of North Dakota's High Altitude Balloon Group.

2

Figure 56 cont. HASP 2008 Payload Application

Figure 56 cont.

PREVIOUS WORK AND ACKNOWLEDGEMENT

As mentioned briefly in the abstract, this work is a continuation of work started at the SLSL, KSC-XA, under the support of Space Florida and its 2007 summer students. This project, although successfully calibrated in the low pressure test bed, failed to provide any flight data due to a telemetry problem shortly after launch. These images are reproduced here, courtesy of Space Florida. Shown in Figure 1 are pictures of the 2007 KSC Intern Balloon Launch at Kelly Park, Florida. These images show the student directed research project mentored by NASA personnel, academic researchers, and Space Florida representatives.

Figure 1- 2007 KSC Intern Balloon Launch at Kelly Park

3

Figure 56 cont. HASP 2008 Payload Application

82

Figure 56 cont.

SENSOR FABRICATION PLAN

Not only is this a validation of design and fabrication, and research into ozone monitoring, it is in fact a general investigation of the affect of pressure on sensor technologies. At 36 km, pressure is roughly less than one percent compared to that at sea level, as seen below in Figure 8. The effect this has on certain sensors limits the accuracy of their absolute molecular measurements. This investigation serves both as the foundation for graduate thesis work and on-going sensor research.

Student Work plan for the fabrication of ozone sensors at the UNF

1. Indium tin oxide (ITO) thin film gas sensors array will be fabricated over glass and alumina substrates (patent pending). Several arrays are fabricated for this project.

2. The surface morphology of sensors are examined using a Scanning Electron Microscope (SEM), and the chemical composition of sensors will be determined using an Energy Dispersive Analysis of X-rays (EDAX) in order to check and verify some of the fabrication parameters of the sensors.

3. Necessary testing of the ITO sensors with test gas will be performed at UNF. Electrical resistance data will be recorded and disseminated. These sensors change their resistance values as a result of ozone concentration.

4. The sensors' array will interface with the printed circuit board (patent pending) via its connection to the 25-pin connector.

5. A miniature, flexible, and low power heater (Minco make) will be integrated on the backside of the sensor arrays. The purpose of the heater is to combat the low temperatures at high altitude and to keep the sensors at a temperature around 25°C. A miniature thermocouple will also be mounted to monitor and control the temperature using an electronic circuit.

6. The sensors' array with heater and printed circuit board mount in the low weight container box.

7. A miniature low power fan will be mounted on the container box so that fan can push the gas molecules over the surface of the sensors at the prescribed rate. This will not affect the balloon's state. A wire mesh will be fixed over the fan in order to filter out dust particles as well as protect the surface of the sensors.

8. The entire box may look similar to the following picture of the sensors' system box, which was fabricated during the summer of 2007. This is shown in Figure 2, along with a PC board containing sensors.

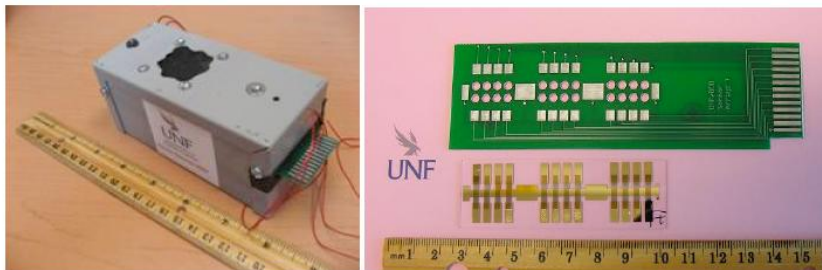Figure 2 – 2007 Summer Sensor Payload and PC Board with Sensors

9. The box containing the sensors, the heater, and the fan system will be delivered to the Dakota Space Society care of Mr. Nathaniel Ambler and his team at UND for further interfacing with the data communication circuit, the temperature control circuit for the heater, and the data storage. All the

4

Figure 56 cont. HASP 2008 Payload Application

Figure 56 cont.

electronic circuit parts will be developed at the University of North Dakota by the local Dakota Space Society and will be tested with the sensors' system on the ground before launch.

10. If required, the necessary modification of sensors and/or circuitry will be performed after testing the electronic communication circuits at UND on a test flight.

TEAM STRUCTURE
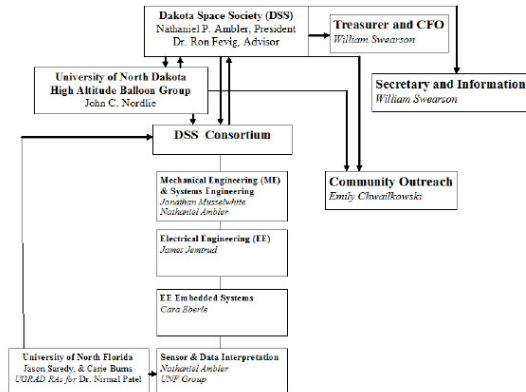
Figure 3 – UND Dakota Space Society Team Structure

Project Engineering Management Competencies:

President of the DSS Consortium and President of the DSS: Nathaniel P. Ambler*
The presiding officer of DSS and his office will execute the overall project. These specific duties include, but are not limited to, the following:
- *Delegating unassigned tasks*
- *Maintaining Project Schedule on Critical Path*
- *Ensuring proper financial and institutional support*
- *Meeting appropriate deadlines and reviews*
- *Fostering continued good-will among prior participants*
- *Approve and submit all financial requests*
- *Utilize prior research experience in this field from KSC, and B.S. in Mechanical Engineering to fill any technical needs*

Treasurer and CFO: William Swearson
The Treasurer and CFO will maintain accurate financial records, and communicate to the individual group leaders the available resources.

Secretary and Information: William Swearson
The Secretary and information officer will maintain appropriate minutes of all consortium meetings, dates, and records. This includes keeping an updated portal of information through the Google group for the UND Hasp Program (http://groups.google.com/group/UND-HASP).

Community Outreach: Emily Chwailkowski*
The community outreach officer will help in organizing local outreach efforts through the Dakota Space Society in conjunction with the Dakota Space Grant Consortium and the UND High Altitude Balloon Group. This involves participating and planning activities for K-12 schools and various local colleges, making presentations to local science and engineering groups, publicizing the project, and creating long-term data about group participants to create an appropriate future impact survey of the project.

5

Figure 56 cont. HASP 2008 Payload Application

Figure 56 cont.

Technical Engineering Management Point of Contacts:
Mechanical Engineering (ME) and Systems Engineering: Jonathan Musselwhite (UND) *et al.*
Electrical Engineering (EE): James Jemtrud (UND) *et al.*
EE Embedded Systems: Carla Eberle (UND) *et al.*
Sensor and Data Interpretation: Jason Saredy (UNF), Carie Burns (UNF), and Nathaniel P. Ambler[*] (UND)

TASKS AND CRITICAL PATH

The initial work break down schedule (WBS) includes the basic tasks required of the HASP project, which includes the Proposal, Integration Plan, Integration Certification, Operation Plan, and Science Report. However, this schedule also includes the strong intent to fly an identical payload locally through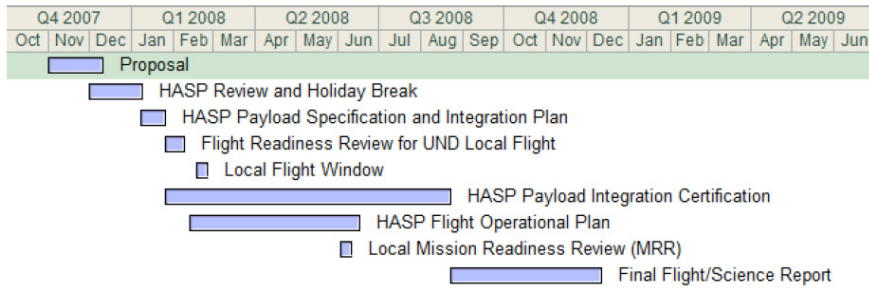 the High Altitude Ballooning group at the University of North Dakota (UND), this task includes creating an identical bus to that of HASP so that all anomalies can be detected in a true flight mode.

Q4 2007			Q1 2008			Q2 2008			Q3 2008			Q4 2008			Q1 2009			Q2 2009		
Oct	Nov	Dec	Jan	Feb	Mar	Apr	May	Jun	Jul	Aug	Sep	Oct	Nov	Dec	Jan	Feb	Mar	Apr	May	Jun

- Proposal
- HASP Review and Holiday Break
- HASP Payload Specification and Integration Plan
- Flight Readiness Review for UND Local Flight
- Local Flight Window
- HASP Payload Integration Certification
- HASP Flight Operational Plan
- Local Mission Readiness Review (MRR)
- Final Flight/Science Report

Name	Duration	%	Assigned	Owner	Work		Start	Finish
Proposal	29 day		Nathaniel Amble	NA			2007-11-7	2007-12-17
HASP Review and Holiday Break	28 day			NA			2007-12-7	2008-1-15
HASP Payload Specification and	15 day			NA			2008-1-14	2008-2-1
Flight Readiness Review for UND	11 day			NA			2008-2-1	2008-2-15
Local Flight Window	3 day			NA			2008-2-24	2008-2-27
HASP Payload Integration Certifi	151 day			NA			2008-2-1	2008-8-29
HASP Flight Operational Plan	90 day			NA			2008-2-19	2008-6-23
Local Mission Readiness Review	3 day			NA			2008-6-9	2008-6-11
Final Flight/Science Report	80 day			NA			2008-8-29	2008-12-18

Figure 4 –Preliminary Task Timeline & Critical Path

HASP INTEGRATION

It is expected that as many as three students (two undergraduates and one graduate) and one faculty member will travel to LSU in late July of 2008 for the integration of the sensor payload onto HASP. It is expected that as many as six students (four undergraduate, and two graduates) and two faculty members will travel to Ft. Sumner for launch of the HASP payload.

PAYLOAD SPECIFICATION

The sensor operates and ozone measurements are processed according to the electronics block diagram shown in Figure 5. Resistance values from the ozone sensor are converted to voltages by the conditioning circuitry, which are then read by an LTC1298-based A/D converter. These values are processed by a BS2-IC microcontroller which

6

Figure 56 cont. HASP 2008 Payload Application

Figure 56 cont.

interfaces with the HASP data handling system. Temperature and pressure sensor readings are processed in a similar manner and are folded into the data stream by the microcontroller. Power from HASP is conditioned by circuitry based on LM78LXX voltage regulators and is provided to each payload electrical subsystem in Figure 5.
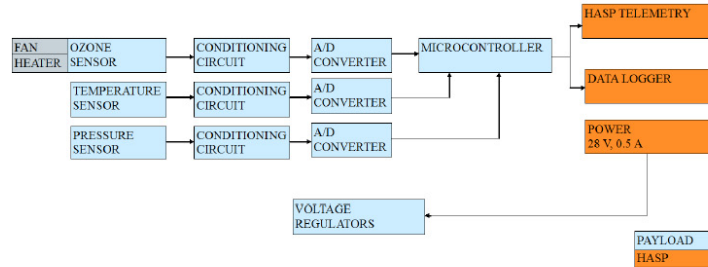
Figure 5 – Electronics Block Diagram

MOUNTING FOOTPRINT

Selection of the small payload dictates the mounting plate that interfaces with the payload. This mounting plate design is provided in the HASP Student Payload Interface Manual (v. 09.09.2007) and is shown below in Figure 6 (Besse, 2007). This mounting plate design will not require modification.
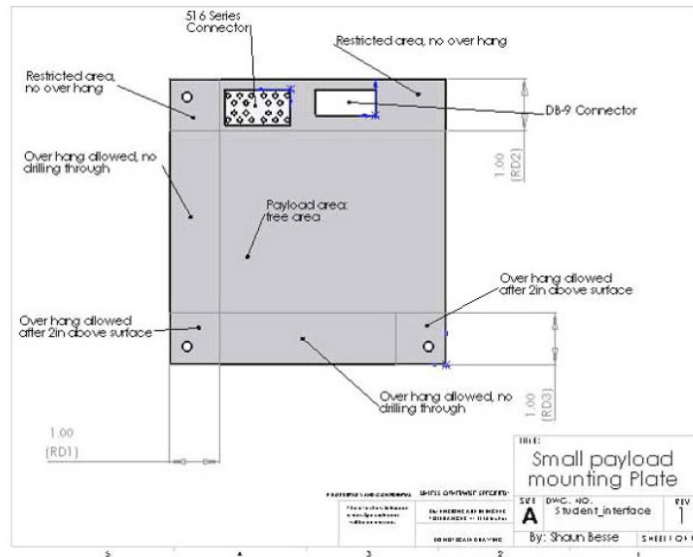
Figure 6 – Mounting Plate (Besse, 2007).

7

Figure 56 cont. HASP 2008 Payload Application

86

Figure 56 cont.

DESIRED LOCATION AND ORIENTATION
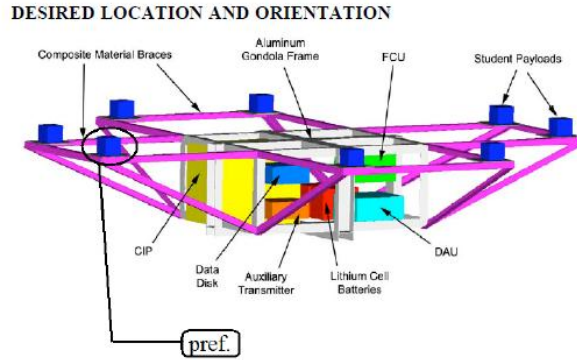
Figure 7 – Proposed HASP Configuration (Guzik and Wefel, 2004)

The requested smaller payload should be oriented on the side away from any solar cells to avoid disparate solar thermal radiation.

PAYLOAD HEIGHT

This payload requested is the small payload; its height will be 30 cm, and the sides will be 15 cm x 15 cm.

MASS BUDGET

The mass budget is itemized below in Table 1.

Table 1 – Itemized Mass Budget

Item:	Mass:
Sensors (including thermistor, and pressure transducer)	450g
SS Data Recorder	250g
Temperature Regulator	300g
Connections	400g
Structure	350g
Total	**1750g**

This is less than the 3 kg limit for the smaller payloads.

POWER BUDGET

The 0.5 Amps at 28 VDC power supplied by HASP adequately accommodates the power requirements for the payload electronics, as well as the heater and fan for the sensor. Table 2 details the preliminary estimate for our power budget

8

Figure 56 cont. HASP 2008 Payload Application

Figure 56 cont.

Table 2 – Itemized Power Budget

Item:	Power requirement:
Payload Electronics	1 W
Sensor Heater	8 W (max.)
Sensor Fan	2 W
Total	**11 W**

This is less than the 14 W limit for the smaller payloads.

THERMAL MODELING

Preliminary heat transfer calculations showed the onboard sensor heater is adequate to keep the sensor at nominal conditions. An additional exploration of the effects of temperature on component integrity is ongoing, and part of the investigation. These initial estimations, based on the prior work performed at KSC-XA, utilized the proposed materials for the walls, and a minimum temperature of -60°C and a general operating temperature of 15°C (found from altitude variation from 0 km to 36 km shown in Figure 8).
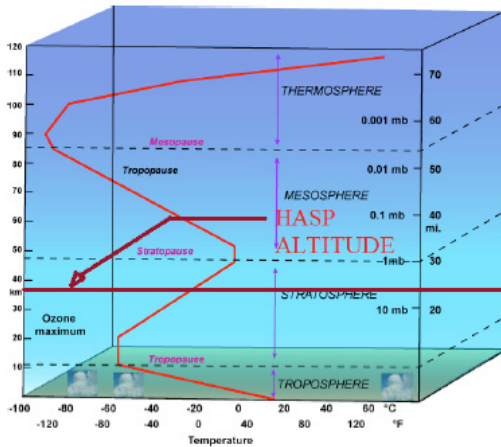
Figure 8 – Modified Altitude Profile (Atkins, 2007)

DOWNLINK SERIAL TELEMETRY RATE

The payload module requires the RS232 HASP telemetry to send the state of resistance to the ground. A data-recording unit will be included with microcontroller in the event that the telemetry link fails. The DB9 connecter is required to the HASP system's telemetry system so that the data can be sent to the base station via the RS232 link. The RS232 link will operate at 1200 baud, with the standard RS232 protocol with eight data bits, no parity, one stop bit, and no flow control. A standard packet will contain the information-formatted vis-à-vis the Student Payload Serial Connection section of the HASP-Student Interface Document.

9

Figure 56 cont. HASP 2008 Payload Application

Figure 56 cont.

UPLINK SERIAL COMMAND RATE

No uplink commands are anticipated.

ANTICIPATED USE OF ANALOG DOWNLIKS

No additional analog downlinks are anticipated.

ANTICIPATED ADDITIONAL DISCRETE COMMANDS

No additional active discrete commands are anticipated.

ANTICIPATED PROCEDURES

Prior to Integration:
    Set initial values for data recorder
    Place sensors in appropriate payload slots
    Insert batteries
    Check all batteries

Integration:
    Mount payload module to HASP
    Connect HASP Power Connector
    Connect HASP Serial Connection
    Test system by recording initial readings and making sure all data is nominal
    Troubleshoot

Pre-Flight Operations:
    Set initial values for data recorder
    Place sensors in appropriate payload slots
    Insert all new batteries
    Check all batteries
    Connect HASP Power Connector
    Connect HASP Serial Connection

Flight Operations:
    Record values for resistance across the sensors

Post-Flight Operations:
    Remove batteries
    Remove data recorder
    Remove payload and sensors for further inspection

10

Figure 56 cont. HASP 2008 Payload Application

Figure 56 cont.

REFERENCES

Guzik, T. Gregory and John P. Wefel. "The High Altitude Student Platform (HASP) for Student-Built Payloads."
35th COSPAR Scientific Assembly. Houston, Texas, 2004. 1-8.

Hansford, Graeme M., et al. "A low cost instrument based on a solid state sensor for balloon-borne atmospheric O3
profile sounding." Journal Environmental Monitoring (2005): 158-162.

HASP – Student Payload Interface Manual, Version 09.07.07, 25 November 2007
< http://laspace.lsu.edu/hasp/documents/public/HASP_Interface_Manual_v90707.pdf>

Atkins, Noel. Survey of Meterology. 10 November 2007
<http://apollo.lsc.vsc.edu/classes/met130/notes/chapter1/vert_temp_all.html>.

11

Figure 56 cont. HASP 2008 Payload Application

90

Figure 56 cont.

BUDGET

The anticipated budget for the project is laid out in Table 2. Support for this project has been generously offered by the North Dakota Space Grant Consortium pending selection of our payload.

Table 2 – Anticipated Budget

Item	Information	Expense
University of North Florida		
Student Research Assistantship	10 hr/week * 4 months	$ 1,600.00
Materials	Chemicals, heater, PCB, box, fan, etc.	$ 1,490.00
Travel & Accommodation	Professor and Student	$ 1,750.00
Incidentals	Shipping, Mailing, etc.	$ 150.00
	Sub-Total	$ 4,990.00
University of North Dakota		
Student Research Assistantship	Summer GRA	$ 3,000.00
Materials	Circuits, Memory, Heater	$ 3,000.00
Travel and Accommodations	Faculty, and Students	$ 9,000.00
Incidentals	Shipping, Mailing, etc.	$ 610.00
	Sub-Total	$ 15,610.00
	Approximate Total	$ 20,600.00

12

Figure 56 cont. HASP 2008 Payload Application

Figure 56 cont.

Biography of PIs

Student Leader:

Nathaniel P. Ambler is a U.S. Citizen, graduate student at the University of North Dakota, Grand Forks, North Dakota. He was awarded a B.S. in Mechanical Engineering in 2005 from the University of Florida where he served as the primary-investigator on an engineering related economic study of aseptic packaging, and as a co-investigator on an effort to automate controls for unmanned vehicles (UAVs, UGVs, and USVs). He worked previously as a teacher of physics and mathematics in secondary education in Seminole County, Florida, and as a researcher in a summer research program at the Kennedy Space Center with NASA. He is currently involved in an on-going research project with NASA mentor Janira A. Ramos, and serves as a graduate teaching assistant (GTA). He currently serves as the President of the Dakota Space Society, which is organizing the local High Altitude Student Platform (HASP) student effort.

Faculty Leaders:

Nirmalkumar G. Patel, Ph.D. is U.S. Citizen, Physics Lecturer and Sensor Scientist at University of North Florida, Jacksonville, Florida. He was awarded his B.S (Physics) in 1976, M.S (Physics-Solid State Electronics) in 1978 and Ph.D. degree (Physics- Semiconductor Thin films Devices) in 1984 from Sardar Patel University, India. He was Professor at Sardar Patel University, during which time he was awarded a DAAD fellowship to work at University of Dortmund, Germany (1986-87), as Visiting Scientist / Professor at the Institute of Chemical and Biological Sensors, Munster, Germany (1996, 1998, 1999 and 2000). He was a PI of Indo-German joint research project on Biosensors for Food and Clinical Analysis. He has 23 years experience in academic work in India and 6 years in USA, and is an established investigator in solid-state gas sensors, with 35 research papers, one patent on biosensors, and one patent pending on nanocrystalline gas sensors arrays. He has been co-investigator on four major sensor research grants funded by the US DOD.

Ronald A. Fevig, Ph.D. is a U.S. Citizen and has a B.A. and M.S. in Mathematics, a M.S. in Space Studies, and a Ph.D. in Planetary Sciences from the University of Arizona. While pursuing his Ph.D. he was heavily involved in a student satellite program that built two CubeSats. He also helped mentor two senior engineering design teams that designed high-altitude balloon payloads. He is currently a post-doctoral researcher and adjunct instructor at the University of North Dakota. In addition to his other responsibilities, he is the faculty advisor for the Dakota Space Society and is a key faculty member involved with the high-altitude ballooning project.

13

Figure 56 cont. HASP 2008 Payload Application

Figure 56 cont.

NORTH DAKOTA

SPACE GRANT CONSORTIUM

Paul Hardersen, Director
(701) 777-4896
hardersen@space.edu

Suezette Rene Bieri, Deputy Director
(701) 777-4856
bieri@space.edu

December 17, 2007

Dakota Space Society
Mr. Nathaniel P. Ambler
Department of Space Studies
Clifford Hall 512
University of North Dakota
4149 University Avenue
Grand Forks, ND 58202-9008

Dear Mr. Ambler,

The North Dakota Space Grant Consortium is pleased to provide financial support of

$20,600 for the student payload, "O3 Sensor Technology Development and Atmospheric

Experimentation," of the Dakota Space Society to fly on HASP.

Sincerely,

Dr. Paul Hardersen

Department of Space Studies
John D. Odegard School of Aerospace Sciences
University of North Dakota
Clifford Hall Room 512
4149 University Avenue Stop 9008
Grand Forks, ND 58202-9008
(701) 777-2480 • FAX (701) 777-3711

UNDAEROSPACE
UNIVERSITY OF NORTH DAKOTA

14

Figure 56 cont. HASP 2008 Payload Application

Figure 56 cont.

HASP Student Payload Application for 2008
Payload Title: O_3 Sensor Technology Development and Atmospheric Experimentation

Name of University Professor / Scientist

Dr. Nirmalkumar G. Patel
Department of Chemistry and Physics
University of North Florida
1 UNF Drive
Jacksonville, Florida 32224

Telephone (Office) 904-620-1670
Cell Phone: 904-200-2855
Email: npatel@unf.edu

Name of UNF Student(s)

(i) Mr. Jason Saredy (Under-Graduate Student, Physics Major and working as a research assistant since last three years with Dr. Patel)
 And / or
(ii) Ms. Carie Burns (Under-Graduate Student, Physics Major and voluntary working with Dr. Patel)

Work plan for the fabrication of ozone sensors

11. Indium tin oxide (ITO) thin film gas sensors array will be fabricated over glass and alumina substrates (patent pending). Several arrays will be fabricated for the project.

12. The surface morphology of sensors will be examined using Scanning Electron Microscope (SEM) and chemical composition of sensors will be determined using Energy Dispersive Analysis of X-rays (EDAX) in order to check and verify some of the fabrication parameters of sensors.

13. Necessary testing of ITO sensors with test gas will be performed at University of North Florida. Electrical resistance data will be provided to Nathan, UND.

14. The sensors array will be interfaced with printed circuit board (Patent pending) and connected with 25-pin connector.

15

Figure 56 cont. HASP 2008 Payload Application

Figure 56 cont.

15. A miniature, flexible and low power heater (Minco make) will be integrated on back side of sensors arrays. The purpose of heater is to combat the low temperature at high altitude and to keep sensors at temperature about 25°C. A miniature thermocouple will also be mounted to monitor and control the temperature using electronics circuit.

16. Sensors array with heater and printed circuit board will be mounted in the low weight container box.

17. A miniature and low power fan with battery will be mounted on the container box so that fan can push the gas molecules over the surface of the sensors. A wire mesh will be fixed over the fan in order to filter out the dust particles as well as protection of surface of the sensors.

18. The entire box may look similar to or better than the following picture of sensors system box, which was fabricated during last summer project.
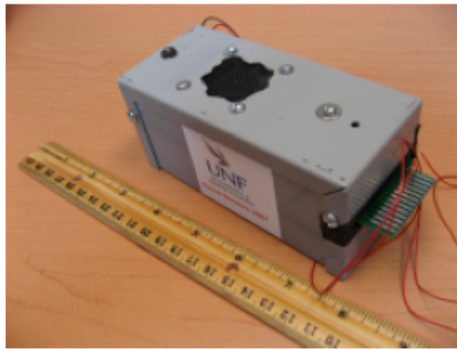
19. The boxes having sensors, heater and fan system will be delivered to Nathan and his team at UND for further interfacing with the data communication circuit, the temperature control circuit for the heater and the storage of data circuit. All the electronic circuit parts will be developed by the other groups of project and will be tested with the sensors system on the ground before launching of a balloon.

20. If required, the necessary modification of sensors or / and circuit parameters will be performed after testing with the electronic communication circuits at UND.

16

Figure 56 cont. HASP 2008 Payload Application

Figure 56 cont.

HASP Student Payload Application for 2008
Payload Title: Sensor Technology Development and Atmospheric Experimentation

Name of University Professor / Scientist

Dr. Nirmalkumar G. Patel
Department of Chemistry and Physics
University of North Florida
1 UNF Drive
Jacksonville, Florida 32224

Telephone (Office) 904-620-1670
Cell Phone: 904-200-2855
Email: npatel@unf.edu

Budget

(1)	Student's salary – 10 hr/week * 4 months (@ $10/hr)	= $ 1600.00
(2)	Materials charges for chemicals, heater, PCB, box, fan, etc	= $ 1490.00
(3)	Travel & accommodation for Professor & Student	= $ 1750.00
(4)	Incidentals (for Shipping / mailing, etc)	= $ 150.00

Total Amount = $ 4990.00

Note: The plus or minus of Budget head # 2, 3 and 4 will be adjusted from each other.

17

Figure 56 cont. HASP 2008 Payload Application

HASP Payload Integration Certification

Payload Title: O₃ Sensor Technology Development & Atmospheric Experimentation

Payload ID: 2008 - 07

Institution: University of North Dakota

Integration Payload Team Leader: Nate Ambler

Contact Information: nathaniel.ambler@und.nodak.edu

Payload has been integrated and is APPROVED FOR FLIGHT OPERATIONS:

_____   8/8/08
T. Gregory Guzik, HASP Director   Date

_____   8/8/08
Michael Stewart, HASP Systems Head   Date

_____   8/8/08
Payload Team Leader   Date

Payload has been integrated, but OUTSTANDING ISSUES NEED TO BE RESOLVED:

_____   _____
T. Gregory Guzik, HASP Director   Date

_____   _____
Michael Stewart, HASP Systems Head   Date

_____   _____
Payload Team Leader   Date

Figure 57. HASP 2008 Payload Flight Readiness Review and Integration Certificate

Figure 57 cont.

HASP Payload Integration Certification

Complete	N/A	LSU Rep	Payload Rep	MECHANICAL
☑	☐	T66		The measured weight of the payload (including the payload plate) is 1.792 kilograms. The typical payload plate weight is 0.581 kilograms. The payload weight without the payload plate is 1.211 kilograms.
☑	☐	T66		Mechanical drawing detailing the major components the payload and specifically how the payload is attached to the payload mounting plate has been provided.
☑	☐	T66		Does the payload contain any hazardous component(s)?

YES   NO
☐   ☑ - Pressurized container
☐   ☑ - Radioactive material
☐   ☑ - Biological Samples
☐   ☑ - Other, list any here:

_____

☐	☑	T66		Documentation detailing all hazardous components has been provided.
☑	☐	T66		The payload is properly secured to the payload plate.
☑	☐	T66		The interior of the payload is properly insulated.
☑	☐	T66		The exterior of the payload is properly shielded and/or insulated.
☑	☐	T66		Other relevant mechanical information has been provided, list any here:

_____

_____

☐	☑	T66		Mechanical issues to be resolved (if so, see attached).

Figure 57 cont. HASP 2008 Payload Flight Readiness Review and Integration Certificate

Figure 57 cont.

HASP Payload Integration Certification

Complete	N/A	LSU Rep	Payload Rep	**POWER**
☑	☐	*TGG*	*(M)*	The measured current draw at 38 VDC is ___100___ mA. *without heater , 208 mA with heater*
☑	☐	*TGG*	*(M)*	A wiring diagram has been provided (applicable if HASP is supplying power to your payload).
☑	☐	*TGG*	*(M)*	Power connection between payload and mounting plate EDAC connector is wired correctly
☑	☐	*TGG*	*(M)*	Other relevant power information has been provided, list any here:
				_____
				_____
				_____
☑	☐	~~H~~ *TGG*	*(M)*	Electrical issues to be resolved (if so, see attached). *change ~~the~~ power up to start with heater off.*

Complete	N/A	LSU Rep	Payload Rep	**THERMAL / VACUUM TESTING**
☑	☐	*TGG*	*(M)*	A thermal test over the temperature range ___−60___ °C to ___60___ °C has been performed.
☑	☐	*TGG*	*(M)*	Test data showing normal payload function during thermal test has been provided.
☑	☐	*TGG*	*(M)*	A vacuum test to ___5___ mbar has been performed..
☑	☐	*TGG*	*(M)*	Test data showing normal payload function during vacuum test has been provided.
☐	☑	*TGG*	*(M)*	Thermal / Vacuum test issues to be resolved (if so, see attached).

Figure 57 cont. HASP 2008 Payload Flight Readiness Review and Integration Certificate

99

Figure 57 cont.

HASP Payload Integration Certification

Complete	N/A	LSU Rep	Payload Rep	COMMUNICATION
☑	☐	TGG		The observed serial data downlink format is: stream or packetized (circle one).
☑	☐	TGG		The observed serial downlink rate is ~~~~ 36 bps.
☑	☐	TGG		The serial downlink is functioning properly.
☑	☐	TGG		The downlink data, retrieved from the HASP website, has been validated by the payload team.
☑	☐	TGG		A list of uplink commands has been provided to the HASP team.
☐	☑	TGG		All ___0___ analog channels being used are functioning properly.
☐	☑	TGG		All ___0___ discrete lines being used are functioning properly.
☑	☐	TGG		All ___2___ uplink commands have been tested and are functioning properly.
☐	☑	TGG		Transmitter frequency _____ MHz verified
☐	☑	TGG		Transmitter power _____ W verified
☐	☑	TGG		Transmitter FCC license verified
☐	☑	TGG		Transmitter functioning normally
☐	☑	TGG		Receiver frequency _____ MHz verified
☐	☑	TGG		Receiver functioning normally
☒	☐	TGG		Communication issues to be resolved (if so, see attached).

Figure 57 cont. HASP 2008 Payload Flight Readiness Review and Integration Certificate

Figure 57 cont.

HASP Payload Integration Certification

Complete	N/A	LSU Rep	Payload Rep	LOGISTICS & PLANNING
☑	☐	TGG	*(signature)*	A list of all payload team members including contact information has been provided.
☑	☐	TGG	*(signature)*	A mission operation plan has been submitted.
☐	☑	TGG	*(signature)*	Logistical and planning issues to be resolved (if so, see attached).

Figure 57 cont. HASP 2008 Payload Flight Readiness Review and Integration Certificate

Figure 57 cont.

HASP Payload Integration Certification

OUTSTANDING ISSUES TO BE RESOLVED

① Change power up so it begins with heater off
— 8/8/08 TGG heater on during startup
② Serial command interface needs to be
implemented correctly. i.e. Table 4
in the Interface Manual.
— 8/8/08 TGG Serial commanding
resolved

Figure 57 cont. HASP 2008 Payload Flight Readiness Review and Integration Certificate

Table 9. HASP Balloon and Ballast Parameters

Balloon Type	Zero pressure, 1 cap CSBF #979
Balloon Size	11.82 million cubic feet
Parachute Diameter	79 feet
HASP Weight	411 pounds
SIP Weight	589 pounds
Balloon Systems	458 pounds
Ballast	542 pounds
Altitude with Ballast	122,500 feet
Altitude without Ballast	126,000 feet
Ballast for Drive-Up	140 pounds
Ballast for Sunset	259 pounds

APPENDIX B

Project Details

The project schedule, Table 10, establishes the project plan. The project plan

formulates the necessary basis to create a work breakdown schedule and the critical path.

Table 10. Project Schedule

Outline of Project Plan
1   Project Overview and Organization
1.1 Summary statement
1.1.1   Specify Mission Statement
1.1.2   Clearly Define Specification
1.1.3   Define Project Composition
1.2 Work Breakdown Structure (WBS)
1.3 Organizational Plan
1.3.1   Address how structure addresses mission
1.3.2   Provide adequate PM controls
1.3.3   Inclusion of milestones
2   Project Scheduling
2.1   Summary statement
2.1.1   Define task precedence relationships
2.1.2   Calculate CPM using Earliest Start and Latest Finish
2.1.2.1   Slack time calculations
2.2 Project Budget
2.3 Resource Allocation
1.3.1   Project Team Formalization
1.3.2   Method of Task Assignment
1.3.3   Delegation of Responsibilities
3   Project Monitoring and Control
3.1   Creation of Metrics
1.1.1   Schedule
1.1.2   Costs
1.1.3   Quality
1.1.4   Risk
3.2 Milestone Reporting
4   Project Termination
4.1   Post-project Evaluation
1.1.1   Evaluate Project Success/failure
4.2 Post-flight Science/Engineering Report
1.3.1   Carry out Data Reduction
1.3.2   Delivery of Report

APPENDIX C

Technical and Engineering Details

Many details relevant to the engineering and technical process require additional attention. This section includes many details regarding the theory of the circuit design, additional schematics, more information on the calibration procedure, a copy of the certification for the OMZ-1108 sensor, and additional electronic relationships.

The use of a Wheatstone bridge forms the fundamentals for the designed circuit. A Wheatstone bridge balances two legs of a bridge circuit to measure the sensor's resistance through a difference measurement. The voltage, which is known and controlled, helps determine resistance following Kirchhoff's second rule seen in the following adaptation,

$$R_x = \frac{R_2 I_2 I_3 R_3}{R_1 I_1 I_x} \qquad \therefore V = \frac{R_x V_s}{R_3 + R_x} - \frac{R_2 V_s}{R_1 + R_2}$$

where R_x resistance, Ohm

             I   current in respective legs, Ampere

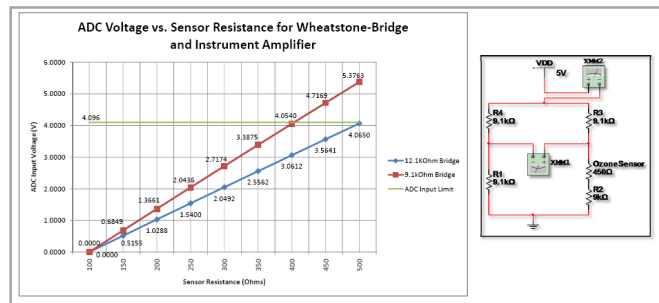This relationship is shown in Figure 58, and with the addition of Table11.

Figure 58. ADC Voltage and Resistance

Table 11. Wheatstone Bridge Voltage to Resistance Outputs

Ozone Sesnor Wheatstone Bridge/Instrumentation Amplifier
Bridge Resistors (R1,R3,R4): 12.1k   R2: 12k

Notes: Full sensor range of **100-500 Ω**
Max bridge current draw of 413.0uA
Max system resolution: 0.492Ω

Sensor Resistance (Ω):	Bridge Output Voltage (mV)	In-Amp Gain A	In-Amp Gain B	Input to ADC Gain A (V)	Input to ADC Gain B (V)
100	0.000	100	10	0.0000	0.00000
150	5.155	100	10	0.5155	0.05155
200	10.288	100	10	1.0288	0.10288
250	15.400	100	10	1.5400	0.15400
300	20.492	100	10	2.0492	0.20492
350	25.562	100	10	2.5562	0.25562
400	30.612	100	10	3.0612	0.30612
450	35.641	100	10	3.5641	0.35641
500	40.650	100	10	4.0650	0.40650

Ozone Sesnor Wheatstone Bridge/Instrumentation Amplifier
Bridge Resistors (R1,R3,R4): 9.1k   R2: 9k

Notes: Full sensor range of **100-400 Ω**
Higher precision than 12.1kΩ bridge
Max bridge current draw of 549.8uA
Max system resolution: 0.296Ω

Sensor Resistance (Ω):	Bridge Output Voltage (mV)	In-Amp Gain A	In-Amp Gain B	Input to ADC Gain A (V)	Input to ADC Gain B (V)
100	0.000	100	10	0.0000	0.00000
150	6.849	100	10	0.6849	0.06849
200	13.661	100	10	1.3661	0.13661
250	20.436	100	10	2.0436	0.20436
300	27.174	100	10	2.7174	0.27174
350	33.875	100	10	3.3875	0.33875
400	40.540	100	10	4.0540	0.40540
450	47.169	100	10	4.7169	0.47169
500	53.763	100	10	5.3763	0.53763

Internal RTD Wheatstone Bridge/Instrumentation Amplifier
Bridge Resistors (R1,R3,R4): 33.5k   R2: 33k

Notes: Full sensor range of **500-1600 Ω**
Temp Range: -100°C to +150°C
Max bridge current draw of 149.2uAuA
Max temperature resolution: ~.2588°C

Temp	Sensor Resistance (Ω):	Bridge Output Voltage (mV)	In-Amp Gain A	In-Amp Gain B	Input to ADC Gain A (V)	Input to ADC Gain B (V)
~-200°C	600	3.726	100	10	0.3726	0.03726
	700		100	10	0.0000	0.00000
	800	11.144	100	10	1.1144	0.11144
	900		100	10	0.0000	0.00000
~-0°C	1000	18.518	100	10	1.8518	0.18518
	1100		100	10	0.0000	0.00000
	1200	25.848	100	10	2.5848	0.25848
	1300		100	10	0.0000	0.00000
	1400	33.136	100	10	3.3136	0.33136
	1500		100	10	0.0000	0.00000
~+150°C	1600	40.380	100	10	4.0380	0.40380

External RTD Wheatstone Bridge/Instrumentation Amplifier
Bridge Resistors (R1,R3,R4): 31.8k   R2: 31.6k

Notes: Full sensor range of **250-1250 Ω**
Temp Range: -200°C to +50°C
Max bridge current draw of 149.2uAuA
Max temperature resolution: ~.2588°C

Temp	Sensor Resistance (Ω):	Bridge Output Voltage (mV)	In-Amp Gain A	In-Amp Gain B	Input to ADC Gain A (V)	Input to ADC Gain B (V)
~-200°C	250	1.964	100	10	0.1964	0.01964
	350		100	10	0.0000	0.00000
	450	9.788	100	10	0.9788	0.09788
	550		100	10	0.0000	0.00000
	650	17.564	100	10	1.7564	0.17564
	750		100	10	0.0000	0.00000
	850	25.291	100	10	2.5291	0.25291
	950		100	10	0.0000	0.00000
~0°C	1050	32.970	100	10	3.2970	0.32970
	1150		100	10	0.0000	0.00000
~+50°C	1250	40.602	100	10	4.0602	0.40602

The overall resulting circuit required a DC-DC converter for the power supplied by the HASP platform through the EDAC 516 connector to supply the heater and fan components of the payload. This initial power supply design is shown in the overall power supply schematic in Figure 59.
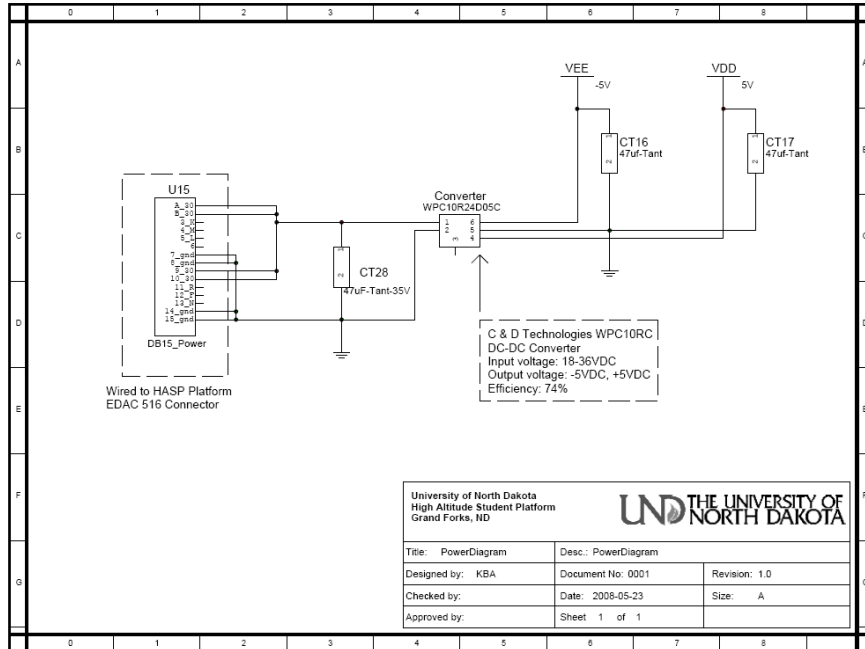
Figure 59. Power Supply Schematic

Further, the use of the Wheatstone bridge to measure resistance is relevant as the signal of interest in calibration and flight for the sensors required the measurement of resistance. The calibration and signal theory that measured this characteristic signal followed the following general sensor signal equations,

$$C' = \frac{Q}{V}(C_o - C) - kC \approx 0$$

$$C = C_o \frac{\frac{Q}{V}}{k + \frac{Q}{V}} \approx C_o \frac{\frac{Q_o}{V} \frac{P^\alpha}{P_o{}^\alpha}}{k + \frac{Q_o}{V} \frac{P^\alpha}{P_o{}^\alpha}}$$

where   C   characteristic signal, Ohm

               Q   volumetric flow rate, $\frac{liters}{minute}$

               P   pressure, Pa

               α diffusivity coefficient, unitless

This procedure, when utilized, as outlined in the main body also required a secondary calibrated source for verification. This certification of calibration for this secondary sensor, the OMC-1108, is included in Figure 60.

Certificate of Calibration

Ozone Solutions
789 7ᵗʰ St NW
Sioux Center, IA 51250
www.ozoneapplications.com
service@ozoneapplications.com
Ph: (712) 722-0337
Fax: (712) 722-1787

Date July 14, 2008

Model Number ___OMC-1108_____

Serial Number_____10804065_____

This is to certify that the instrument described above was calibrated in our facilities according to the manufacturer's procedures

The calibration was performed with an Advanced Pollution Instruments 401X O3 Photometric Calibrator – Serial Number 331. This analyzer is certified to be NIST traceable and is calibrated according to API specification in their facility.

The calibration of the sensor is checked several times over several hours of testing. The calibration data is entered with the serial number, customer and date in our permanent calibration database.

Calibration Performed by:

Joel Leusink

Date of Calibration _____July 10, 2008

Figure 60. Certificate of OMC-1108 Calibration

The main ozone sensor however was not the only signal of interest. The measurement of temperature was crucial to the flight and similarly took in measurements of resistance, these measurements came from an onboard platinum-RTD. This RTD follows

108

the traditional Callendar-Van Dusen relationship shown below for the low temperature regime,

$$R_T = R_o[1 + AT + BT^2 + CT^3(T - 100)]$$

where R_T resistance , Ohm

                T   temperature, $^\circ$C

                A   constant from calibration $\approx$ 3.9083 x 10^{-3} $^\circ$C^{-1}

                B   constant from calibration $\approx$ -5.775 x 10^{-7} $^\circ$C^{-2}

                C   constant from calibration $\approx$ -4.183 x 10^{-12} $^\circ$C^{-4}

Finally, the relationship between the voltage and resistance important to these signals came in two forms of resolution: high and low. These resolution modes each had their own characteristics, which both shared the same near perfect linear relationship through Ohm's law. This relationship is shown in Figure 61.
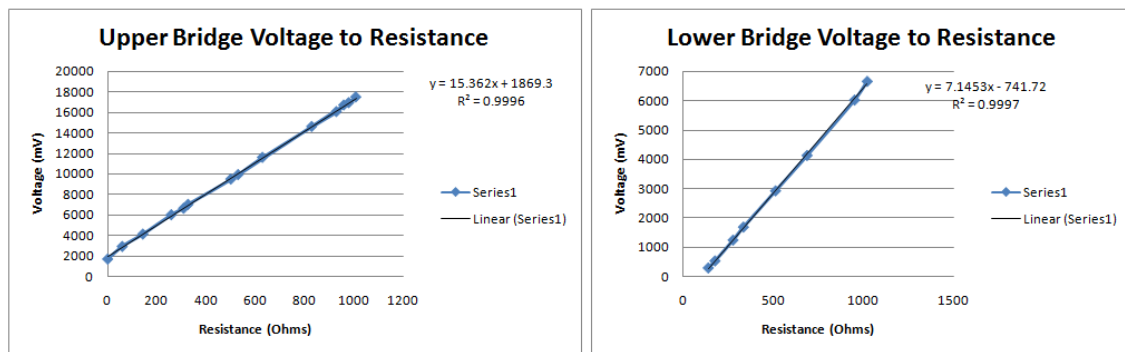

Figure 61. Voltage to Resistance

APPENDIX D

Sensor Details and Operating Principles

The sensor arrays tested all included 24 sensors on a board that connected to the circuitry via a ribbon cable. These sensors on the array followed a standard convention of labeling according to keep sensors distinct as shown in Figure 62.
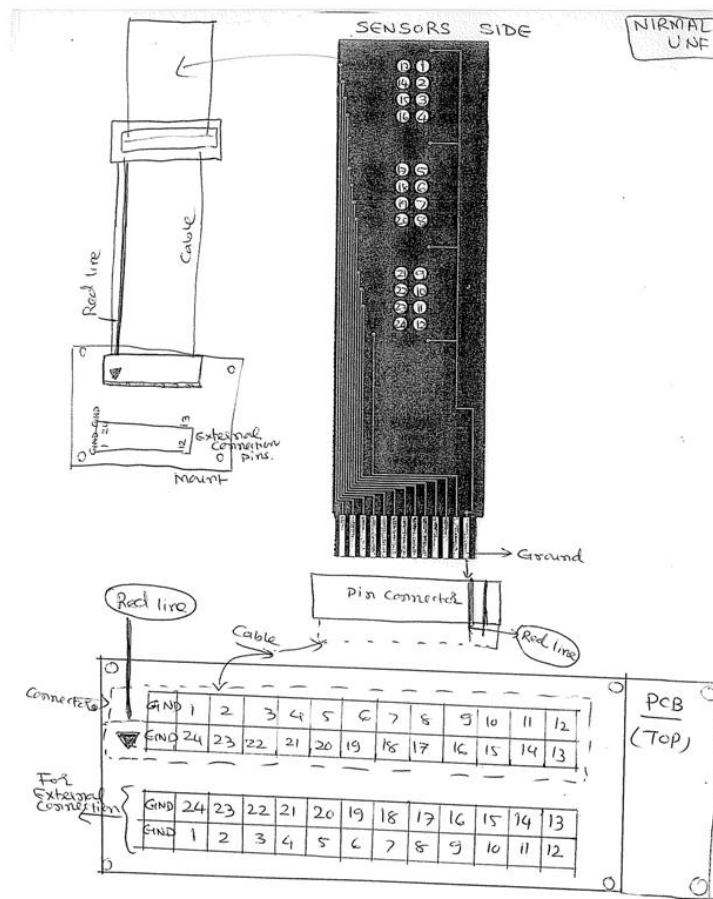

Figure 62. Sensor Numbering

Each of the sensors arrays had different baseline conditions depending on the deposition parameters; however, each were initially tested for reactivity using the reducing gas, acetylene, as shown in Figure 63.
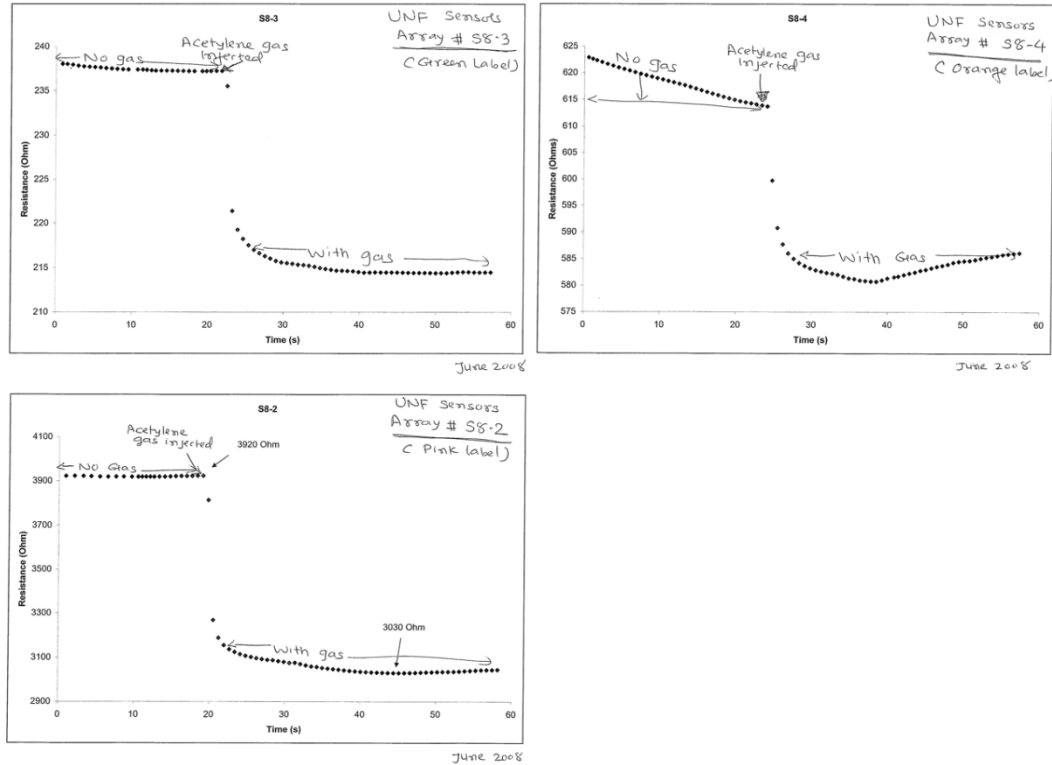

Figure 63. Initial Sensor Test

The behaviors of the sensors follow basic semiconductor atomic and quantum behaviors. The utility of the structure of the ITO film relies on the fact that tin atoms occupy the less distorted octahedral b sites of the In_2O_3 crystalline lattice expanding its lattice parameter from roughly 10.117 Å to up to 10.125 Å with 6% tin doping (Nadaud *et al.* 1988). The resulting electrical behavior of the ITO thin film act as traditional conductors. This metal oxide conductor is a form of a degenerate semiconductor and is largely governed by the mentioned solid-state physics considerations.

REFERENCES

Ambler, N. P., and N G. Patel, "SOLID-STATE SENSOR BEHAVIOR IN REDUCED-PRESSURE ENVIRONMENTS DEMONSTRATION USING AN EXPERIMENTAL INDIUM TIN OXIDE OZONE GAS SENSOR FOR OZONE SOUNDING," IAC Congress, 2008, C2.I.17

Carrico, Barbara, Saredy, J., Tracy, L.,N G. Patel, J. Garner and L. Gasparov, "Measurement of the DC Resistance of Semiconductor Thin Film Gas Systems: Comparison to Several Transport Models." Journal of Applied Physics, 2007, Vol. 102, Issue, 83, 714-721

Chan, C.Y., Y.S. Li, J.H. Tang, Y.K. Leung, M.C. Wu, L.Y. Chan, C.C. Chang, S.C. Liu,"An Analysis on Abnormally Low Ozone in the Upper Troposphere over Subtropical East Asia in Spring 2004." Atmospheric Environment, Vol. 41, Issue 17, June 2007, 3556-3564

Chang, K.S., R.T. Farrell, J.W. Snellen. "Thermal properties of metalized plastic and polyethylene sheeting: a direct calorimetric assessment." Ergonomics, Volume 28, Issue 11, November 1985. 1557 – 1562.

Chapman, S., "A theory of upper atmospheric ozone." Memoirs of the Royal Meteorological Society. 1930. 3 (26). 103-25.

Demore, W. B., C. J. Howard, S. P. Sander, A. R. Ravishankara, " Chemical Kinetics and Photochemical Data for Use in Stratospheric Modeling." JPL Publication 97-4, 1997, Evaluation number 12.

Department of Defense. "Systems Engineering Fundamentals." Defense Acquisition Press. January 2001. 31.

Guzik, T. Gregory and John P. Wefel. "The High Altitude Student Platform (HASP) for Student-Built Payloads." 35th COSPAR Scientific Assembly. Houston, Texas, 2004. 1-8.

Guzik, T. G., S. Besse, A. Calongne, A. Dominique, S. B. Ellison, R. Gould, D. Granger, D. Olano, D. Smith, M. Stewart and J. P. Wefel. "Development of the High Altitude Student Platform." COSPAR, 2006, PSB1-0043-06

Hansford, Graeme M., Ray A. Freshwater, Ronald A. Bosch, R. Anthony Cox, Roderic L. Jones, Keith F. E. Pratt and David E. Williams. "A low cost instrument based on a solid state sensor for balloon-borne atmospheric O_3 profile sounding." Journal Environmental Monitoring, 2005, 7, 158-162.

Haenni, W.H., H.J. Boving, A.M. Perret, M. van Eesbeek, J. Matcham. "High Temperature Electronics Conference 1998." HITEC. 1998 Fourth International Volume, Issue 14-18, Jun 1998, 234 – 237

O'Hanlon, John F., A User's Guide to Vacuum Technology. New York: John Wiley & Sons, 1980.

Honour, Eric C. "Understanding the Value of Systems Engineering." INCOSE Conference, 2004

HASP – Student Payload Interface Manual, Version 09.07.07, 25 November 2007 <laspace.lsu.edu/hasp/documents/public/HASP_Interface_Manual_v90707.pdf>

Jacobson, Mark Z. "Fundamentals of Atmospheric Modeling." Cambridge University Press, 2005

Klastorin, Ted. "Project Management, Tools and Trade-Offs." John Wiley & Sons. University of Washington. 13, 72. 2004.

Kludze, A.K. *"The Impact of Systems Engineering on Complex Systems,"* Conference on Systems Engineering Research, University of Southern California, Los Angeles, CA, 2004.

Korotcenkov, G., *"Metal oxides for solid state gas sensors. What determines our choice?"* Material Science Engineering. B 139, 2007: 1-23.

Korotcenkov, G., *"The role of morphology and crystallographic structure of metal oxides in response of conductometric- type gas sensors,"* Material Science Engineering. R 61, 2008: 1-39.

Korotcenkov, G., J. R. Stetter, "Comparative study of SnO2- and In2O3- based ozone sensors," G. Hunter, S. Bhansali, and R. Mukundan (eds.), Sensors, Actuators, and Microsystems (General) 211th ECS Meeting, May 6-May 10, 2007, Chicago, Illinois, ECS Transactions, 6 (20), 2008: 29-41

Kumar Krishen. "New technology innovations with potential for space applications." Acta Astronautica, volume 63. 1-4, 324-333.

Marenco, C. "Long Term Evolution of Ozone at the Mid-Latitudes of the Northern Hemisphere." European Geophysical Society, XVII General Assembly, Edinburgh, 6-10 April 1992.

Maylor, H. and R. Vidgen, "Complexity in Project-based operations: a grounded model and its Implications for theory and practice." (2006).

Might, R.J. and W. A. Fischer. "The Role of Structural Factors in Determining Project Management Success." IEEE Transactions on Engineering Management EM-32, no. 2, May 1985.

Nadaud, N., N. Lequeux, M. Nanot, J. Jové, and T. Rosinel. "Structural Studies of Tin-Doped Indium Oxide (ITO) and $In_4Sn_3O_{12}$." Journal of Solid State Chemistry, 1998, Vol. 135. 140-148.

Patel, N. G., P. D. Patel, and V. S. Vaishnav. "Indium Tin Oxide (ITO) Thin Film Gas Sensor for Detection of Methanol at Room Temperature." Actuators B: Chemical, 2003, Vol. 96. 180-189.

Pinto, J. and D. Slevin. "Critical Factors in Successful Project Implementation," IEEE Transactions on Engineering Management EM-34, no. 1. Feb. 1987. 22-27.

Project Management Institute (PMI). A Guide to the Project Management Body of Knowledge (PMBOK® Guide). Newton Square, Pa., 2000.

Project Management Institute. Practice Standard for Work Breakdown Structures. Second Edition. Global Standard Press. 2006.

Randel, William J., Richard S. Stolarski, M. Derek, Derek M. Cunnold, Jennifer A, Logan, M. J. Newchurch, Joseph M. Zawodny. "Trends in the Vertical Distribution of Ozone." Science. 10 September 1999, Vol. 285. No. 5434. 1689- 1692.

Shenhar, A. J. "One Size Does Not Fit All Projects: Exploring Classical Contingency Domains." Management Science 74, no. 3, March 2001. 394-414.

Shenhar, Aaron J., and Don Dvir. "Reinventing Project Management." Harvard Business School Press. 2007.

Soffian, Asan. "Project Success in Relation with Organizational Roles and Capabilities and Project Managers' Skills and Capabilities." University of Strathclyde. November 2003.

Solomon, Susan, "STRATOSPHERIC OZONE DEPLETION: A REVIEW OF CONCEPTS AND HISTORY." Reviews of Geophysics, August 1999, 37, 3, 275–316

Vaishnav, V. S., Parasbhai D. Patel, and N.G. Patel. "Preparation and Characterization of Indium Tin Oxide Thin Films for their Application as Gas Sensors." Thin Solid Films, 2005, Vol. 487, 277-282

Vaishnav, V.S., Parasbhai D. Patel, and N. G. Patel. "Indium Tin Oxide Thin Film Gas Sensors for Detection of Ethanol Vapours." Thin Solid Films, 2005, Vol. 490. 94-100.

Vaishnav, V.S., Parasbhai D. Patel, and N.G. Patel. "Indium Tin Oxide Thin-Film Sensor for Detection of Volatile Organic Compounds (VOCs)." Materials and Manufacturing Processes, 2006, Vol. 21, 257-261

Wells, Don, R. Cubert, and A. Rao, "Agile Development Methods Extreme Programming." University of Florida. 2nd Edition. 2004.

Youker, Robert. "Organizational Alternatives for Project Managers." Project Management Quarterly. Vol. VIII, No. 1, March 1997.

APPENDICES

To my loving parents and friends